SANDIA REPORT

SAND2011-8012
Unlimited Distribution
Printed December 2011

Linear Diffusion into a Faraday Cage

K. C. Chen
Y. T. Lin
L. K. Warne
K. O. Merewether

Prepared by
Sandia National Laboratories
Albuquerque, New Mexico 87185 and Livermore, California 94550

Sandia National Laboratories is a multi-program laboratory managed and operated by Sandia Corporation, a wholly owned subsidiary of Lockheed Martin Corporation, for the U.S. Department of Energy's National Nuclear Security Administration.

Issued by Sandia National Laboratories, operated for the United States Department of Energy by Sandia Corporation.

Available to DOE and DOE contractors from

U.S. Department of Energy
Office of Scientific and Technical Information
P.O. Box 62
Oak Ridge, TN 37831

Telephone: (865) 576-8401
Facsimile: (865) 576-5728
E-Mail: reports@adonis.osti.gov
Online ordering: http://www.osti.gov/bridge

Available to the public from

U.S. Department of Commerce
National Technical Information Service
5285 Port Royal Rd.
Springfield, VA 22161

Telephone: (800) 553-6847
Facsimile: (703) 605-6900
E-Mail: orders@ntis.fedworld.gov
Online order: http://www.ntis.gov/help/ordermethods.asp?loc=7-4-0#online

SAND2011-8012

Unlimited Distribution
Printed December 2011

Linear Diffusion into a Faraday Cage

K. C. Chen
Nuclear Safety Assessment,
Y. T. Lin
Weapon Surety and EM Engineering,
L. K. Warne
Electromagnetic Theory
K. O. Merewether
Weapon Surety and EM Engineering,

Sandia National Laboratories
P. O. Box 5800
Albuquerque, New Mexico 87185

Abstract

Linear lightning diffusion into a Faraday cage is studied. An early-time integral valid for large ratios of enclosure size to enclosure thickness and small relative permeability ($\mu/\mu_0 \leq 10$) complemented by an exact residue expansion is used for this study. Existing solutions for nearby lightning impulse responses of electrically thick-wall enclosures are refined and extended to calculate the nearby lightning magnetic field (H) and time-derivative magnetic field (HDOT) inside enclosures of varying thickness caused by a decaying exponential excitation. For a direct strike scenario, the early-time integral for a worst-case line source outside the enclosure caused by an impulse is simplified and numerically integrated to give the interior H and HDOT at the location closest to the source as well as a function of distance from the source. H and HDOT enclosure response functions for decaying exponentials are considered for an enclosure wall of any thickness. Simple formulas are derived to provide a description of enclosure interior H and HDOT as well. Direct strike voltage and current bounds for a single-turn optimally-coupled loop for all three waveforms are also given.

Acknowledgement

The authors are grateful to Dr. Kelvin Lee for his valuable comments that result in a more comprehensive presentation.

Contents

Figures

Tables

Linear Diffusion into a Faraday Cage

Executive Summary

An impulse is used as an idealized waveform for approximating a high altitude electromagnetic pulse (HEMP) when treating the magnetic diffusion into a metallic enclosure [1]. A unit step on the other hand is used to calculate the maximum voltage induced on an optimal coupling loop inside a metallic enclosure and on the opposite side of the enclosure wall by lightning [2]. The rationale of these treatments is clear. A thick enclosure wall allows the use of an impulse; a thin wall needs to use a unit step. The questions that arise in deciding which approach to take are, "What is the quantitative criterion for determining which one is more accurate? What is the relevant parameter? What errors are incurred if the criterion is violated?"

The parameter most relevant to the diffusion penetration is the diffusion time ($\tau_d = \Delta^2\mu\sigma$) of the enclosure wall where μ, σ and Δ are the permeability, conductivity and thickness of the wall material. Table 1 lists various $\alpha\tau_d$ where α is the decay constant of the lightning waveform. All of these thicknesses are used in various aerospace applications. The table shows that the diffusion time is both large and small compared to the fall time of the lightning waveform, depending on the thickness, so that neither the impulse approximation, nor the step-function approximation is universally valid.

In the frequency domain, the skin depth δ is a familiar quantity for shielding. When the skin depth for an incident magnetic field with ω as the angular frequency is small compared to the enclosure wall thickness, i.e., $\delta = \sqrt{2/\omega\mu\sigma} < \Delta$, the magnetic field is attenuated as it penetrates the wall. The higher the frequency the greater the attenuation. Letting $\omega = 2/t$, leads to $t < \tau_d$. For $t \ll \tau_d$, the magnetic field is greatly attenuated. The smaller the time the greater the attenuation.

Table 1. $\alpha\tau_d$ values for different enclosure wall thicknesses and for different lightning decay constants.

Δ (wall thickness in inches)	$\tau_d = \Delta^2\mu\sigma$ for 6061 Aluminum Alloy	$\alpha\tau_d$	
		$\alpha = 3466$ (1% lightning)	$\alpha = 13864$ (50% lightning)
1/2	5.27 ms	18.27	73
1/4	1.32 ms	4.567	18.27
1/8	329 μs	1.142	4.567
1/16	82 μs	0.2855	1.142
1/32	21 μs	0.0714	0.2855

The decaying exponential waveform characterizes the principal energy contribution of naturally occurring physical phenomena, e.g., lightning. The decaying exponential response closely describes the transient behavior and is the response of interest in many physical problems. The decay constant α is inversely proportional to the fall time of the waveform. Therefore, $\alpha\tau_d$ is proportional to the ratio of diffusion time to the fall time and is the transition parameter. Limiting cases are simple and easier to calculate and serve as useful models. When $\alpha \to 0$ and the fall time goes to infinity, the decaying exponential becomes a unit step that contains low frequencies. This is considered a thin limit because low frequencies penetrate the enclosure wall. When $\alpha \to \infty$ and the fall time goes to zero, the decaying exponential becomes an impulse that contains high frequencies. In the thick limit, we consider how high frequencies penetrate the wall.

This report varies $\alpha\tau_d$ through the transition range from thin to thick. Figure 1 is peak interior HDOT for nearby lightning enclosure interior fields. Strictly speaking, the unit step response is only valid for $\alpha\tau_d = 0$ and the impulse response is only valid for $\alpha\tau_d \to \infty$; however, either model can be used to approximate the problem under study. The peak HDOT determines the peak induced voltage and therefore we will emphasize our discussion on HDOT. For voltage calculations in an externally uniform field drive like HEMP and nearby lightning, the spatial variation of the nearby lightning H and HDOT inside the enclosure is assumed to be constant. For direct strikes, the spatial variation of the HDOT waveform is, in general, unknown and therefore the direct calculation of a voltage bound is also included. The current bound is also used to illustrate the importance of avoiding multi-point grounds.

We compared unit step, impulse, and decaying exponential responses and found that approximate HDOT peaks for decaying exponentials can be obtained by combining the unit step coupling and the impulse coupling (treating them as independent, for the former is dominated by low frequencies and the latter is dominated by high frequencies). A parallel "combination" of the unit step coupling and the impulse coupling yields an approximate formula for peak HDOT:

$$\frac{1}{HDOT_{in}^{e}} = \frac{1}{HDOT_{in}^{s}} + \frac{1}{HDOT_{in}^{i}} \qquad (1)$$

where superscript "e" is for decaying exponential, superscript "*s*" is for unit step and superscript "*i*" is for impulse and subscript "*in*" is for interior field. Figure 1 shows the peak decaying exponential response compared to the peak unit step and the peak impulse responses for nearby lightning. Note that 0.8876 is the peak response of coupling from the unit step, 5.7118 is the slope of the peak response of the coupling from the unit impulse and $\frac{1}{\alpha\tau_d}$ is the impulse moment. These numerical values obtained by solving limiting cases are fully discussed in the section on numerical results.

The approximation in Figure 1 makes use of (1) in combining the unit step contribution with the impulse contribution.

$$Peak\ HDOT_{in}^{e}(\xi\tau_d/H_{ex}) \approx \frac{1}{\frac{1}{0.8876}+\frac{\alpha\tau_d}{5.7118}} \quad (2)$$

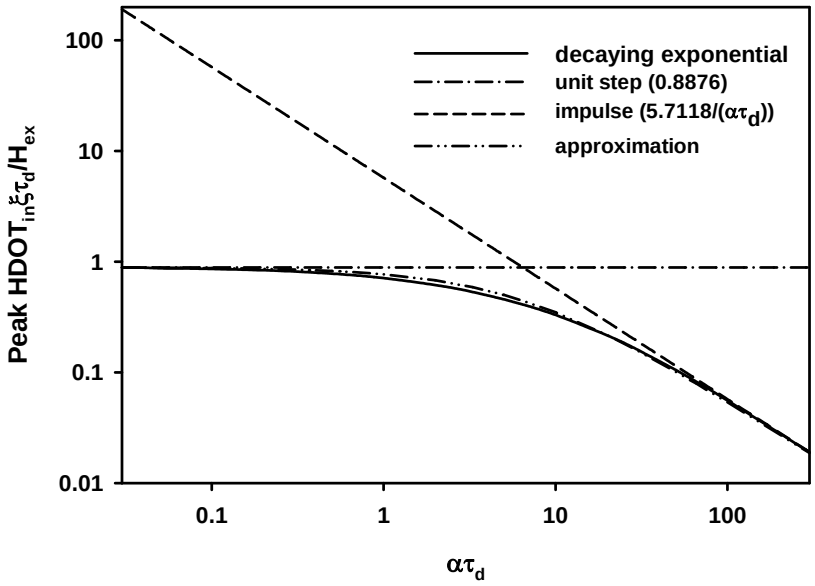

Figure 1. This figure shows the peak decaying exponential response compared to the peak unit step and the peak impulse response. Note the unit step and impulse intersects at $\alpha\tau_d = 6.4351$ where either waveform overestimates the peak derivative compared to the decaying exponential.♣ $\xi = 6.088$ is used for obtaining peak responses.

The scale factor $\xi\tau_d$ is the product of enclosure geometric factor and diffusion time. The geometric factor is $\xi = \frac{\mu_0}{\mu}\frac{V}{S\Delta}$ where *V* is the volume and *S* is the surface of the enclosure. As an example a cylindrical enclosure with diameter of $2a = 2\ ft$, length of $b = 6\ ft$ and $\Delta = 20\ mils$, *ξ = 257.3*. Note that Figure 1 is calculated with *ξ = 6.088*. Scaled peak responses are not very sensitive to the ξ value. In the section on numerical results, small variations for different ξ's will be discussed. The peak unit step and impulse responses intersect at $\alpha\tau_d = 6.4351$. At this value of $\alpha\tau_d$, the error is approximately a factor of *2* in either the impulse or step responses. Large errors can incur if the unit step is applied to the thick wall ($\alpha\tau_d$ is large) or if the impulse response is applied to thin wall ($\alpha\tau_d$ is small). HEMP has a decay constant $\alpha = 4 \times 10^6$ [3]. The intersection point corresponds to $\tau_d = 1.61\ \mu s$, or approximately 9 mil aluminum foil. For the impulse response to be accurate, the enclosure wall has to be at least *20 mils* in thickness.

Consider now a HEMP (*Electric Field Peak =50 kV/m* and *Magnetic Field Peak =133 A/m*) is incident on a cylindrical enclosure discussed before ($2a = 0.61\ m$ and $b = 1.83\ m$). We

♣ The corresponding intersection for peak H response (Figure 24) is $\alpha\tau_d = 0.1458$. An adequate model for describing HDOT may not be adequate for describing H and vice versa.

assume a wall thickness $\Delta = 20\ mils$, a magnetic field perpendicular to the axis of the cylinder, and an optimum coupling loop oriented to capture a maximum penetrant magnetic flux. The induced voltage is the time derivative of the magnetic flux through the loop. Let us use an impulse model as shown in Figure 1. 20 mil-aluminum alloy wall has $\tau_d = 8.4\ \mu s$, $\alpha\tau_d = 33.6$ and the geometric factor $\xi = 257.3$,

$$V = \mu_0 \frac{dH}{dt} 2ab = \mu_0 HDOT_{in} 2ab = \frac{\mu_0 H_{ex}}{\xi \tau_d} \frac{5.7118}{\alpha\tau_d} 2ab \approx 14.5\ millivolts.$$

Equation (2) for calculating the voltage of a decaying exponential waveform gives *12.2 millivolts*.

Similarly, the nearby peak magnetic field is *320 A/m.* Using the same cylindrical enclosure for the HEMP problem, the induced voltage for the maximum coupling loop as defined before is *35 millivolts* for the impulse model and *29.3 millivolts* for the more accurate decaying exponential.

The direct lightning model assumed in this report is one for which the lightning current is adjacent to the enclosure but electrically insulated from the enclosure (Figure 2). The lightning channel may have high potential and the assumed lightning line source is not easily realizable for a small separation between the lightning carrying cable and the enclosure. However, the worst-case coupling can be approached when lightning strikes a well-insulated cable that is isolated from the enclosure but their separation is sufficient to withstand the high potential. The relevancy of the model should be based on the potential physical configuration that might be susceptible to this particular threat.

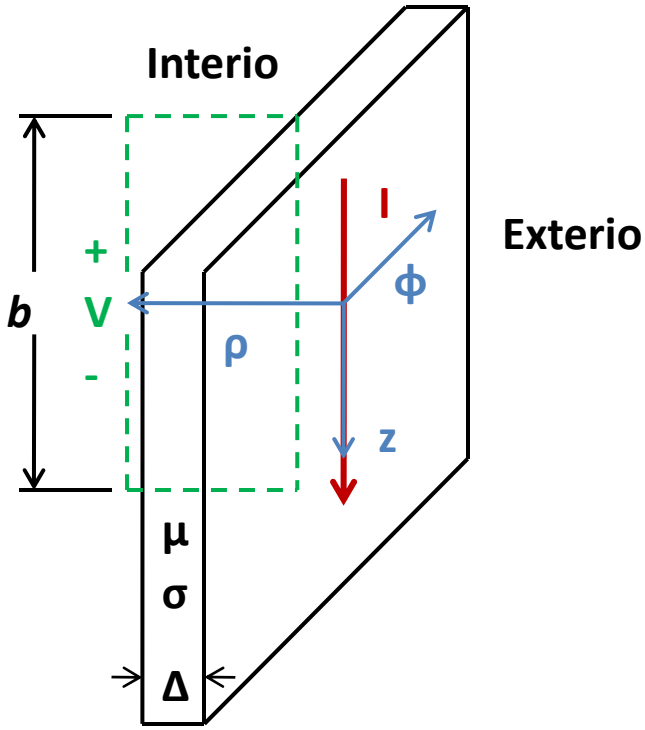

Figure 2. Direct lightning strike to an insulated cable parallel to the enclosure wall and a maximum coupling loop.

Peak HDOT for a direct strike next to the enclosure is given in Figure 3. The unit step coupling peak is *0.2516* and the slope of the unit impulse coupling peak is *4.1608*. The approximation in Figure 3 makes use of (1) for $\rho = \Delta,\ \mu = \mu_0$ and I = the direct strike peak current as

$$Peak\ HDOT_{in}^{e}(\tau_d\, \Delta/I) \approx \frac{1}{\frac{1}{0.2516}+\frac{\alpha\tau_d}{4.1608}} \tag{3}$$

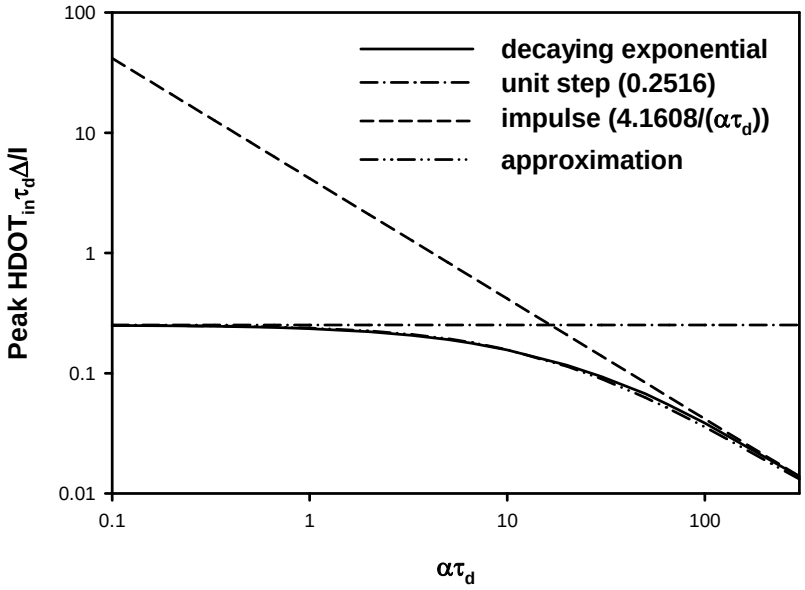

Figure 3. HDOT peak ($\rho = \Delta$) for the decaying exponential and an approximation are compared to the unit step and impulse responses. This value determines the maximum voltage induced on an optimally coupled loop. The enclosure wall has $\mu = \mu_0$.

Note that the intersection of the unit step and the impulse peaks occurs at $\alpha\tau_d = 16.5374$ (Figure 3). For 1-percentile lightning, the decay constant is determined to be $\alpha = 3466$. A ½-inch aluminum wall thickness has $\alpha\tau_d = 18.27$ (Table 1). At this value of $\alpha\tau_d$ and *b* as defined in Figure 2 is *1.83m*,

$$V < \int_{\Delta}^{\infty} \mu_0 HDOT_{in}|_{\rho=\Delta} \frac{\Delta^2 b d\rho}{\rho^2} \approx \mu_0 HDOT_{in}|_{\rho=\Delta} b\Delta = \frac{\mu_0 2\times10^5}{0.00527} 0.2516 \times 1.83 \approx 21.95\ volts \tag{4}$$

for the unit step case. Equation (3) gives 10.4 volts for the decaying exponential.

HDOT values in the enclosure indicate what induced voltage on a given loop might be. However, because the spatial dependence of the HDOT waveform is unknown the induced loop voltage waveform that is the integration of the HDOT waveform on the loop area cannot be accurately calculated. The voltage bound on an optimally coupled loop is a useful alternative for describing the enclosure interior direct strike lightning coupling (Figure 4). Note the close

agreement between the unit step response of *0.2516* for HDOT (Figure 3) and the unit step response 0f *0.2552* for the voltage bound (Figure 4). This is because the HDOT for the unit step has an approximate spatial variation of ($\approx \frac{1}{\rho^2}$).

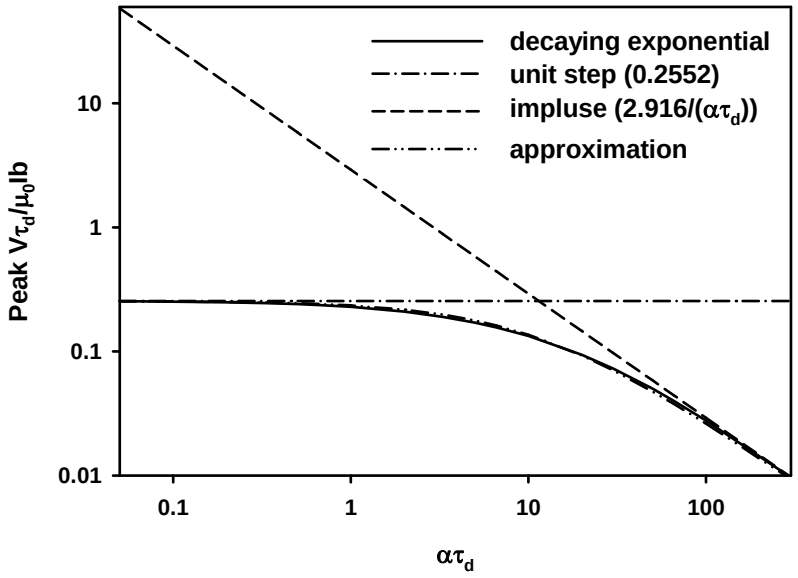

Figure 4. Peak voltage bound for direct strikes. The intersection of the peak unit step voltage and the peak impulse voltage occurs at $\alpha\tau_d = 11.4263$.

The unit step voltage bound for the direct strike problem (Figure 2) just discussed can be calculated by (Figure 4)
$V = 0.2552\frac{\mu_0}{\tau_d}Ib \approx \frac{0.2552\times\mu_0}{0.00527}2\times10^5\times1.83 \approx 22.27\ volts.$

The peak impulse voltage bound (Figure 4) is somewhat smaller than the voltage obtained from peak HDOT (Figure 3) because HDOT from the impulse drops off much faster than $\frac{1}{\rho^2}$. The approximation in Figure 4 is a formula similar to (3):

$$V\tau_d/\mu_0 Ib \approx \frac{1}{\frac{1}{0.2552}+\frac{\alpha\tau_d}{2.916}} \qquad (5)$$

The more accurate decaying exponential voltage bound (5) is thus $V \approx 0.0982\ \frac{\mu_0 Ib}{\tau_d} \approx 8.57\ volts.$

HDOT for $\rho = \Delta$ that gives the maximum induced voltage of an optimally coupled loop is a universal response and can be scaled for any enclosure wall thickness Δ by noticing the impulse solution is scaled by $(\tau_d)^2\Delta$ and thus is inversely proportional to Δ^5. Similarly, the unit step HDOT solution is inversely proportional to Δ^3. The corresponding induced voltage is scaled by Δ^{-4} for the impulse and Δ^{-2} for the unit step, which agrees with voltage bounds (5). As an

example, the induced voltage (5) for a 1/8-inch aluminum enclosure ($\alpha\tau_d = 1.142$) with same geometry and 1/8-in wall thickness is $V \approx 0.232\ \frac{\mu_0 Ib}{\tau_d} \approx 324\ volts$.

We must emphasize at this point that there is no reliable way to know which one of the two models (unit step or impulse) to use because the intersection point in Figure 1, Figure 3 and Figure 4 cannot be determined a priori. For example, how do we know $\alpha\tau_d$ of 1.142 is too small for using the impulse model? If the impulse model is used for calculating the peak voltage bound, the resulting estimated voltage is approximately a factor of *11* too high.

On the other hand, although either the unit step or the impulse model may overestimate the peak response, the peak obtained from the model is always conservative; the resulting design based on either model will have adequate shielding.

The procedure for deriving the approximate expression (1) for the enclosure interior peak HDOT as a function of $\alpha\tau_d$ can be used to address the situation. When both the unit step and impulse HDOT are known, an accurate fit function is available for use. Furthermore, the technique of using a fit function is applicable to other diffusion problems. For instance, the insulated conductor that is struck by lightning can be only a small distance away from the enclosure. In this case, solving for the unit step and impulse responses is considerably simpler than the decaying exponential response. The fit function for decaying exponentials can thus be constructed with the simpler unit step and impulse responses.

Equation 4 can be integrated to describe the short-circuit current (*i*) on the optimally coupled loop shown in Figure 2. Note that the induced voltage *V* on the left hand side of (4) is the same as $\frac{d}{dt}(Li)$ and $HDOT_{in}|_{\rho=\Delta}$ on the right hand side is the same as $\frac{d}{dt}H_{in}|_{\rho=\Delta}$ the current on the short-circuit coupling loop can therefore be expressed as

$$i < \frac{\mu_0}{L}H_{in}|_{\rho=\Delta} b\Delta \approx \frac{2\pi I}{\cosh^{-1}\frac{(\rho-\Delta)}{r_0}}\frac{0.2516}{18.27} \approx 2.7\ kA$$

where the loop inductance *L* is assumed to arise from images on enclosure walls that dominate the impedance of the loop, a is the outer radius of the enclosure and r_0 is the wire radius♦. The reduction for the loop current from the impulse to decaying exponential is determined later and found to be approximately 10% lower. A typical current bound for a perfectly conducting loop is thus high and hence multi-point grounds must be avoided [4]. If there is a series capacitance in the loop (e.g., an incidental open switch or other openings in the circuit), the loop current will be small because the impedance for the capacitance is very large at this frequency range.

♦ 0.2516 is from Figure 4 and $\frac{2\pi}{\cosh^{-1}\frac{(\rho-\Delta)}{r_0}} \approx 1$ is used. This is an order-of-magnitude estimate. The actual inductance can be considerably lower than the value obtained from the assumption.

Other useful approximations are the application of averaging to a convolution integral (28) and an ad hoc use of averaging to a two-parameter integral (57).

Finally, the double exponential waveform does not provide a good description of HDOT for the lightning waveform. The time derivative of a double exponential waveform that starts from a maximum value and decays in time on the order of $\frac{1}{\beta}$, where β is the rate-of-rise constant, does not resemble the time derivative of the lightning current. Therefore, the transparency limit ($\Delta \to 0$) for solutions given in this report is not realistic and should not be taken.

Introduction

A Faraday cage is an enclosure composed of a continuous system of conductors, such that the potential difference between any two points on the cage is zero, when exposed to an electrostatic field. Although the definition is limited to electrostatic fields, Faraday cages are also effective in transient applications. In such cases, although potential differences and average fields are not identically zero, they are reduced dramatically from what they would have been in the absence of the shield. As a result, they are used in virtually all high-consequence or mission-critical applications to mitigate the effects of electrical and electromagnetic environments.

Faraday cages constructed as metallic enclosures must be evaluated for their attributes of shielding effectiveness against external electrical stresses. Enclosures of interest here are metallic cases. The external electrical stresses are nearby and direct lightning threats. Nearby solutions are useful for situations where the distance from the lightning current to the enclosure is much greater than the enclosure linear dimension. Direct strike solutions give a worst-case coupling to the enclosure interior.

Nearby lightning can couple to the critical circuits inside the enclosure only through magnetic fluxes. However, direct lightning strikes can penetrate the imperfect Faraday cage through insults on specific enclosure physical features. First, the metallic enclosure wall must be thick enough to provide attenuation for lightning, not only for reducing the magnetic flux coupling, but also for stopping the lightning continuing current from burning through the wall. Second, the bolts used for connecting the enclosure must be evaluated for their contact impedances and the bolt spacing must be small so that no excessive voltage will appear on the joint. Lastly and most important of all is that any line penetration must be stopped. Use of lightning surge arrestors, inductors, fuses and robust switches are recommended to stop lightning that might be attached to the line penetrations from reaching protected circuits. These circuits must be evaluated for all three different threats.

This report first considers only the linear diffusion by extending the existing nearby solution of impulse magnetic field coupling into a thick-wall enclosure [1] to enclosures of arbitrary thickness using an early-time integral and a residue expansion for a decaying exponential excitation. The limiting cases of the impulse and the unit step excitation are used to illustrate the magnetic coupling to an enclosure. Decaying exponential response functions, uniformly valid for all thicknesses, are introduced for constructing the solution. The wide transition for H and HDOT from very thick to the thin limit is covered by numerical curves as well as approximate analytical formulas.

The worst-case magnetic coupling to an enclosure from a direct lightning strike is then treated. The situation when the lightning current flows in a conductor in close proximity to the enclosure, but is insulated from the metallic enclosure case such that the magnetic flux from lightning can optimally couple to the enclosure interior, is the worst case. If lightning attaches

to the enclosure metal case the lightning current will be distributed on the enclosure case so that the magnetic coupling to the enclosure interior will be reduced.

For a direct strike, a previous paper [2] treats the maximum penetration of a step function enclosure response that applies to a situation with $\tau_d \ll \tau_f$ (where τ_d is the diffusion time of the enclosure wall and τ_f is the fall time of the incident waveform). This report applies the basic formulation given in [2] to arbitrary wall thicknesses and the lightning waveform is treated as a decaying exponential waveform. The solution is also numerically studied for distant fields. Approximate formulas are derived to facilitate the understanding of the relevant physics. Again, decaying exponential response functions, uniformly valid for all thicknesses, are introduced for constructing the solution. Voltage and current bounds for all three waveforms are also given.

The organization of the report: (A) executive summary provides a description of major accomplishments of the report, (B) subsections in the introduction present the parameters of lightning, the distinction between the nearby and direct lightning, and relevant works on linear diffusion, (C) sections on numerical results give complete waveforms for all limiting cases and all peak enclosure interior parameters are summarized in tables, (D) sections on technical details are given in the order of general solutions, nearby lightning, direct lightning for impulses and for decaying exponentials, and voltage and current bounds for direct strikes, (E) all supporting figures are gathered in one section, followed by conclusions.

Parameters of Lightning

The parameters of lightning (such as peak amplitude, peak rise rate, pulse width, and total action) are statistical in nature. Statistical study of the frequency of the various lightning parameters [5, 6] indicated that they are reasonably well described by lognormal distributions, which are straight lines on logarithmic probability paper. Consequently, the full distributions are described by two points, which are the 50-percentile and 1-percentile worst-case levels (or the 50-percentile and 1-percentile occurrence levels). The most important parameters are shown below in Table 2.

We therefore assume that the return stroke can be represented by an exponential pulse of the form

$$i(t) = I\left(e^{-\alpha t} - e^{-\beta t}\right)u(t) = If(t) \approx Ie^{-\alpha t}u(t) \tag{6}$$

which is a two-parameter waveform in current amplitude *I* and α. In terms of the time to half maximum t_{50} or action *G*, the decay constant α is given by

$$\alpha = \frac{\ln 2}{t_{50}} \tag{7}$$

or

$$\alpha = \frac{I^2}{2G}, \tag{8}$$

where

$$G = \int_0^\infty i^2(t)dt \,. \tag{9}$$

Table 2. Lightning Environment: return stroke and flash parameters.

RETURN STROKE PARAMETERS	*1 %*	*50 %*
Peak Current (kA)	*200.*	*30.*
Time to Peak (μs)	*0.1-15.*	*3.*
Maximum Rate of Rise (kA/μs)	*400.*	*150.*
Time to Decay to Half Maximum (μs)	*10.-500.**	*50.*
Amplitude of Continuing Current (A)	*30.-700.*	*150.*
Duration of Continuing Current (ms)	*500.*	*150.*
FLASH PARAMETERS		
Number of Strokes	*>20.*	*4.*
Interstroke Interval (ms)	*10.-500.*	*60.*
Total Flash Duration (ms)	*30.-1000.*	*180.*
Total Charge Transfer (C)	*350.*	*15.*
Action [$\int I^2 dt$] (A^2-s)	$3.\times 10^6$	$5.\times 10^4$

Notes: * The decay time has been revised downward in recent years; however, according to the best available data, the action, which is a measure of the total impulse strength, is still 3×10^6 A^2-*s* at the one-percentile occurrence level. 200 μs was discussed by Ciano and Pierce [5].

If we fix *I = 200 kA* and assume a decay time of *500 μs* (see Table 2), the corresponding action is 14.4×10^6 A^2-*s*, which is almost a factor of five larger than the one-percentile action for the entire flash. On the other hand, if we choose the decay constant to satisfy the one-percentile action, the time to half maximum is a little over *100 μs*, which is not necessarily a value that would give rise to a maximum interior field. If we choose the decay constant to maximize the total impulse charge,

$$Q = \int_0^\infty i(t)dt = \frac{I}{\alpha}\,, \tag{10}$$

such a choice also maximizes the interior field. Therefore, if we assume the impulse charge *Q* is equal to its one-percentile value of *40 C* (see Appendix A) and add a *50*-percent safety margin, the time to half maximum $t_{50} \approx 200$ μs, and the total action $G = 5.8 \times 10^6$ A^2-s. Under these assumptions, the decay constant is

$$\alpha = \ln(2)/(200\ \mu\text{s}) = 3466\ \text{s}^{-1} \tag{11}$$

Parameter β in (6) is determined by maximum rate of rise in Table 2:

$\beta \approx \frac{\frac{dI}{dt}}{I} \approx 2 \times 10^6\ sec^{-1}$ (1-percentile severity levels) or $0.75 \times 10^6\ sec^{-1}$ (*50-percentile* severity levels). A *1-percentile* peak current is used for all calculations.

Nearby vs. Direct-Strike Lightning

Nearby lightning is a normal environment, which is an expected logistical and operational environment that the system is required to survive without degradation in operational reliability. Based on practical considerations, the nearby lightning environment is *defined* as the magnetic field due to a *20-kA* return stroke at *10 m* or a *200-kA* return stroke at *100 m*, where, for a vertical lightning channel, the magnetic field *H* at a distance ρ is given by

$$H(t) = \frac{i(t)}{2\pi\rho}. \tag{12}$$

The peak value of this magnetic field is

$$H_{ex}^{pk} \approx 320 \text{ A/m}.$$

Lightning strikes closer than *10 m* or those that produce larger fields than the above are considered direct strikes. Direct-strike lightning is an abnormal environment for aeronautical systems.

Relevant Works on Linear Diffusion

Kaden investigated diffusion for canonical geometries in the frequency domain in [7]; Bedrosian and Lee [1], [8] summarized Kaden's enclosure diffusion from a plane wave incident magnetic field for EMP applications as

$$\frac{H_{in}}{H_{ex}} \approx \frac{1}{cosh\sqrt{s\tau_d} + \eta\sqrt{s\tau_d} sinh\sqrt{s\tau_d}} \tag{13}$$

where $\eta = \frac{\mu_0 a}{\mu\Delta}$ for parallel plates and $2a$ is the plate separation; $\eta = \frac{\mu_0 a}{2\mu\Delta}$ for a cylindrical shell and *a* is the radius of the cylinder; $\eta = \frac{\mu_0 a}{3\mu\Delta}$ for a spherical shell and a is the radius of the sphere. Bedrosian and Lee generalized the definition of geometric factor η to (19) to be given later.

A plane wave incident on a single plate does not simulate how the magnetic flux leaves the enclosure and cannot be used to model the enclosure diffusion for a nearby lightning field. However, for a line source next to the enclosure wall the magnetic flux can cross the enclosure wall on one side and leave the enclosure on the other side and therefore a single plate is used to treat a direct strike to an insulated cable adjacent to the enclosure.

There is evidence that the single plate model for direct strike is quite adequate for describing an arbitrary enclosure. Merewether [9] calculated the maximum HDOT inside a ½-in-thick- 2-D cylindrical shell with a one-percentile lightning return stroke striking an adjacent insulated conductor using a current waveform of

$$I(t) = \hat{I}\,\frac{\left(\frac{t}{\tau_1}\right)^m}{1+\left(\frac{t}{\tau_1}\right)^m} e^{-\frac{t}{\tau_2}} \qquad (14)$$

where parameters *m,* $\hat{I}$ *,* τ_1 *and* τ_2 were adjusted to match a given peak amplitude, peak rate , and fall time ($m = 10$ seems to give the best fit to measured data). Frequency-domain solutions were transformed using *65,536-*, or *131,072*-point Fast Fourier Transforms (FFTs) and the HDOT so obtained agrees with the single plate model calculation to approximately 2%.

Numerical Results

This section summarizes all useful parameters calculated by (A) providing complete waveforms for limiting cases ($\alpha\tau_d = 0;\ \alpha\tau_d = \infty$), (B) describing simple fit functions for peaks for these parameters that were discussed in the executive summary in tables and (C) summarizing peak responses of all identified parameters for representative values of $\alpha\tau_d$. The enclosure interior parameters are:

- H and HDOT for nearby lightning,
- H and HDOT at $\rho = \Delta$ and $\rho = 10\Delta$ for direct strike lightning ($\mu = \mu_0$ and $\mu = 10\mu_0$),
- Voltage and current bounds for direct strike lightning.

Waveforms for Fundamental Solutions

Figure 5 gives the nearby lightning H inside the enclosure for an impulse that corresponds to $\alpha\tau_d = \infty$, or can be used as HDOT for a unit step that corresponds to $\alpha\tau_d = 0$.

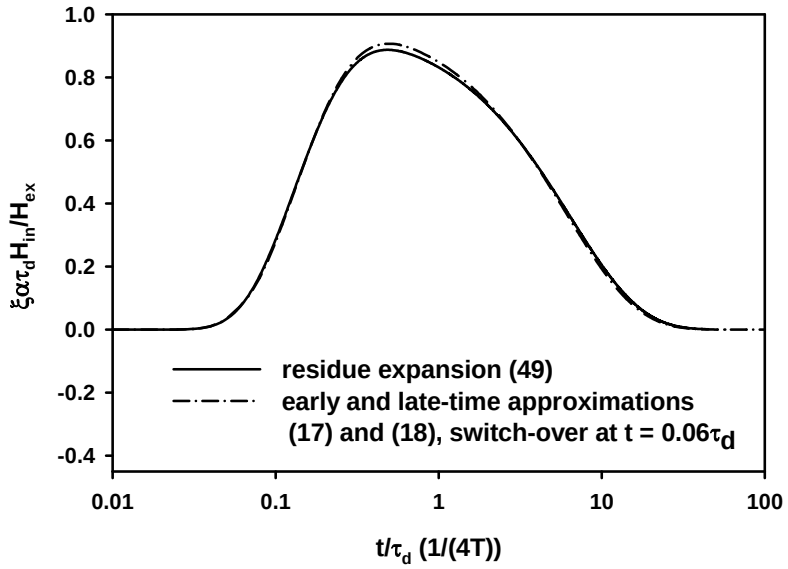

Figure 5. Normalized H for an impulse is shown with normalized time. This can be used for HDOT for a unit step. The pulse width of the interior field determines the procedure for obtaining the actual penetrating field. Relevant parameters are $t_p = 0.47\tau_d$, $t_{50} = 0.13\tau_d$ and $4.64\tau_d$. (17) is compared to (49) and found to be 2.72% too high. $\xi = 6.088$ is used.

Figure 5 shows the pulse width of the impulse response H as approximately $4.5\tau_d$. Figure 6 on the other hand shows the pulse width of the HDOT for an impulse ($\alpha\tau_d = \infty$) as approximately $0.13\tau_d$. HDOT for a unit step has a wide pulse and thus is dominated by low frequencies, while HDOT for an impulse has a narrow pulse width and is thus dominated by high frequencies. Most figures are computed with $\xi = 6.088$. Figure 7 compares H for two different values of ξ. Figure 8 compares HDOT for three different values of ξ.

The unit step responses for two values of ξ (Figure 9) obtained by integrating H shown in Figure 5 approaches the static limit. Figure 10 shows a corresponding case for direct strikes.

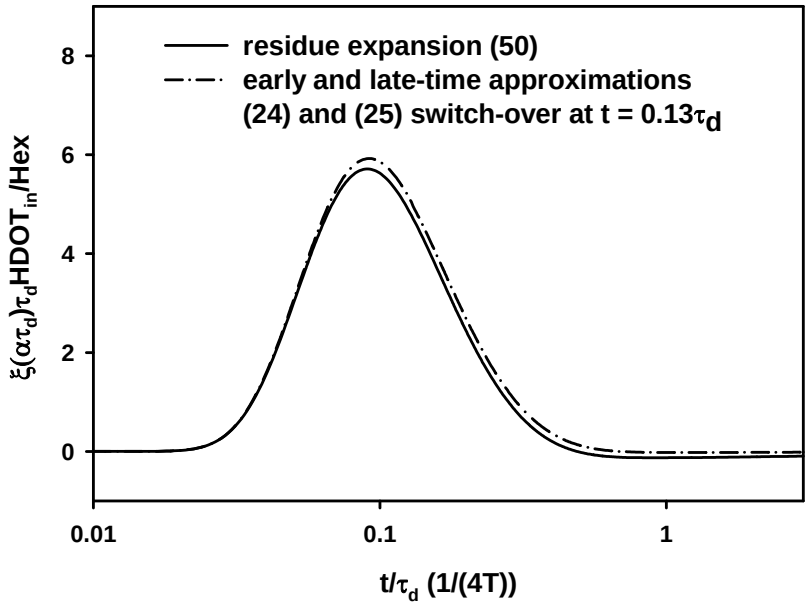

Figure 6. Normalized HDOT for an impulse is shown with normalized time. The pulse width of the interior field determines the procedure for obtaining the actual penetrating field. Relevant parameters are $t_p = 0.092\tau_d$, $t_{50} = 0.049\tau_d$ and $0.18\tau_d$. (24) is compared to (50) and found to give 3.68% too high in peak. $\xi = 6.088$ is used.

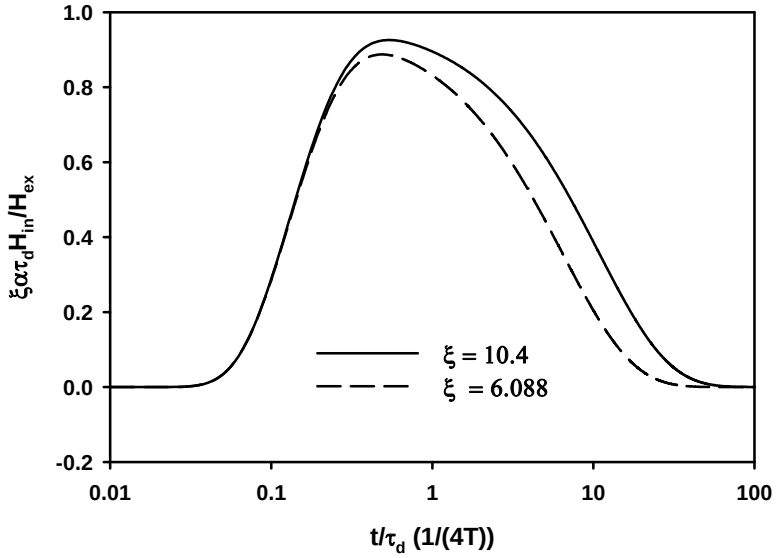

Figure 7. Normalized H for an impulse with two different ξ's. The peak for ξ=10.4 is 0.926 occurring at 0.5392; the peak for ξ=6.088 is 0.8876 occurring at 0.49.

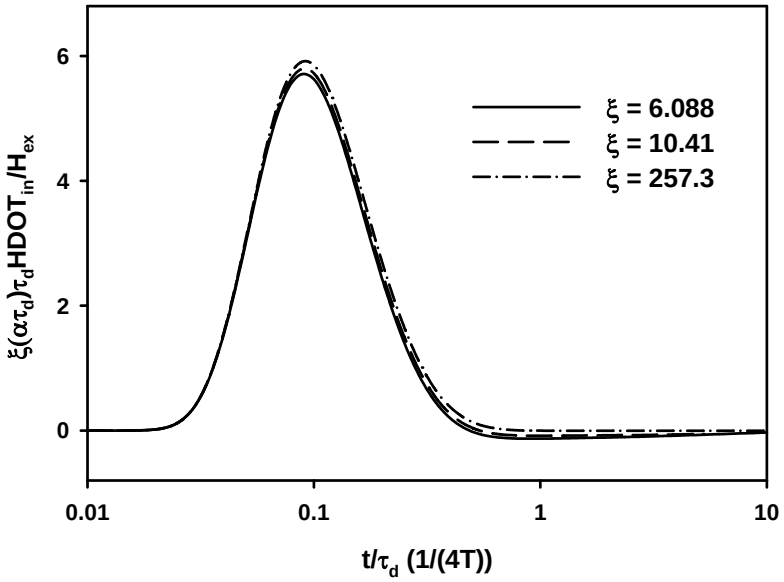

Figure 8. HDOT Comparisons for different ξ: HDOT peak 5.7118 at 0.09 for ξ = 6.088, 5.7973 at 0.0912 for ξ = 10.41 and 5.9179 at 0.092 for ξ = 257.3.

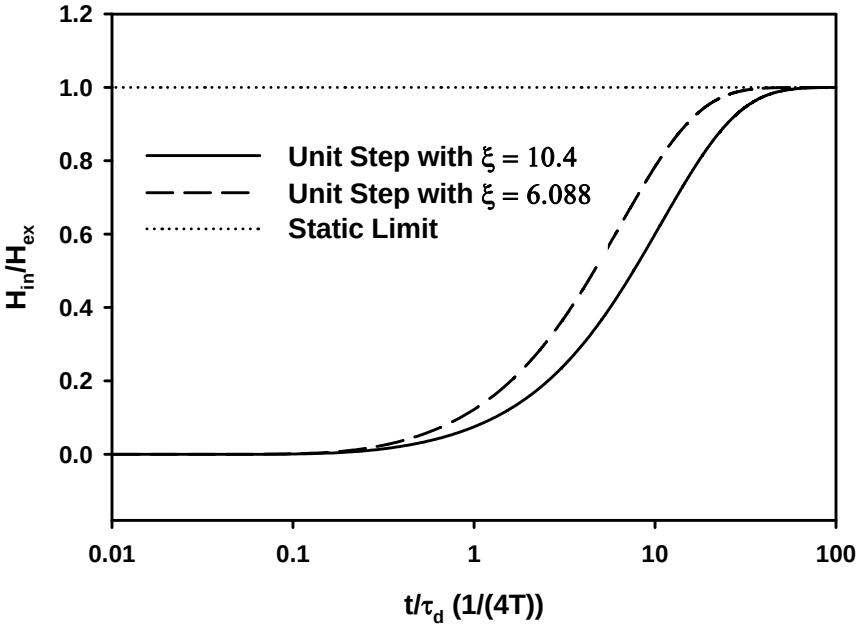

Figure 9. Normalized H for a unit step is shown with normalized time. The enclosure for large ξ appears to rise slower to the steady state in the normalized time, but because ξ is inversely proportional to Δ and τ_d is inversely proportional to the square of Δ it actually rises a lot faster.

Direct strike pulse widths for impulse responses H and HDOT at $\rho = 10\,\Delta$ shown in Figure 11 and Figure 12 appear to be approximately the same as those for the nearby fields shown in

Figure 5 and Figure 6 and thus they approach a plane field limit. Note that for $\rho = \Delta$, the pulse width of H is approximately $0.32\tau_d$ and the pulse width of HDOT is approximately $0.06\tau_d$.

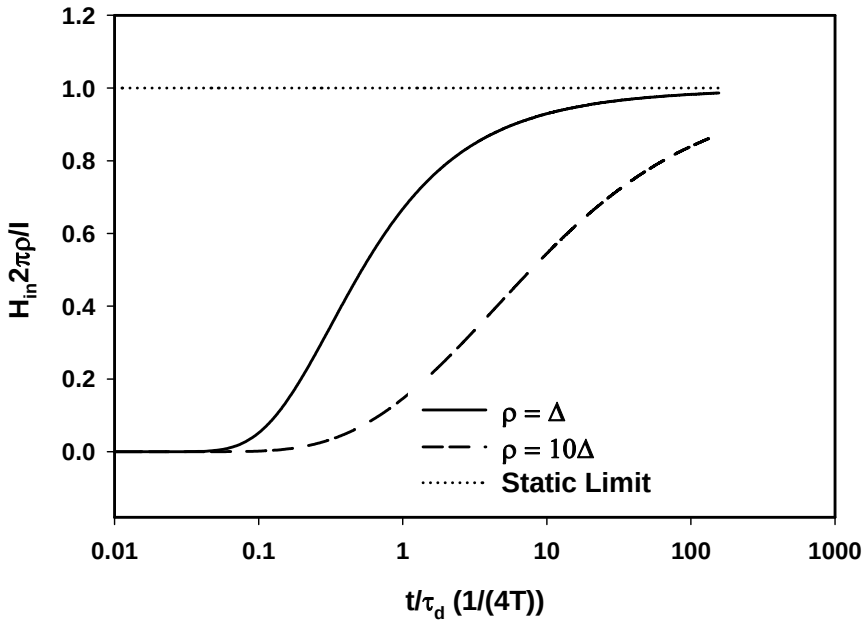

Figure 10. Normalized Unit Step H Responses for Direct Lightning Strikes ($\mu = \mu_0$).

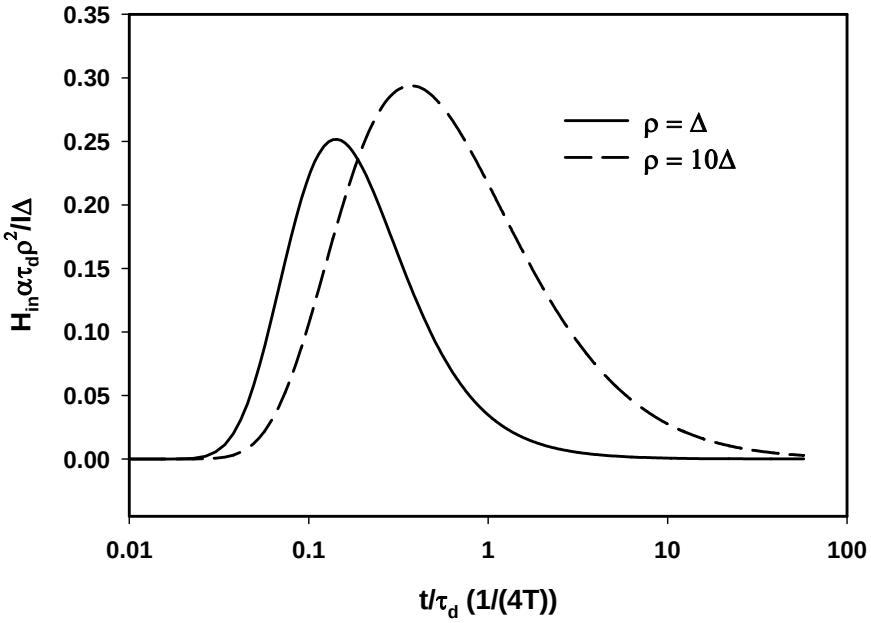

Figure 11. Normalized Impulse H Responses for Direct Lightning Strikes($\mu = \mu_0$). For $\rho = \Delta$, relevant parameters are $t_p = 0.14\tau_d$, $t_{50} = 0.065\tau_d$ and $0.39\tau_d$. For $\rho = 10\Delta$, relevant parameters are $t_p = 0.36\tau_d$, $t_{50} = 0.12\tau_d$ and $1.8\tau_d$.

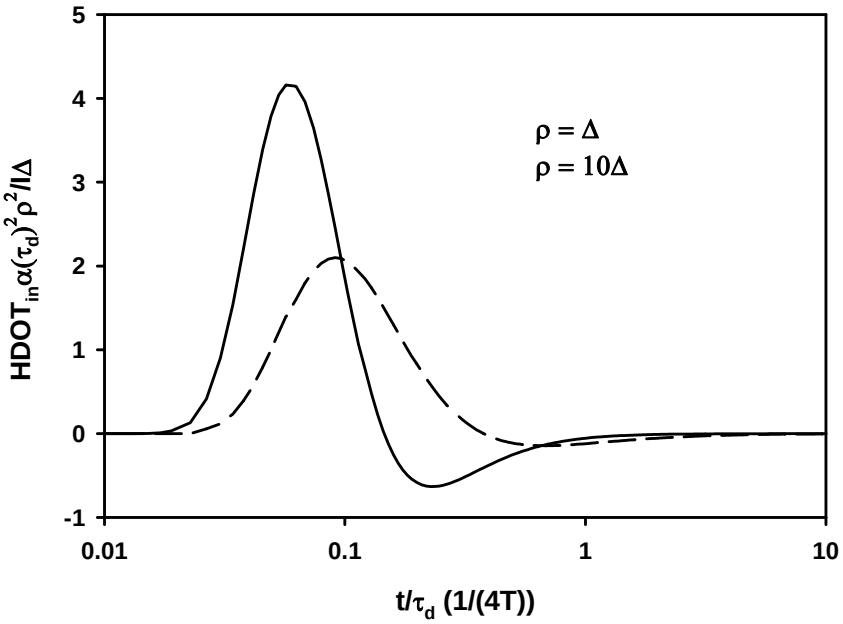

Figure 12. Normalized Impulse HDOT Responses for Direct Lightning Strikes $(\mu = \mu_0)$. For $\rho = \Delta$, relevant parameters are $t_p = 0.06\tau_d$, $t_{50} = 0.037\tau_d$ and $0.097\tau_d$. For $\rho = 10\Delta$, relevant parameters are $t_p = 0.09\tau_d$, $t_{50} = 0.05\tau_d$ and $0.18\tau_d$.

Since the magnetic permeability of the enclosure wall enters into the nearby enclosure solutions through diffusion time τ_d only, the nearby result is applicable to moderate values of $\nu = \mu/\mu_0$. The solution for direct strikes given later is a function the magnetic permeability. We present direct lightning fundamental solutions for $\mu = 10\mu_0$. Figure 13 gives the comparison of the static limit derived in [2] as $\frac{1}{2\pi\Delta}\frac{2\nu ln(\nu)}{\nu^2-1}$ and magnetic fields at different distances obtained by the early-time integral . H and HDOT as a function of ρ for $\mu = 10\mu_0$ somewhat differ from those for $\mu = \mu_0$. For $\mu = \mu_0$, they vary as $\frac{1}{\rho^2}$; for $\mu = 10\mu_0$, they are shown in Figure 14 and Figure 15. Again, these responses are the limiting cases of H or HDOT responses in the thin and thick limits.

For direct strikes, the spatial dependence of the HDOT waveform inside the enclosure is unknown and the induced voltage cannot be obtained accurately. Fortunately, the voltage bounds for an impulse and a unit step on a one-turn optimally coupled loop shown in Figure 2 can be calculated. Their waveforms are shown in Figure 16 and Figure 17. Figure 17 can also be used for the current bound on a short-circuit one-turn optimally coupled loop for an impulse. The voltage bound peak for an impulse (Figure 16) occurs at a time closer to the peak HDOT arrival time at $\rho = \Delta$ than that at $\rho = 10\Delta$ (Figure 12). The voltage bound peak for a unit step (Figure 17) occurs at a time closer to the peak HDOT arrival time at $\rho = \Delta$ than that at $\rho = 10\Delta$ (Figure 11).

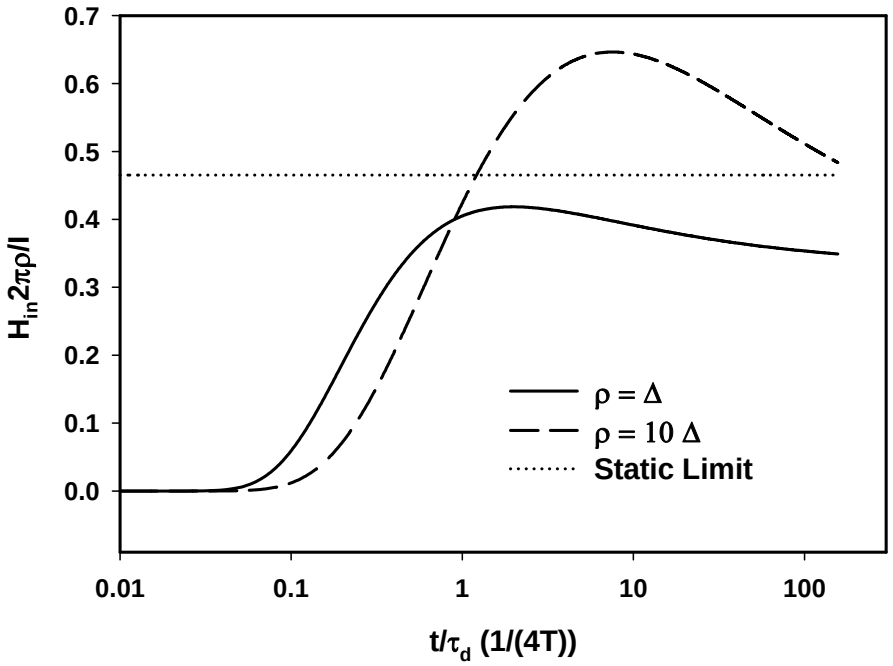

Figure 13. Unit step responses for $\rho = \Delta$ and $\rho = 10\Delta$ are compared to the static limit obtained previously in [2] $(\mu = 10\mu_0)$. The deviation from static limit is caused by the inaccuracy of the early-time integral.

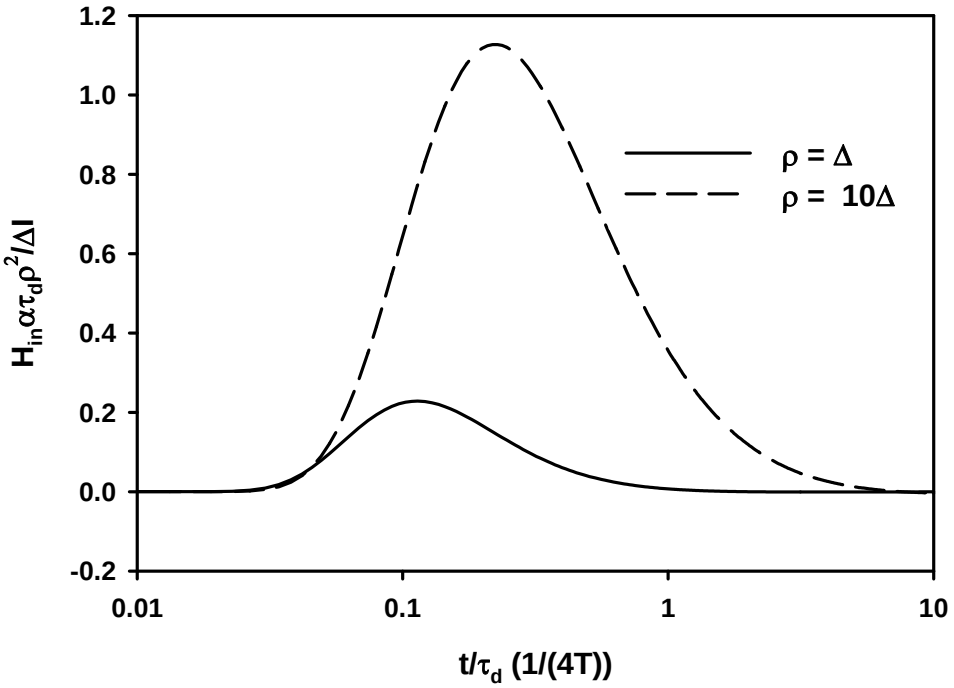

Figure 14. Normalized Impulse H Responses for Direct Lightning Strikes$(\mu = 10\mu_0)$. It appears that the magnetic field varies as $\frac{1}{\rho}$ rather than $\frac{1}{\rho^2}$.

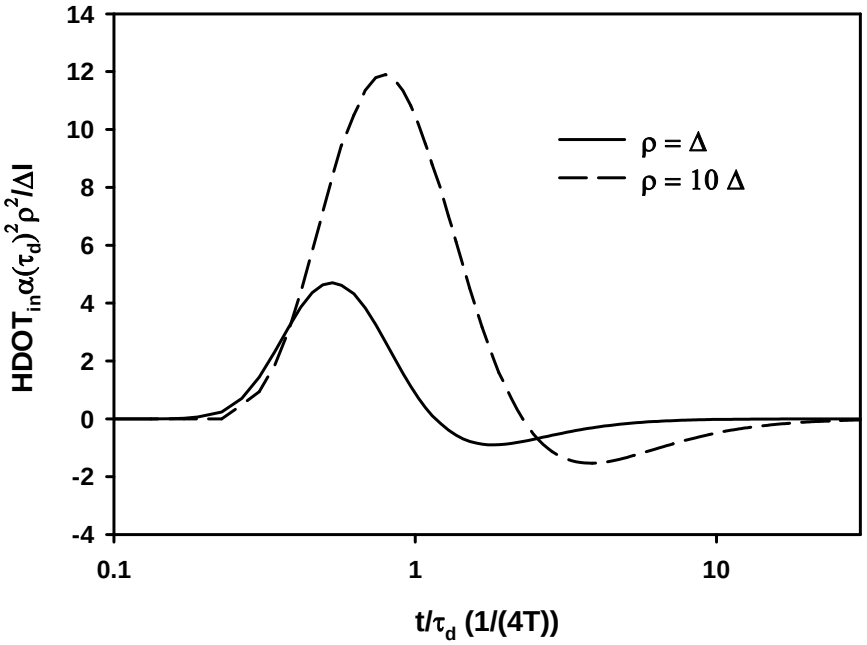

Figure 15. Normalized Impulse H Responses for Direct Lightning Strikes $(\mu = 10\ \mu_0)$. It appears that the magnetic field varies as $\frac{1}{\rho^{3/2}}$.

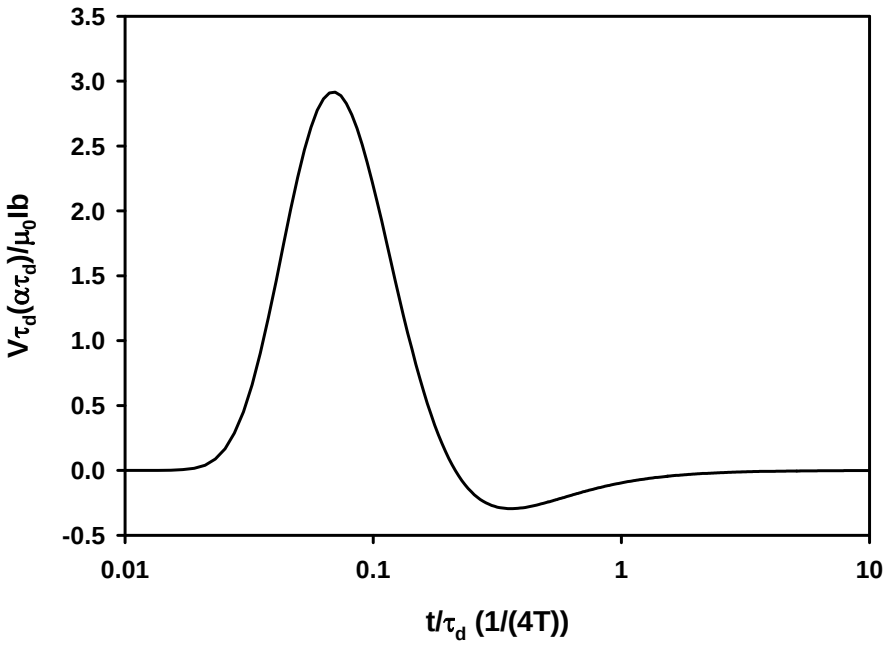

Figure 16. Voltage bound for an optimally coupled loop under impulse excitations ($\mu = \mu_0$). The peak value is *2.918* occurring at *0.069*.

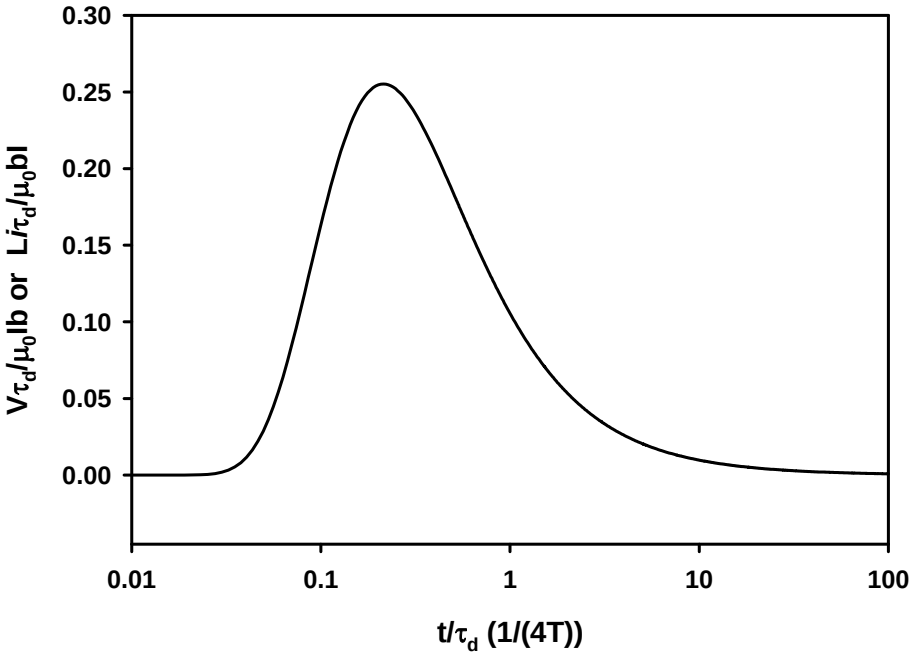

Figure 17. Voltage bound for an optimally coupled loop under unit step excitations ($\mu = \mu_0$). Alternatively, this can be used for current bounds for an impulse excitation. The peak value is *0.2552* occurring at *0.215*.

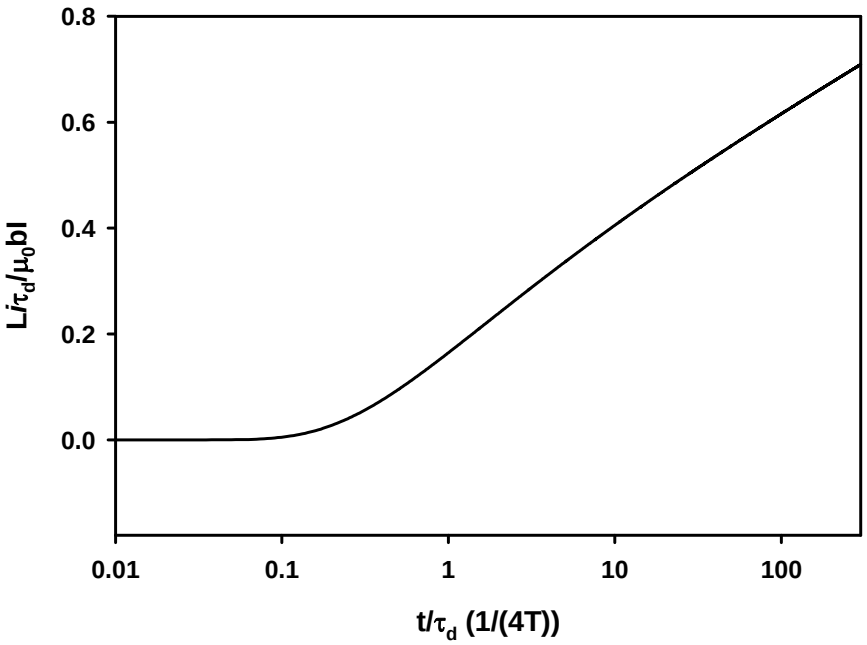

Figure 18. Current bound for an optimally coupled loop under a unit step excitation ($\mu = \mu_0$). As $t/\tau_d \rightarrow \infty$, the vertical value approaches *2.862*.

Figure 18 for current bounds for a unit step ($\mu = \mu_0$) that is based on the total flux path through the loop as the upper limit extends to infinity reflects the limitation of the model. Since the static magnetic field varies as $\frac{1}{\rho}$, the flux should diverge. In practice, a truncation of the upper limit to the actual enclosure dimension should give a more realistic number. Thus, H given in Figure 10 ($\mu = \mu_0$) and Figure 13 ($\mu = 10\,\mu_0$) should be used for calculating the total magnetic flux linking, and the current bound for, the loop.

Figure 19 and Figure 20 give corresponding voltage bounds for $\mu = 10\,\mu_0$; the comments given for Figure 16 and Figure 17 ($\mu = \mu_0$) are applicable to this case. Figure 21 is also limited by similar reasoning to that given for Figure 18.

We have completed discussions for the relevant waveforms for the limiting cases and will continue by discussing simple fit functions of decaying exponential peaks as discussed in the executive summary.

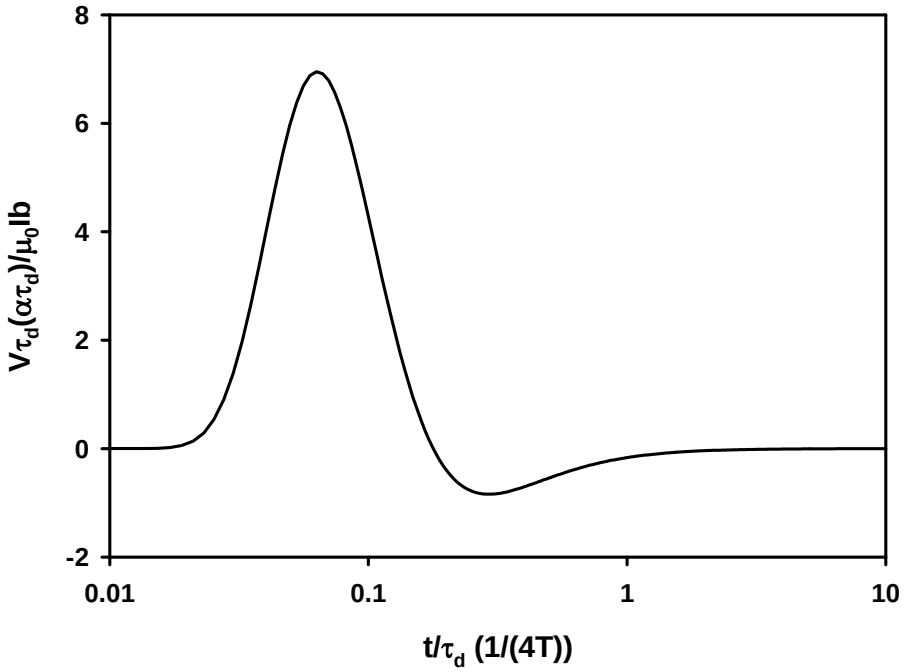

Figure 19. Voltage bound for an optimally coupled loop under an impulse excitation (μ = 10 μ_0). The peak value is *6.946* occurring at *0.0625*.

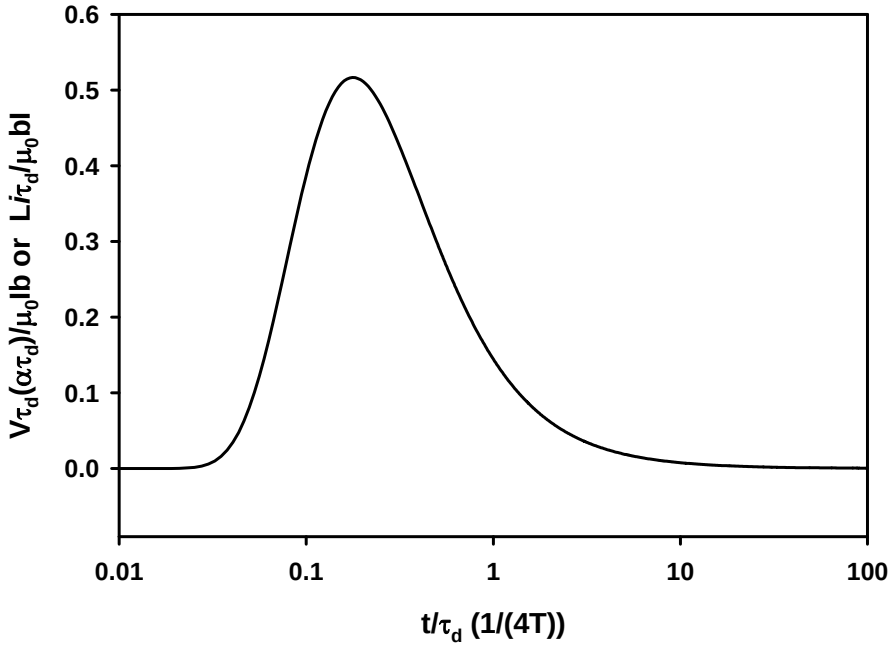

Figure 20. Voltage bound for an optimally coupled loop under a unit step excitation ($\mu = 10\mu_0$). Alternatively, this can be used for current bounds for an impulse excitation. The peak value is *0.5167* occurring at *0.1764*.

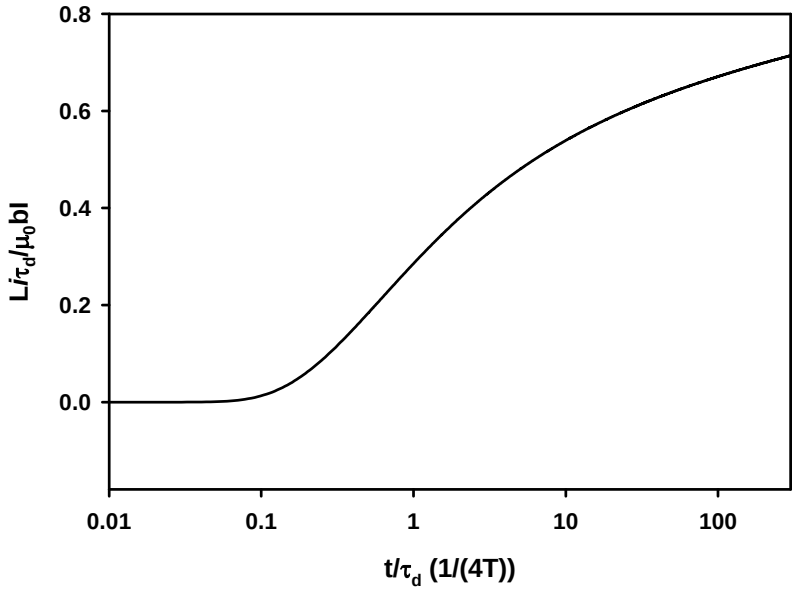

Figure 21. Current bound for an optimally coupled loop under a unit step excitation ($\mu = 10\mu_0$). As $t/\tau_d \rightarrow \infty$, the vertical value approaches *1.458*.

Fit Functions for Peak Responses

Let us summarize the fit functions (2), (3) and (5) as

$$g^e = \frac{1}{\frac{\alpha\tau_d}{l}+\frac{1}{m}}\ ,\ g^i = \frac{l}{\alpha\tau_d}\ ,\ g^s = m \tag{15}$$

where the subscript "e" for the decaying exponential, "*i*" for impulse and "s" for unit step and its parameter given in Table 3. "*b*" is the length of the loop in the direction of the lightning current as defined in Figure 2.

Table 3. Parameters for Approximate Formula (15) for Peak HDOT and Voltage Bounds.

Environment	Physical Quantity	Field point	Permeability	Approximation Parameters		
				g	l	m
Nearby Lightning	HDOT	Everywhere inside enclosure	$\mu \le 10\mu_0$	$\frac{HDOT_{in}\,\xi\tau_d}{H_{ex}}$	5.7118 (*ξ=6.088*)	0.8876 (*ξ=6.088*)
Direct Lightning	HDOT	$\rho = \Delta$	$\mu = \mu_0$	$\frac{HDOT_{in}\tau_d\Delta}{I}$	4.1608	0.2516
Direct Lightning	HDOT	$\rho = 10\Delta$	$\mu = \mu_0$	$\frac{HDOT_{in}\rho^2\tau_d}{I\Delta}$	2.0997	0.2938
Direct Lightning	HDOT	$\rho = \Delta$	$\mu = 10\mu_0$	$\frac{HDOT_{in}\tau_d\Delta}{I}$	4.7065	0.2281
Direct Lightning	HDOT	$\rho = 10\Delta$	$\mu = 10\mu_0$	$\frac{HDOT_{in}\rho^2\tau_d}{I\Delta}$	11.8978	1.1272
Direct Lightning	Voltage Bound	Single-Turn Loop	$\mu = \mu_0$	$\frac{V\tau_d}{\mu_0 Ib}$	2.916	0.2552
Direct Lightning	Voltage Bound	Single-Turn Loop	$\mu = 10\mu_0$	$\frac{V\tau_d}{\mu_0 Ib}$	6.949	0.5167

The 1st, 2nd and 6th row of data in Table 3 correspond to fit functions (2), (3) and (5), respectively. In Table 3, the numerical values for l are obtained from peaks of Figure 5, Figure 11, Figure 14, Figure 17 and Figure 20, and for m are from peaks of Figure 6, Figure 12, Figure 15, Figure 16 and Figure 19, respectively.

Figure 22 as summarized in the 3rd row of data ($\rho = 10\Delta$) in Table 3 is relevant to the coupling loop located away from the enclosure wall. The intersection of the unit step and the impulse peaks occurs at $\alpha\tau_d = 7.15$, which is not very different from the nearby lightning value shown in Figure 1 but very different from the direct strike value for $\rho = \Delta$ (Figure 3). The closeness of these values in these two cases is closely related to the pulse widths of their fundamental solutions (Figure 6 and Figure 12). Figure 23 and Figure 24 or Row 4 and 5 of data in Table 3 give the corresponding comparison for $\mu = 10\mu_0$ and are applicable to magnetic steel with low permeability. Figure 25 gives the peak voltage bounds for $\mu = 10\mu_0$.

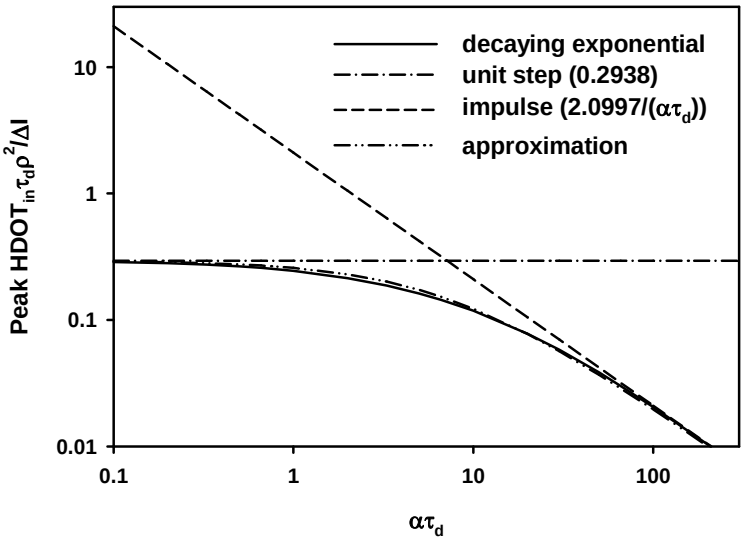

Figure 22. HDOT peak at $\rho = 10\Delta$ for decaying exponential and an approximation are compared to those of the unit step and the impulse excitations. The intersection for the unit step and impulse peaks occurs at $\alpha\tau_d = 7.1467$, which is 11% greater than that for the nearby lightning case shown in Figure 1. The enclosure wall has $\mu = \mu_0$.

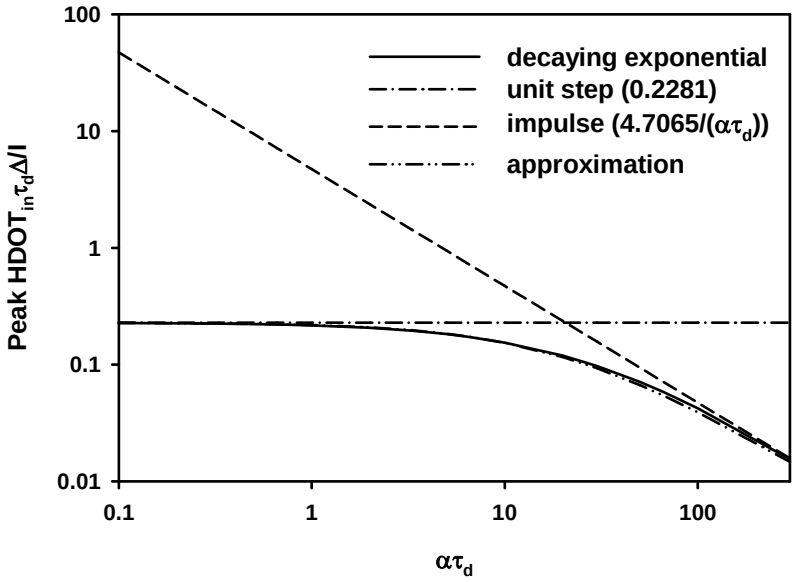

Figure 23. HDOT peak ($\rho = \Delta$) for the decaying exponential and an approximation are compared to the unit step and the impulse responses. This value determines the maximum voltage induced on an optimally coupled loop. The intersection of unit step and impulse peak occurs at $\alpha\tau_d = 20.6335$. The enclosure wall has $\mu = 10\mu_0$.

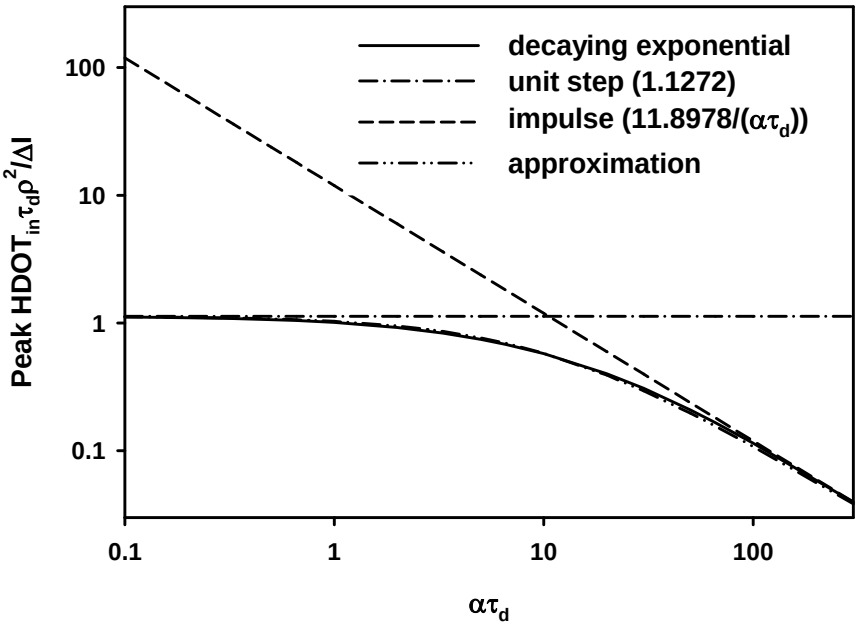

Figure 24. HDOT peak at $\rho = 10\Delta$ for decaying exponential and an approximation are compared to those of the unit step and the impulse excitations. The intersection of unit step and impulse peak occurs at $\alpha\tau_d = 10.5552$. The enclosure wall has $\mu = 10\mu_0$.

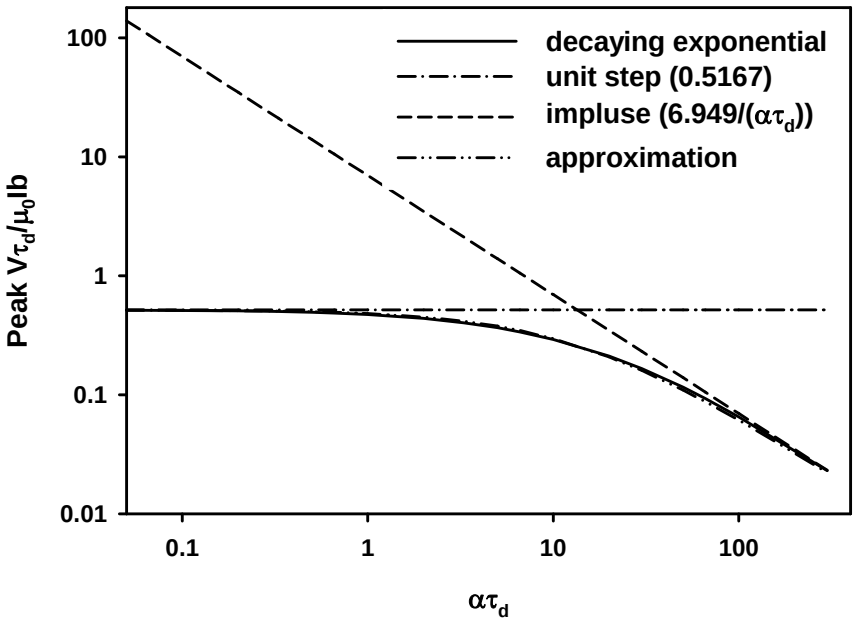

Figure 25. Peak voltage bounds for direct strikes. The intersection of unit step and impulse peak occurs at $\alpha\tau_d = 13.4488$. ($\mu = 10\,\mu_0$).

The fit function for peak H is

$$h^e = \frac{1}{\frac{\alpha\tau_d}{m}+\frac{1}{n}}\ ,\quad h^i = \frac{m}{\alpha\tau_d}\ ,\quad h^s = n \tag{16}$$

where parameters are defined in Table 4. Parameters in the table are: "*i* " is the current , "*L"* is the inductance of a single-turn loop and "*b*" is the length of loop along the lightning current (Figure 2). Here we assume the inductance is dominating when calculating current bounds, however, the resistance can be dominating and voltage bounds are more relevant in practical situations.

Table 4. Parameters for Approximate Formula (16) for Peak H and Current Bounds. "*i*" is the short-circuit current for the optimum coupled loop with length *b along the lightning current*.

Environment	Physical Quantity	Field point	Permeability	Approximation Parameters		
				h	m	n
Nearby Lightning	H	Everywhere inside enclosure	$\mu \le 10\mu_0$	$\frac{H_{in}\xi}{H_{ex}}$	0.8876 (*ξ=6.088*)	6.088 (*ξ=6.088*)
Direct Lightning	H	$\rho = \Delta$	$\mu = \mu_0$	$\frac{H_{in}\Delta}{I}$	0.2516	0.1592
Direct Lightning	H	$\rho = 10\Delta$	$\mu = \mu_0$	$\frac{H_{in}\rho^2}{I\Delta}$	0.2938	1.592
Direct Lightning	H	$\rho = \Delta$	$\mu = 10\mu_0$	$\frac{H_{in}\Delta}{I}$	0.2281	0.0666
Direct Lightning	H	$\rho = 10\Delta$	$\mu = 10\mu_0$	$\frac{H_{in}\rho^2}{I\Delta}$	1.1272	1.0288
Direct Lightning	Current Bound	Single-Turn Loop	$\mu = \mu_0$	$\frac{Li}{\mu_0 Ib}$	0.2552	NA
Direct Lightning	Current Bound	Single-Turn Loop	$\mu = 10\mu_0$	$\frac{Li}{\mu_0 Ib}$	0.5167	NA

The fit function for current bounds is not given because the total magnetic flux linking the short-circuit loop is large for the unit step compared to that for the impulse.

Comparisons of enclosure interior peak H for decaying exponential numerical value, unit step, impulse and approximation given in Table 4 are given in Figure 26 (nearby), Figure 27 (direct strike $\rho = \Delta\ \ \mu = \mu_0$), Figure 28 (direct strike $\rho = 10\Delta\ \ \mu = \mu_0$), Figure 29 (direct strike $\rho = \Delta$ $\mu = 10\mu_0$),Figure 30 (direct strike $\rho = 10\Delta\ \ \mu = 10\mu_0$).

There is an important difference between the accuracy of the fit function presented in Table 3 for HDOT and that presented in Table 4 for H: Both HDOT for the unit step and HDOT for the impulse are pulses and the resulting approximation has relatively small errors. The unit step H

is not a pulse, and thus the governing parameter $\alpha\tau_d$ has to be extremely small before approaching the unit step response and the fit function incurs a large error in that limit. Nevertheless, we include a description of the fit function.

As discussed before, because the unit step current bounds can be obtained by other consideration, only impulse model and numerical decaying exponential peaks are given for current bounds in Figure 31 and Figure 32.

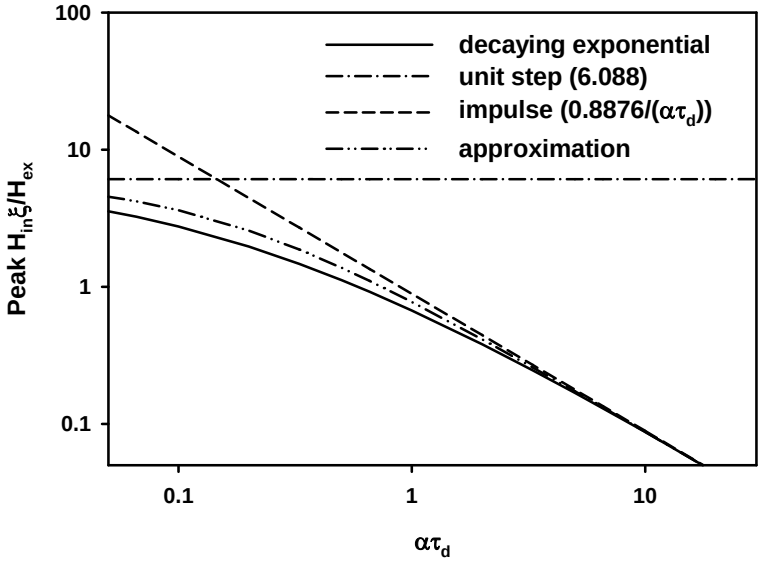

Figure 26. Peak H for nearby lightning ($\mu = \mu_0$). The unit step and impulse intersection is at $\alpha\tau_d = 0.1458$. The unit step peak shown is 6.088 (the value of ξ).

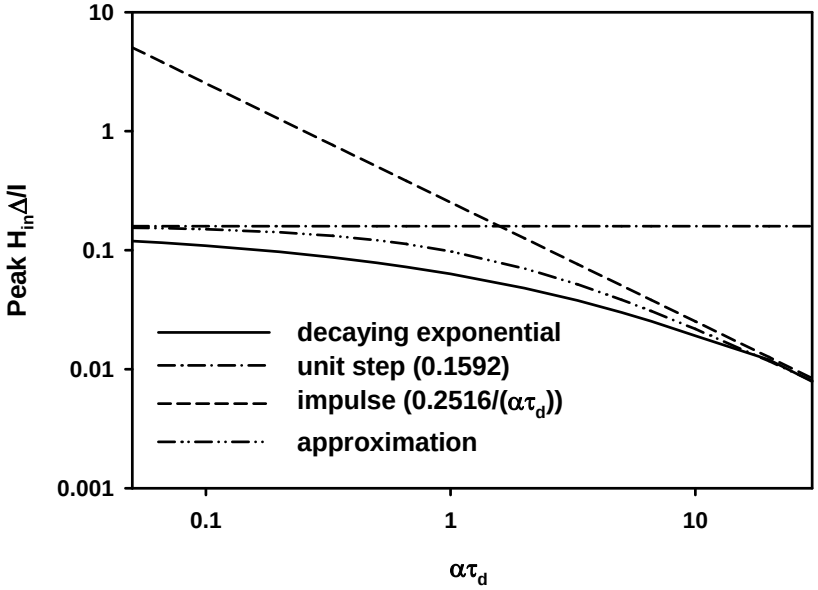

Figure 27. Peak H for direct strikes at $\rho = \Delta$. The intersection of unit step and impulse peak occurs at $\alpha\tau_d = 1.5804$. ($\mu = \mu_0$).

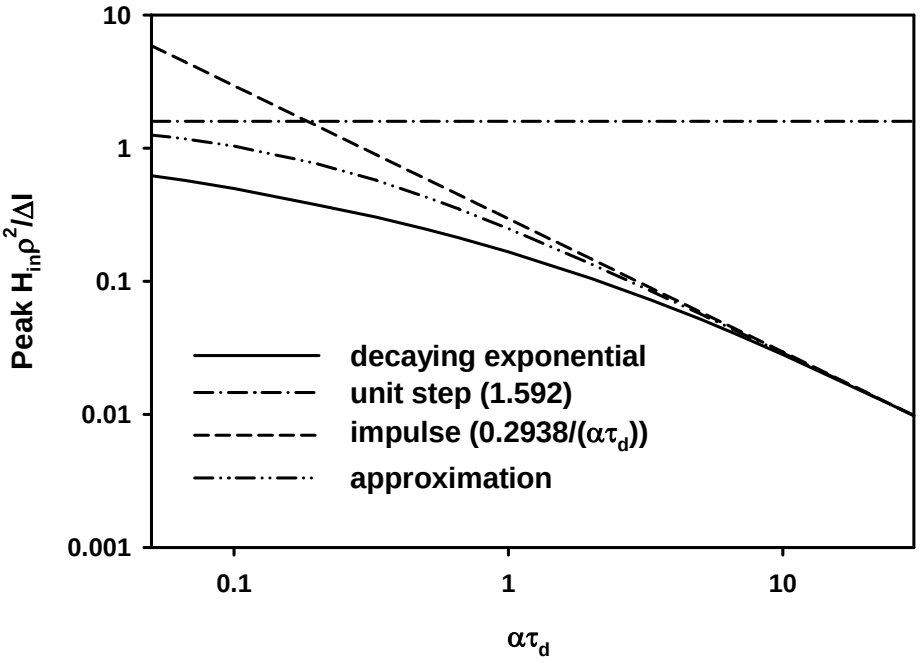

Figure 28. Peak H for direct strikes at $\rho = 10\Delta$. The intersection of unit step and impulse peak occurs at $\alpha\tau_d = 0.1845$. ($\mu = \mu_0$).

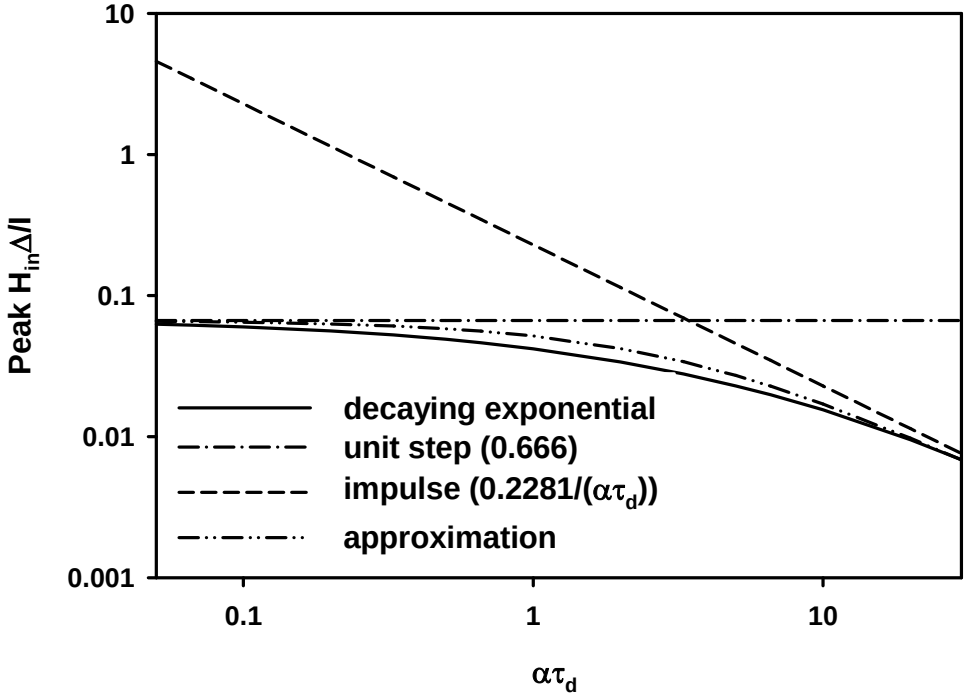

Figure 29. Peak H for direct strikes at $\rho = \Delta$. The intersection of unit step and impulse peak occurs at $\alpha\tau_d = 3.4249$. ($\mu = 10\mu_0$).

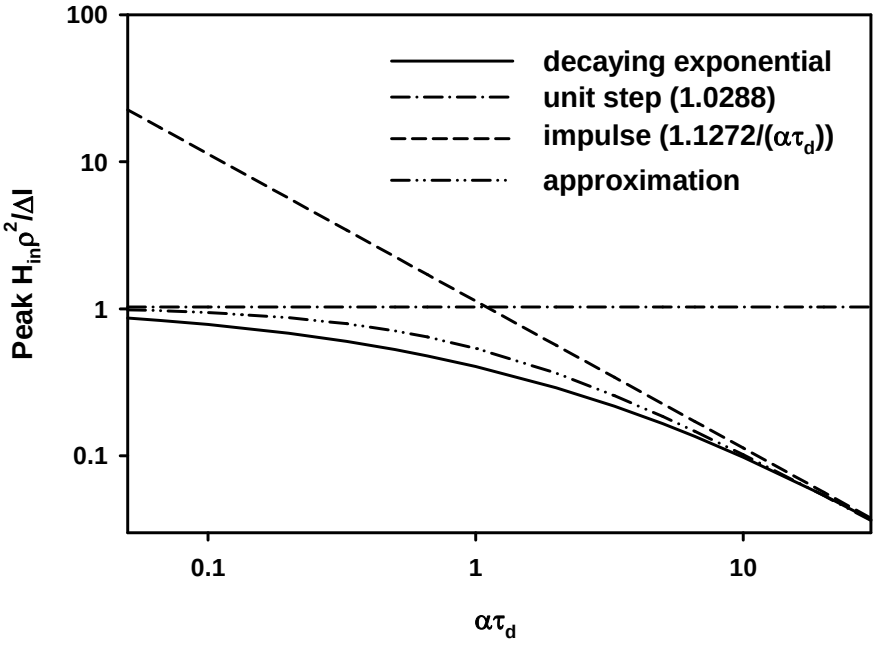

Figure 30. Peak H for direct strikes at $\rho = 10\Delta$. The intersection of unit step and impulse peak occurs at $\alpha\tau_d = 1.0956$. ($\mu = 10\,\mu_0$).

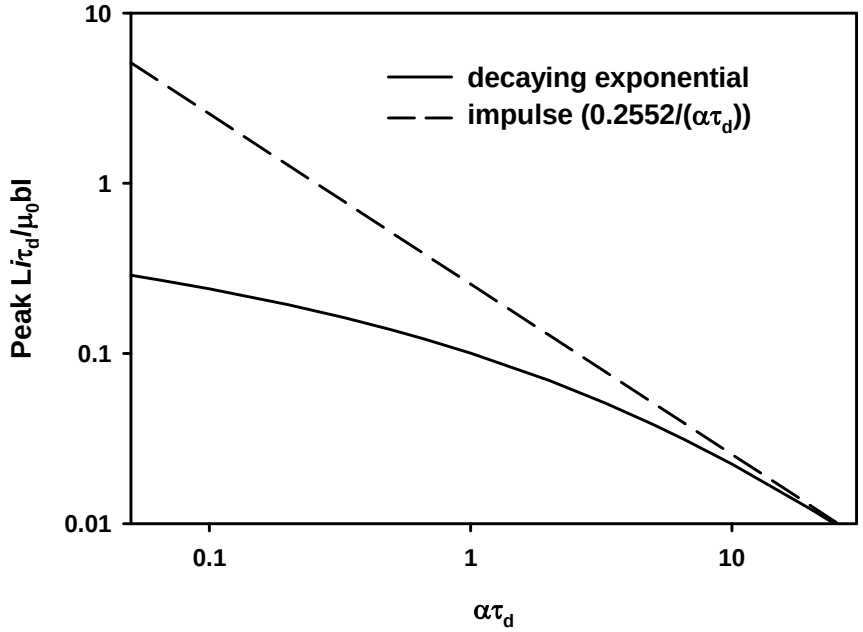

Figure 31. Current bound for a short-circuit loop shown in Figure 2 ($\mu = \mu_0$). The unit step current bound is not given because more accurate limit can be obtained from the actual loop geometry.

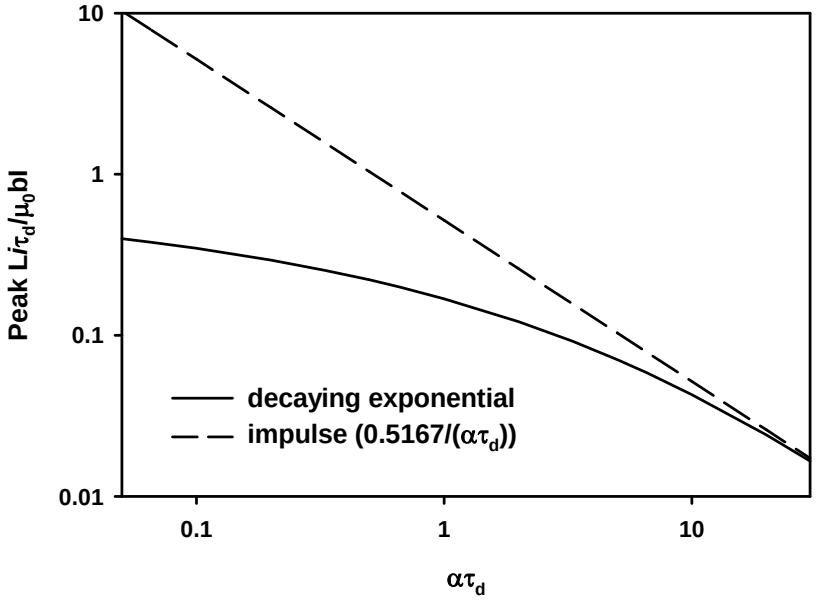

Figure 32. Current bound for a short-circuit loop shown in Figure 2 ($\mu = 10\mu_0$). The unit step current bound is not given because more accurate limit can be obtained from the actual loop geometry.

Comparison of Decaying Exponential Peaks with the Fit Function

In order to gain accuracy when using the peak response given in this report, we include a comparison of the numerical result and fit function for representative value of the governing parameter. Table 5 provides the actual numerical value followed by the value from the fit function for various HDOT and voltage bounds.

The loop voltage of the EMP example given in the executive summary was estimated to be *12.2 milliv*olts using the fit function (2). Notice the discrepancy between the actual numerical value and the approximation for $\alpha\tau_d = 30$ is *2%* higher for the actual numerical value. This gives the more accurate loop voltage as *12.4 millivolts*. Using numbers given in caption of Figure 8 accounting for ξ of *257.3* the loop voltage is *12.8 millivolts*.

The loop voltage of the lightning problem for ½-in enclosure is estimated from (5) to be *8.57 volts*. The discrepancy between the numerical value and the approximation for a voltage bound with $\alpha\tau_d = 20$ is *1.6%* higher for the numerical value, resulting in a loop voltage of *8.69 volts*.

Table 6 compares actual numerical evaluation of H with the approximate fit functions and gives the actual current bounds for representative governing parameters. As discussed before, the errors incurred by the H fit functions are greater than those for HDOT.

Table 5. Comparison of HDOT and Voltage Actual Peaks with Approximate Formula (15). The Actual Peak is followed by the Approximation indicated by (A) in Each data Entry.

$\alpha\tau_d$ value	Nearby HDOT Peak (ξ=6.088)	Direct HDOT Peak $\rho = 10\Delta$, $\mu = \mu_0$	Direct HDOT Peak $\rho = \Delta$, $\mu = \mu_0$	Direct HDOT Peak $\rho = \Delta$, $\mu = 10\mu_0$	Direct HDOT Peak $\rho = 10\Delta$, $\mu = 10\mu_0$	Direct Voltage Bound $\mu = \mu_0$	Direct Voltage Bound $\mu = 10\mu_0$
0.05	0.8730 0.8808 (A)	0.2507 0.2508 (A)	0.2904 0.2918 (A)	0.2275 0.2275 (A)	1.1208 1.1219 (A)	0.2537 0.2541 (A)	0.5142 0.5148 (A)
0.066	0.8688 0.8786 (A)	0.2504 0.2506 (A)	0.2894 0.2911 (A)	0.2273 0.2274 (A)	1.1182 1.1202 (A)	0.2532 0.2537 (A)	0.5134 0.5142 (A)
0.1	0.8602 0.874 (A)	0.2498 0.2501 (A)	0.2871 0.2897 (A)	0.2269 0.2270 (A)	1.1138 1.1166 (A)	0.2522 0.253 (A)	0.5117 0.5129 (A)
0.2	0.8371 0.8608 (A)	0.2480 0.2486 (A)	0.2811 0.2858 (A)	0.2257 0.2259 (A)	1.1005 1.1062 (A)	0.2492 0.2508 (A)	0.5069 0.5091 (A)
0.33	0.8103 0.8443 (A)	0.2458 0.2467 (A)	0.2739 0.2808 (A)	0.2242 0.2245 (A)	1.0839 1.0930 (A)	0.2455 0.248 (A)	0.5009 0.5053 (A)
0.5	0.7805 0.8236 (A)	0.2430 0.2442 (A)	0.2654 0.2746 (A)	0.2221 0.2227 (A)	1.0636 1.0762 (A)	0.2410 0.2445 (A)	0.4933 0.4982 (A)
0.66	0.7562 0.805 (A)	0.2403 0.2419 (A)	0.2581 0.269 (A)	0.2203 0.2210 (A)	1.0458 1.0609 (A)	0.2371 0.2413 (A)	0.4865 0.4925 (A)
1	0.7111 0.7682 (A)	0.2351 0.2373 (A)	0.2446 0.2577 (A)	0.2166 0.2176 (A)	1.0097 1.0297 (A)	0.2292 0.2347 (A)	0.4730 0.4809 (A)
2	0.6155 0.6771 (A)	0.2214 0.2245 (A)	0.2144 0.2296 (A)	0.2066 0.2079 (A)	0.9220 0.9476 (A)	0.2099 0.2172 (A)	0.4389 0.4498 (A)
3.3	0.5325 0.5867 (A)	0.2064 0.2097 (A)	0.1871 0.201 (A)	0.1951 0.1966 (A)	0.8338 0.8587 (A)	0.1905 0.198 (A)	0.4033 0.4149 (A)
5	0.4575 0.4995 (A)	0.1902 0.1932 (A)	0.1620 0.1729 (A)	0.1824 0.1836 (A)	0.7448 0.7649 (A)	0.1710 0.1775 (A)	0.3664 0.3767 (A)
6.6	0.4061 0.4382 (A)	0.1776 0.1798 (A)	0.1444 0.1527 (A)	0.1722 0.1728 (A)	0.6794 0.6935 (A)	0.1565 0.1618 (A)	0.3382 0.3466 (A)
10	0.3304 0.3475 (A)	0.1563 0.1568 (A)	0.1183 0.1225 (A)	0.1542 0.1536 (A)	0.5751 0.5788 (A)	0.1334 0.1361 (A)	0.2922 0.2963 (A)
20	0.2157 0.2161 (A)	0.1167 0.1139 (A)	0.0780 0.0773 (A)	0.1190 0.1158 (A)	0.4001 0.3894 (A)	0.0941 0.0928 (A)	0.2112 0.2078 (A)
30	0.1603 0.1568 (A)	0.0934 0.0894 (A)	0.0583 0.0565 (A)	0.0972 0.0930 (A)	0.3073 0.2934 (A)	0.0729 0.0704 (A)	0.1660 0.1599 (A)

Table 6. Comparison of H and Current Actual Peaks with Approximate Formula (16). The Actual Peak is followed by the Approximation indicated by (A) in Each data Entry.

$\alpha\tau_d$ value	Nearby H Peak (ξ=6.088)	Direct H Peak $\rho = \Delta$, $\mu = \mu_0$	Direct H Peak $\rho = 10\Delta$, $\mu = \mu_0$	Direct H Peak $\rho = \Delta$, $\mu = 10\mu_0$	Direct H Peak $\rho = 10\Delta$, $\mu = 10\mu_0$	Direct Current Bound $\mu = \mu_0$	Direct Current Bound $\mu = 10\mu_0$
0.05	3.5566 4.5333 (A)	0.1191 0.1543 (A)	0.6210 1.2526 (A)	0.0626 0.0728 (A)	0.8642 0.9839 (A)	0.2879	0.3977
0.066	3.2370 4.1908 (A)	0.1153 0.1528 (A)	0.5710 1.1726 (A)	0.0617 0.0724 (A)	0.8344 0.9703 (A)	0.2684	0.3776
0.1	2.7487 3.6111 (A)	0.1088 0.1497 (A)	0.4970 1.0325 (A)	0.0600 0.0717 (A)	0.7829 0.9428 (A)	0.2396	0.3466
0.2	1.9653 2.5668 (A)	0.0967 0.1413 (A)	0.3740 0.764 (A)	0.0561 0.0695 (A)	0.6820 0.87 (A)	0.1934	0.2929
0.33	1.4678 1.8655	0.0869 0.1317 (A)	0.3030 0.571 (A)	0.0525 0.0668 (A)	0.5997 0.7907 (A)	0.1619	0.2534
0.5	1.1178 1.3744 (A)	0.0782 0.1209 (A)	0.2464 0.4292 (A)	0.0489 0.0637 (A)	0.5275 0.7064 (A)	0.1373	0.2209
0.66	0.9186 1.1015 (A)	0.0723 0.1123 (A)	0.2120 0.3479 (A)	0.0463 0.0609 (A)	0.4783 0.642 (A)	0.1219	0.1996
1	0.6721 0.7747 (A)	0.0631 0.0975 (A)	0.1661 0.248 (A)	0.0419 0.0559 (A)	0.4053 0.5379 (A)	0.1003	0.1687
2	0.3813 0.4136 (A)	0.0481 0.0703 (A)	0.1051 0.1345 (A)	0.0339 0.0449 (A)	0.2903 0.3641 (A)	0.0692	0.1215
3.3	0.2460 0.2576 (A)	0.0378 0.0516 (A)	0.0725 0.0843 (A)	0.0278 0.0357 (A)	0.2174 0.2564 (A)	0.0508	0.0919
5	0.1685 0.1725 (A)	0.0300 0.0382 (A)	0.0518 0.0567 (A)	0.0229 0.0282 (A)	0.1654 0.1849 (A)	0.0382	0.0707
6.6	0.1300 0.1316 (A)	0.0253 0.0308 (A)	0.0408 0.0433 (A)	0.0198 0.0236 (A)	0.1355 0.1465 (A)	0.0311	0.0584
10	0.0874 0.0875 (A)	0.0191 0.0217 (A)	0.0281 0.0288 (A)	0.0155 0.0174 (A)	0.0980 0.1016 (A)	0.0224	0.0429
20	0.0442 0.0441 (A)	0.0120 0.0117 (A)	0.0145 0.0146 (A)	9.5e-3 9.882e-3 (A)	0.0538 0.0534 (A)	0.0122	0.0241
30	0.0295 0.0294 (A)	7.89e-3 7.97e-3 (A)	9.8e-3 9.734e-3 (A)	6.847e-3 6.895e-3 (A)	0.0368 0.0362 (A)	8.336e-3	0.0166

General Diffusion Solutions for Enclosure

The diffusion time for the enclosure wall is discussed in Table 1. The diffusion time gives us an indication of the shielding effectiveness of the enclosure wall, however the peak and he waveform of actual penetrating responses are determined by the penetration parameter $\alpha\tau_d$ as discussed in the executive summary. This section discusses the enclosure interior H and HDOT from the unit step and impulse excitations for nearby as well as direct lightning. The nearby enclosure solution is more well-known and is used as an example for our discussion.

Nearby lightning responses for H and HDOT to an impulse existing in the literature are shown in Figure 5 and Figure 6.

In this case, for parallel planes, infinite cylinders, and spheres, the impulse magnetic field within the enclosure is independent of position and is given by [1]

$$H_{in}^{(1)} \approx \frac{2H_{ex}}{\sqrt{\pi}\xi\alpha\tau_d}\frac{1}{\sqrt{t/\tau_d}}e^{-\frac{\tau_d}{4t}},\ t/\tau_d \le 0.06^{\blacklozenge} \tag{17}$$

$$H_{in}^{(2)} \approx \frac{H_{ex}}{\xi\alpha\tau_d}\left[e^{-\frac{t}{\tau_d\xi}} - 2e^{-\frac{\pi^2 t}{\tau_d}} + 2e^{-\frac{4\pi^2 t}{\tau_d}}\right],\ t/\tau_d > 0.06 \tag{18}$$

where ξ is the previously discussed geometrical parameter for the enclosure given by

$$\xi = \frac{\mu_0}{\mu}\frac{V}{S\Delta}. \tag{19}$$

That (17) and (18) agrees within 1% at $t = 0.06\,\tau_d$ does not mean the peak is accurate to less than 1%. An exact residue expansion is given in (49) and (17) and (18) give a peak of 2.72% too high. At the peak, the quantity in brackets in (18) is approximately equal to one[♣], so that

$$H_{in}^{peak} \approx \frac{H_{ex}}{\xi\alpha\tau_d} \tag{20}$$

or, noting that the surface resistance of the wall and cavity inductance are given by

$$R = \frac{1}{\sigma\Delta} \text{ and } L = \frac{\mu_0 V}{S} \tag{21}$$

respectively, the parameter ξ can be written in the form

$$\xi = \frac{L}{R\tau_d} \tag{22}$$

and therefore

$$H_{in}^{peak} \approx \frac{H_{ex}}{\xi\alpha\tau_d} = \frac{RH_{ex}}{\alpha L} \tag{23}$$

The early-time HDOT formula is found to be

$$\frac{dH_{in}^{(1)}}{dt} \approx \frac{2H_{ex}}{\sqrt{\pi}\xi\alpha(\tau_d)^2}\left[-\frac{1}{2\left(\frac{t}{\tau_d}\right)^{3/2}} + \frac{1}{4\left(\frac{t}{\tau_d}\right)^{5/2}}\right]e^{-\frac{\tau_d}{4t}},\ \mathrm{t}/\tau_d \le 0.13 \tag{24}$$

The corresponding late-time HDOT formula is given in [8]

♦ [1] uses *0.1* for the boundary between the early-time formula and the late-time formula. The difference between the two formulas at *0.1* is *5.47%*. At *0.06*, the difference is only *0.45%.*

♣ Numbers for two different ξ's are shown in Figure 7.

$$\frac{dH_{in}^{(2)}}{dt} \approx -\frac{H_{ex}}{\xi\alpha(\tau_d)^2}\left[\frac{1}{\xi^2}e^{-\frac{t}{\tau_d\xi}} - 2\pi^2 e^{-\frac{\pi^2 t}{\tau_d}} + 8\pi^2 e^{-\frac{4\pi^2 t}{\tau_d}}\right], \mathrm{t}/\tau_d > 0.13 \quad (25)$$

At $\mathrm{t}/\tau_d = 0.13$, the percentage difference is *0.56%*. Similarly, the peak derivative of the internal magnetic field is given by [1]

$$\frac{dH_{in}^{peak}}{dt} \approx \frac{6RH_{ex}}{L\alpha\tau_d} = \frac{6H_{ex}}{\xi\alpha\tau_d^2} \quad (26)$$

The numerical coefficient 6♥ comes from the essential singularity of (17) and thus (24) (Figure 6). (24) gives the peak 3.68% too high when compared to (50) for $\xi = 6.008$.

Figure 5 can be used for the HDOT unit step response. Figure 6 provides HDOT for the impulse response, which is much narrower in pulse width than the HDOT unit step response. The H unit step response is obtained by integrating (17) and (18) and shown in Figure 9.

If we assume $b = 72$ inches and $2a = 24\ inches$, the geometric factor of (19) is $\xi \approx 10.4$. If b remains the same and $2a = 12\ inches$, $\xi \approx 5.6$. $\xi = 6.088$ is used to obtained nearby lightning figures. The geometric factor is not included in the direct strike model because only the planar structure is treated. The corresponding direct lightning responses for H and HDOT unit step and impulse responses are shown in Figure 10, Figure 11 and Figure 12

Given $f(t)$ as defined in (6) and an impulse response of the enclosure $H_{in}^{i}(t')$, the enclosure interior HDOT can be expressed as

$$\frac{dH_{in}^{e}}{dt} = \frac{d}{dt}\left[\int_0^t \alpha f(t')H_{in}^{i}(t-t')\,dt'\right] \quad (27)$$

The superscript "*e*" has been introduced to $H_{in}$to represent a decaying exponential. Two limiting cases where solutions are simplified considerably are the thick limit and thin limit:

If $\frac{1}{\alpha}$ is much less than the pulse width of the H or HDOT response function shown in Figure 5 or Figure 6, the thick limit applies. Figure 5 and Figure 6 approximate that limit as:

$$H_{in}^{e} = \int_0^t \alpha f(t')H_{in}^{i}(t-t')\,dt' \approx H_{in}^{i}(t-\langle t\rangle) \quad (28)$$

$$\frac{dH_{in}^{e}}{dt} = \int_0^t \alpha f(t')\frac{dH_{in}^{i}(t-t')}{dt'}dt' \approx \frac{dH_{in}^{i}(t-\langle t\rangle)}{dt} \quad (29)$$

Here

$$\langle t\rangle = \frac{\int_0^t t'[exp(-\alpha t')-exp(-\beta t')]dt'}{\int_0^t [exp(-\alpha t')-exp(-\beta t')]dt'} \approx \frac{[1-exp(-\alpha t)]-\alpha t exp(-\alpha t)}{\alpha[1-exp(-\alpha t)]} \quad (30)$$

and superscript "i" represents the impulse response. Therefore, the thick approximation is only a time delay of the H or HDOT impulse response function.

Two comments are in order: First, (28) is derived by expanding $H_{in}^{i}(t-t')$ as a function of t' in the integral in terms of Taylor series around $\langle t\rangle$ and select $\langle t\rangle$ such that the first order contribution vanishes [10]: $\int_0^t f(t')\,(t'-\langle t\rangle)dt' = 0$. Second, Microsoft® Excel® can be used

♥ Numerical coefficients for three different ξ's from (50) are shown in Figure 8.

for quick numerical evaluation. To see how well (28) and (30) works, we refer to Figure 40 and Figure 41.

On the other hand, if $\frac{1}{\alpha}$ is somewhat greater than the pulse width of the H or HDOT response function shown in Figure 5 and Figure 6, then the enclosure wall can be considered as thin and the thin approximation applies:

$H_{in}^{e} = \int_0^t H_{in}^{i}(t')\alpha f(t-t')\,dt' \approx f(t)\alpha \int_0^{t/\tau_d} \alpha\tau_d\, H_{in}^{i}(t/\tau_d)d(t/\tau_d) \approx f(t)H_{in}^{s}(t) \approx H_{in}^{s}(t)exp(-\alpha t)$ (31)

$\frac{dH_{in}^{e}}{dt} = \int_0^t \frac{dH_{in}^{i}(t\prime)}{dt\prime}\alpha f(t-t')dt' \approx f(t)H_{in}^{i}(t) \approx H_{in}^{i}(t).$ (32)

superscript "s" represents the unit step response. The time-delay formulas are not derived here because calculating time delay requires evaluating the moment for $H_{in}^{i}(t)$ and $\frac{dH_{in}^{i}(t)}{dt}$ and the resulting formula is too cumbersome to apply.

Equations (28) and (31) are for H, while (29) and (32) are for HDOT. Approximations (28), (29), (31) and (32) can be explained by their Laplace transforms. Transforming time to its normalized time $\frac{t}{\tau_d}$, the Laplace transform of the decaying exponential is $\frac{1}{\alpha\tau_d+s\prime}$. In a thick limit ($\alpha\tau_d \to \infty$), the decaying exponential transform becomes $\frac{1}{\alpha\tau_d}$ and its response response becomes $\frac{1}{\alpha\tau_d}\ H_{in}^{i}$. In a thin limit ($\alpha\tau_d \to 0$), the decaying exponential transform becomes $\frac{1}{s\prime}$ and its response becomes H_{in}^{s}.

A word of caution. Equation (32) does not apply to the rise portion of the incident field $-exp(-\beta t)$, i.e., the condition for using (32): β has to be somewhat greater than $\frac{1}{\tau_d}$. Otherwise the interior HDOT will rise faster than the incident HDOT. The double exponential waveform does not describe the HDOT of the incident field very well and the resulting transparent limit is not valid.

Nearby Lightning Responses for Decaying Exponential and for Unit Step Waveforms

This section starts with utilizing existing nearby lightning formulas for constructing the solution for decaying exponential and unit step excitations and ends with accurate numerical solutions based on residue expansion of known solutions.

Consider an exterior nearby lightning magnetic field, H_{ex}, with a decaying exponential waveform. The early-time integral for the interior cavity field of an enclosure is the approximation below [1]

$$H_{in} = \frac{H_{ex}}{2\pi i}\int_{c-i\infty}^{c+i\infty} \frac{e^{st}}{(s+\alpha)\left[\cosh\sqrt{s\tau_d} + \xi\sqrt{s\tau_d}\sinh\sqrt{s\tau_d}\right]} ds$$
$$\approx \frac{2H_{ex}}{2\pi i}\int_{c-i\infty}^{c+i\infty} \frac{e^{-\sqrt{s\tau_d}}e^{st}}{(s+\alpha)\left(1+\xi\sqrt{s\tau_d}\right)} ds \approx \frac{2H_{ex}}{2\pi i}\int_{c-i\infty}^{c+i\infty} \frac{e^{-\sqrt{s\tau_d}}e^{st}}{(s+\alpha)\xi\sqrt{s\tau_d}} ds \quad (33)$$

The Laplace transform can be inverted when a partial fraction is applied to the first multiplicative factor in the denominator of the integrand. The remaining expressions are tabulated in [11]. Note the left hand side of (33) is valid for all time, while the right hand side is for the early time only and ξ is large. The time-domain response for the right hand side integral can be written as

$$H_{in}^{(1)} = \frac{iH_{ex}}{\xi\sqrt{\alpha\tau_d}} exp(-\alpha\, t)\left[exp\left(i\sqrt{\alpha\tau_d}\,\right) erfc\left(i\sqrt{\alpha t} + \sqrt{T}\right) - exp\left(-i\sqrt{\alpha\tau_d}\,\right) erfc\left(-i\sqrt{\alpha t} + \sqrt{T}\right)\right] \quad (34)$$

where $erfc(x) = \frac{2}{\sqrt{\pi}}\int_x^\infty e^{-t^2} dt$ (35)

or

$H_{in}^{(1)} = -\frac{2H_{ex}}{\xi\sqrt{\alpha\tau_d}} exp(-\alpha\, t) Im\left[exp\left(i\sqrt{\alpha\tau_d}\,\right) erfc\left(i\sqrt{\alpha t} + \sqrt{T}\right)\right]$. Note superscript "(1)" represents early time and superscript "(2)" will represent late time.

Identities $w(iz) = e^{z^2} erfc(z)$ and $w(-x+iy)) = \overline{w(x+iy)}$ are used to show

$$H_{in}^{e(1)}\left(\frac{t}{\tau_d}, \alpha\tau_d\right) = \frac{2H_{ex}}{\xi\sqrt{\alpha\tau_d}} e^{-T} Im\left[w\left(\sqrt{\alpha t} + i\sqrt{T}\right)\right] \quad (36)$$

The thin-wall limit of a unit step response can be verified by letting $\alpha \to 0$. The result is

$$H_{in}^{s(1)} = \frac{2H_{ex}}{\xi\sqrt{\tau_d}}\left[2\sqrt{\frac{t}{\pi}} exp(-T) - \sqrt{\tau_d} erfc\left(\sqrt{T}\right)\right] \quad (37)$$

Although (36) and (37) give reasonable bounds for the time-domain responses, the use of impulse responses is restricted to $\frac{t}{\tau_d} < 0.06$. For $t/\tau_d \geq 0.06$, the following equation are derived:

$$H_{in}^{e(2)} = \frac{H_{ex}}{\xi\tau_d}\left[-\left(\frac{1}{\alpha-\frac{1}{\xi\tau_d}} - \frac{2}{\alpha-\frac{\pi^2}{\tau_d}} + \frac{2}{\alpha-\frac{4\pi^2}{\tau_d}}\right)e^{-\alpha\, t} + \frac{1}{\alpha-\frac{1}{\xi\tau_d}}e^{-\frac{t}{\xi\tau_d}} - \frac{2}{\alpha-\frac{\pi^2}{\tau_d}}e^{-\frac{\pi^2 t}{\tau_d}} + \frac{2}{\alpha-\frac{4\pi^2}{\tau_d}}e^{-\frac{4\pi^2 t}{\tau_d}}\right] \quad (38)$$

for the decaying exponential. However, because using the late-time expression (9) for the early time causes a large error, (38) cannot be used directly. The correction in the early-time error can be accounted for $t > 0.06\tau_d$ by adding

$$\Delta H_{in}^{e}(t) = \int_0^{0.06\tau_d}\left[H_{in}^{(1)}(t') - H_{in}^{(2)}(t')\right]e^{\alpha t'}dt'e^{-\alpha t} \quad (39)$$

where $H_{in}^{(1)}(t')$ and $H_{in}^{(2)}(t')$ are given by (17) and (18).

For $t/\tau_d \geq 0.06$, the interior field is thus given by

$$H_{in}^{e(2)}\left(\frac{t}{\tau_d}, \alpha\tau_d\right) = \frac{H_{ex}}{\xi}\left[-\left(\frac{1}{\alpha\tau_d-\frac{1}{\xi}} - \frac{2}{\alpha\tau_d-\pi^2} + \frac{2}{\alpha\tau_d-4\pi^2}\right)e^{-\alpha\, t} + \frac{1}{\alpha\tau_d-\frac{1}{\xi}}e^{-\frac{t}{\xi\tau_d}} - \frac{2}{\alpha\tau_d-\pi^2}e^{-\frac{\pi^2 t}{\tau_d}} + \frac{2}{\alpha\tau_d-4\pi^2}e^{-\frac{4\pi^2 t}{\tau_d}}\right] + \Delta H_{in}^{e}(t) \quad (40)$$

By letting $\alpha \to 0$ the unit step response can be shown to be:

$$H_{in}^{s(2)} = \frac{H_{ex}}{\xi}\left[\left(\xi - \frac{2}{\pi^2} + \frac{2}{4\pi^2}\right) - \xi e^{-\frac{t}{\xi\tau_d}} + \frac{2}{\pi^2}e^{-\frac{\pi^2 t}{\tau_d}} - \frac{2}{4\pi^2}e^{-\frac{4\pi^2 t}{\tau_d}}\right]. \quad (41)$$

Again, for $\frac{t}{\tau_d} \geq 0.06$, a correction term must be added to (41):

$$\Delta H_{in}^{s}(t) = \int_0^{0.06\tau_d}\left[H_{in}^{(1)}(t') - H_{in}^{(2)}(t')\right]dt' \quad (42)$$

Thus,

$$H_{in}^{s(2)} = \frac{H_{ex}}{\xi}\left[\left(\xi - \frac{2}{\pi^2} + \frac{2}{4\pi^2}\right) - \xi e^{-\frac{t}{\xi\tau_d}} + \frac{2}{\pi^2}e^{-\frac{\pi^2 t}{\tau_d}} - \frac{2}{4\pi^2}e^{-\frac{4\pi^2 t}{\tau_d}}\right] + \Delta H_{in}^{s}(t) \quad (43)$$

Finally, the double exponential response can also be written as

$$H_{in}^{de} = H_{in}^{e}\left(\frac{t}{\tau_d}, \alpha\tau_d\right) - H_{in}^{e}\left(\frac{t}{\tau_d}, \beta\tau_d\right) \quad (44)$$

Here (36) is used for $\frac{t}{\tau_d} < 0.06$ and (40) is used for $\frac{t}{\tau_d} \geq 0.06$. Superscript "de" represents the double exponential response.

The HDOT for exponential decaying responses can be obtained by observing an identity

$$\frac{dH_{in}^{e}}{dt/\tau_d}\left(\frac{t}{\tau_d}, \alpha\tau_d\right) = H_{in}^{i}\left(\frac{t}{\tau_d}\right) - \alpha\tau_d H_{in}^{e}\left(\frac{t}{\tau_d}, \alpha\tau_d\right) \quad (45)$$

The first term on the right is the impulse response (17) and (18) and the only dependent variable in the second term is the decaying exponential response. (45) is obtained by writing the impulse response as the sum of the decaying exponential and its time derivative from the corresponding functions in the transformed domain.

The left hand side of (33) can be evaluated exactly by the residue expansion. First, the integral on the left hand side of (33) is transformed from s-plane to z-plane with the transformation $z = \sqrt{s\tau_d}$. The resulting integral is

$$H_{in} = \frac{2H_{ex}}{2\pi i} \int_{\Gamma} \frac{z e^{z^2 \frac{t}{\tau_d}}}{(z^2+\alpha\tau_d)[\cosh z + \xi z \sinh z]} dz \qquad (46)$$

where the contour Γ is shown in Figure 33.

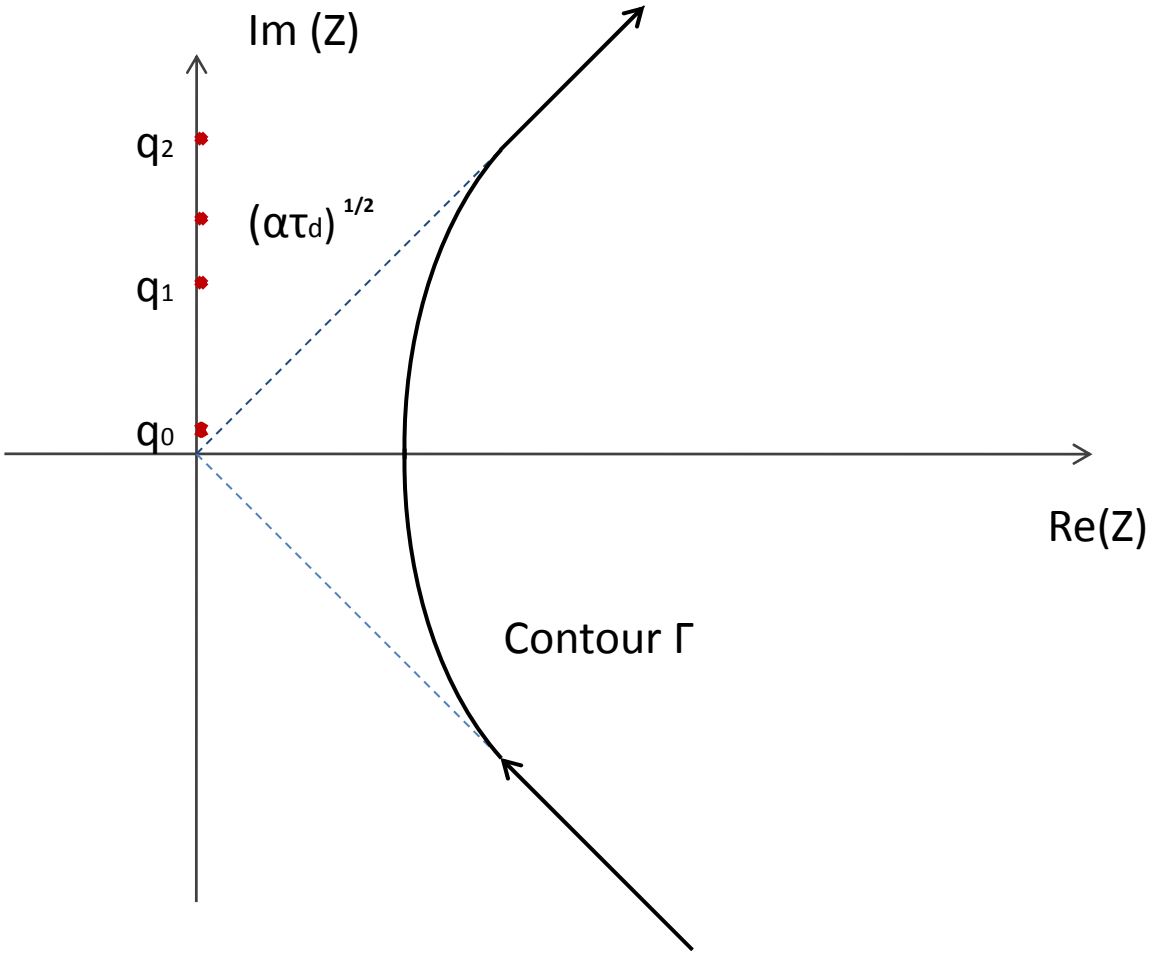

Figure 33. The contour in the z-plane .

Equation (43) has only poles. They are located at $z = i\sqrt{\alpha\tau_d}$ and $z_n = iq_n$ where q_n satisfy

$F(q) = cosq - \xi q sinq = 0$. An iterative equation can be used to determine the root location:

$q_{n+1} = q_n - \frac{F(q_n)}{F'(q_n)}$ where $F'(q) = -(\xi+1)sinq - \xi qcosq.$ The initial guess for the m[th] roots for ($n = 0,1,2, \dots$) are $q_{n=0}\,(0) = \frac{1}{\sqrt{\xi}}$ and $q_{n=0}\,(m) = m\pi,\ m = 1,2,3.$

The residue expansion can be written as

$$\frac{H_{in}}{H_{ex}} = \sum_{m=0}^{\infty} \frac{2q_m e^{-q_m^2 \frac{t}{\tau_d}}}{(\alpha\tau_d - q_m^2)[\xi q_m cosq_m + (\xi+1)sinq_m]} + \frac{e^{-\alpha t}}{cos\sqrt{\alpha\tau_d} - \xi\sqrt{\alpha\tau_d}sin\sqrt{\alpha\tau_d}} \tag{47}$$

$$\frac{HDOT_{in}\tau_d}{H_{ex}} = -\sum_{m=0}^{\infty} \frac{2q_m^3 e^{-q_m^2 \frac{t}{\tau_d}}}{(\alpha\tau_d - q_m^2)[\xi q_m cosq_m + (\xi+1)sinq_m]} - \frac{\alpha\tau_d e^{-\alpha t}}{cos\sqrt{\alpha\tau_d} - \xi\sqrt{\alpha\tau_d}sin\sqrt{\alpha\tau_d}} \tag{48}$$

One can derive an expression for a double pole caused formed by overlapping $\sqrt{\alpha\tau_d}$ by one of the q_n's. However, it is not needed here. In a similar manner, Impulse H and HDOT responses are given

$$\frac{H_{in}\alpha\tau_d}{H_{ex}} = \sum_{m=0}^{\infty} \frac{2q_m e^{-q_m^2 \frac{t}{\tau_d}}}{\xi q_m cosq_m + (\xi+1)sinq_m} \tag{49}$$

$$\frac{HDOT_{in}(\alpha\tau_d)\tau_d}{H_{ex}} = -\sum_{m=0}^{\infty} \frac{2q_m^3 e^{-q_m^2 \frac{t}{\tau_d}}}{\xi q_m cosq_m + (\xi+1)sinq_m} \tag{50}$$

The unit step response is a simple integration of (49)

$$\frac{H_{in}^s}{H_{ex}} = \sum_{m=0}^{\infty} \frac{2\left(1 - e^{-q_m^2 \frac{t}{\tau_d}}\right)}{q_m[\xi q_m cosq_m + (\xi+1)sinq_m]} \tag{51}$$

The accuracy of peak responses is determined by the location of dominating poles rather than the number of poles included in the calculation. Because the residue expansion is extremely accurate and convenient for numerical calculations, (47) through (51) are used to obtain all nearby lightning responses.

Direct-Strike Response for Impulse

For the direct-strike case, the maximum internal fields and pin-level voltages are induced when the lightning channel is inclined at an acute angle with respect to the enclosure wall or for a direct strike to an insulated conductor that is parallel and very close to the outer surface of the wall (Figure 2). Direct attachment with the lightning channel oriented perpendicular to the shield wall results in smaller voltages [12,13]. The impulse response is examined in great detail to exhibit the general features of the enclosure interior field from a direct strike.

Derivation of Transverse Magnetic Fields inside the Enclosure from a Longitudinal Current Filament

Consider the problem of calculating the transverse magnetic fields on the opposite side of an electrically thick wall (of thickness Δ) due to a parallel current filament with time dependence $i(t) = I\,e^{-\alpha t}u(t)$. According to Reference 2, the early-time approximation for replacing $\cosh(\xi\Delta) \sim \sinh(\xi\Delta) \sim \frac{1}{2}e^{\xi\Delta}$ in the magnetic vector potential gives

$$A_z^{tot} \sim \frac{2\mu_0 I}{\pi}\int_1^\infty \frac{\beta^2/\nu}{\left(\sqrt{\beta^2-1}+\beta/\nu\right)^2\sqrt{\beta^2-1}}\frac{1}{2\pi i}\int_{r-i\infty}^{r+i\infty}\frac{e^{st-F(\beta)\sqrt{s\tau_d}}}{s+\alpha}\,ds d\beta \qquad (52)$$

where $\nu = \mu/\mu_0$ and

$$F(\beta) = \beta + \left(\frac{\rho}{\Delta}-1\right)\sqrt{\beta^2-1} \qquad (53)$$

Note that Δ is the wall thickness and ρ the transverse radial distance from the filament center. The integration over β represents a superposition of solutions that satisfy Laplace's equation. The validity of (52) for enclosure applications is that $\rho \ll 2a$, where $2a$ is the enclosure dimension.

The magnetic field expression can be simplified by recognizing that for $\tau_d >> t_{50}$, the lightning source behaves as an impulse $\alpha \to \infty$. Under this approximation, the inverse Laplace Transform becomes

$$A_z^{tot} \sim \frac{2\mu_0 I}{\pi\alpha}\int_1^\infty \frac{(\beta^2/\nu)}{\left(\sqrt{\beta^2-1}+\beta/\nu\right)^2\sqrt{\beta^2-1}}\frac{1}{2\pi i}\int_{r-i\infty}^{r+i\infty} e^{st-F(\beta)\sqrt{s\tau_d}}\,ds d\beta$$

The magnetic vector potential can be simplified as [11]

$$A_z^{tot} \sim \frac{2\mu_0 I}{\pi\alpha}\int_1^\infty \frac{(\beta^2/\nu)F(\beta)\tau_d^{1/2}}{\left(\sqrt{\beta^2-1}+\beta/\nu\right)^2\sqrt{\beta^2-1}}\frac{e^{-[F(\beta)]^2\frac{\tau_d}{4t}}}{2\sqrt{\pi t^3}}\,d\beta$$

The magnetic field is given by

$$H_x = -\frac{1}{\mu_0}\frac{\partial}{\partial\,\rho}A_z^{tot} \sim \frac{2I}{\pi\Delta\alpha}\int_1^\infty \frac{(\beta^2/\nu)\tau_d^{1/2}}{\left(\sqrt{\beta^2-1}+\beta/\nu\right)^2}\{1-2T[F(\beta)]^2\}\frac{e^{-[F(\beta)]^2\frac{\tau_d}{4t}}}{2\sqrt{\pi t^3}}\,d\beta$$

$$H_x \sim -\frac{8I}{\alpha\Delta\tau_d}\left(\frac{T}{\pi}\right)^{3/2}\int_1^\infty \frac{(\beta^2/\nu)}{\left(\sqrt{\beta^2-1}+\beta/\nu\right)^2}\{1-2T[F(\beta)]^2\}e^{-[F(\beta)]^2T}d\beta \quad (54)$$

where $\mathrm{T} = \tau_\mathrm{d}/4\mathrm{t}$.

For $\nu = 1$, this is simplified to

$$H_x = -\frac{8I}{\alpha\Delta\tau_d}\left(\frac{T}{\pi}\right)^{3/2}\int_1^\infty \beta^2\left(\beta-\sqrt{\beta^2-1}\right)^2\{1-2T[F(\beta)]^2\}e^{-[F(\beta)]^2\frac{\tau_d}{4t}}d\beta \quad (55)$$

For $\frac{\rho}{\Delta}-1=0$,

$$H_x \sim -\frac{8I}{\alpha\Delta\tau_d}\left(\frac{T}{\pi}\right)^{3/2}\int_1^\infty \beta^2\left(\beta-\sqrt{\beta^2-1}\right)^2\{1-2T\beta^2\}e^{-\beta^2T}d\beta \quad (56)$$

Note that (54) can be used to evaluate the magnetic field away from the wall.
Let $\lambda = \frac{\rho}{\Delta}-1$ and $u=\beta^2$-1, (54) can also be expressed as

$$\frac{4I}{\alpha\Delta\tau_d}\left(\frac{T}{\pi}\right)^{3/2}\int_0^\infty \frac{\sqrt{1+u}/\nu}{\left(\sqrt{u}+\sqrt{1+u}/\nu\right)^2}\left\{1-2T\left[\sqrt{1+u}+\lambda\sqrt{u}\right]^2\right\}e^{-\left[\sqrt{1+u}+\lambda\sqrt{u}\right]^2}du \quad (57)$$

For $\nu = 1$,

$$H_x \sim -\frac{4I}{\alpha\Delta\tau_d}\left(\frac{T}{\pi}\right)^{3/2}\int_0^\infty\left[2(1+u)^{\frac{3}{2}}-(1+u)^{\frac{1}{2}}-2\sqrt{u}(1+u)\right]\left\{-2T\left[\sqrt{1+u}+\lambda\sqrt{u}\right]^2\right\}e^{-\left[\sqrt{1+u}+\lambda\sqrt{u}\right]^2T}du \quad (58)$$

Equations (53) through (58) can be used for the numerical evaluation of magnetic field and its derivative inside the enclosure.

Averaging and Truncation Approximations for Maximum Magnetic Fields

Equation (56) or (58) with $\lambda = 0$ gives the maximum magnetic field inside the enclosure and can be expressible in terms of a finite number of simple functions:

$$H_x \approx \frac{-4I}{\alpha\Delta\tau_d}\left(\frac{T}{\pi}\right)^{3/2}e^{-T}\left\{-2-\frac{8}{T}+\left(2-\frac{12}{T}\right)\left[\frac{1}{T}+\frac{\pi^{1/2}}{2T^{3/2}}e^T erfc\sqrt{T}\right]+\frac{2\pi^{1/2}}{T^{1/2}}+\frac{5\pi^{1/2}}{T^{3/2}}+\frac{12\pi^{1/2}}{2T^{5/2}}\right\} \quad (59)$$

However, averaging and truncation approximations [2], [14] are expressed in terms of elementary functions.

An averaging technique gives

$$H_x \approx \frac{-4I}{\alpha\Delta\tau_d}\left(\frac{T}{\pi}\right)^{3/2}e^{-T}\left[2\left(1+\frac{1}{T}\right)^{3/2}-\left(1+\frac{1}{T}\right)^{1/2}-2\frac{1}{\sqrt{T}}\left(1+\frac{1}{T}\right)\right]\left[1-2T\left(1+\frac{1}{T}\right)\right]\frac{1}{T} \quad (60)$$

Averaging for $\nu \neq 1$ is

$$H_x \approx \frac{4IT^{1/2}}{\alpha\Delta\tau_d\pi^{3/2}}e^{-T}\frac{\nu\sqrt{1+\frac{1}{T}}}{\left(\nu\sqrt{\frac{1}{T}}+\sqrt{1+\frac{1}{T}}\right)^2}[2T+1] \quad (61)$$

Alternatively, the truncation method gives

$$H_x \approx \frac{4I}{\alpha\Delta\tau_d \pi^{3/2}} e^{-T}\left\{-\frac{8T}{3}-\frac{28}{15}-\frac{12}{35T}+\frac{8}{7}T^{5/2}\left[\left(1+\frac{1}{T}\right)^{7/2}-1\right]-\frac{4}{5}T^{5/2}\left[\left(1+\frac{1}{T}\right)^{5/2}-1\right]-\frac{4}{5}T^{3/2}\left[\left(1+\frac{1}{T}\right)^{5/2}-1\right]+\frac{2}{3}T^{3/2}\left[\left(1+\frac{1}{T}\right)^{3/2}-1\right]\right\} \quad (62)$$

Averaging for Magnetic Fields Away from the Source Wall

Critical circuitry may be located far away from the enclosure wall and are not subjected to the large field near the line source. This discussion provides simple averaging formulas for describing magnetic field away from the wall.

Averaging is defined as

$$\int_1^\infty e^{-yT}\,dy = \frac{e^{-T}}{T}$$

or

$$\int_0^\infty \left(\sqrt{1+u}+\lambda\sqrt{u}\right)\left(\frac{1}{\sqrt{1+u}}+\frac{\lambda}{\sqrt{u}}\right)e^{-\left[\sqrt{1+u}+\lambda\sqrt{u}\right]^2 T}du = \frac{e^{-T}}{T}$$

Note that

$$\langle y\rangle = \frac{\int_0^\infty y e^{-y(u)T}\frac{dy}{du}du}{\int_0^\infty e^{-y(u)T}\frac{dy}{du}du} = 1+\frac{1}{T}$$

Rather than using averaging alone, we also impose consistency in mapping and define

$$\langle u\rangle = \frac{\int_0^\infty u e^{-y(u)T}\frac{dy}{du}du}{\int_0^\infty e^{-y(u)T}\frac{dy}{du}du} = \frac{1}{T_1}$$

So that

$$1+\frac{1}{T} = \left(\sqrt{1+1/T_1}+\lambda/\sqrt{T_1}\right)^2 \quad (63)$$

The averaging result is thus given by

$$H_x \sim -\frac{4IT^{1/2}e^{-T}}{\pi^{3/2}\alpha\Delta\tau_d}\left[2\left(1+\frac{1}{T_1}\right)^{3/2}-\left(1+\frac{1}{T_1}\right)^{1/2}-\frac{2}{\sqrt{T_1}}\left(1+\frac{1}{T_1}\right)\right]\frac{2T+1}{\left(\sqrt{1+\frac{1}{T_1}}+\frac{\lambda}{\sqrt{T_1}}\right)\left(\frac{1}{\sqrt{1+\frac{1}{T_1}}}+\lambda\sqrt{T_1}\right)} \quad (64)$$

and for $\nu \neq 1$

$$H_x \sim \frac{4IT^{1/2}e^{-T}}{\pi^{3/2}\alpha\Delta\tau_d}\left[\frac{\nu\sqrt{1+\frac{1}{T_1}}}{\left(\nu\sqrt{\frac{1}{T_1}}+\sqrt{1+\frac{1}{T_1}}\right)^2}\right]\frac{2T+1}{\left(\sqrt{1+\frac{1}{T_1}}+\frac{\lambda}{\sqrt{T_1}}\right)\left(\frac{1}{\sqrt{1+\frac{1}{T_1}}}+\lambda\sqrt{T_1}\right)} \quad (65)$$

Numerical Examples for Impulse Responses

Maximum Magnetic Field in the Enclosure

Approximate formulas only involve elementary functions. Equations (56), (58) with $\lambda = 0$, and (59) were evaluated numerically for I = 200 kA, α = ln(2)/(200 μs), $\mu = \mu_0$, σ = 2.6 × 10^7 S/m, and Δ = 0.5 inches. The maximum magnetic field inside an enclosure is 2.2 ×10^5 A/m at approximately 0.76 ms. The results are compared in Figure 34, which shows that the truncation result gives a more accurate peak and the averaging formula gives a somewhat lower peak value. Figure 35 shows the numerical derivatives of the magnetic field given by (56), (58) with $\lambda = 0$, and (59). The peak time derivative of the magnetic field derived is 6.8×10^8 A/m/s at 0.3 ms. Truncation gives slightly higher HDOT in Figure 35.

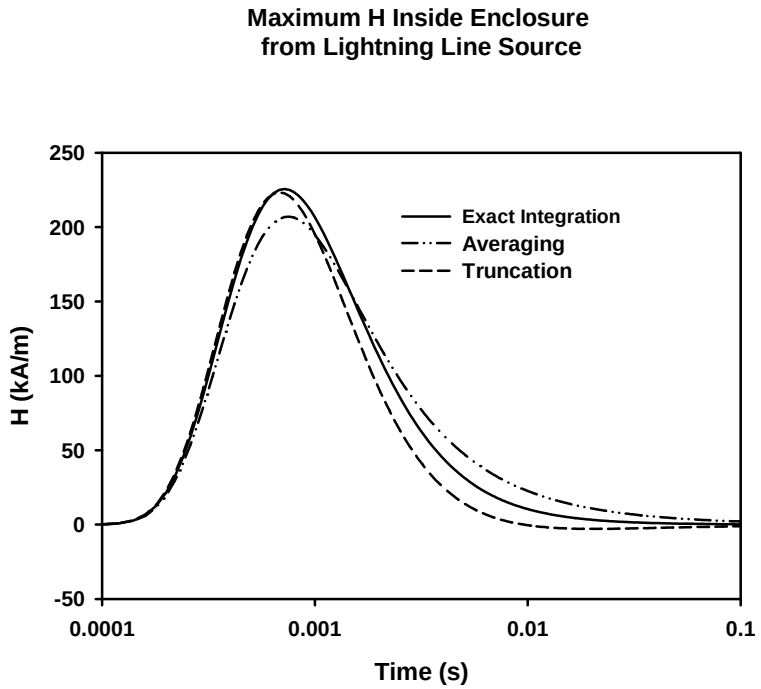

Figure 34. Comparison of the maximum magnetic field inside an enclosure by various methods: exact integration, averaging, and truncation method.

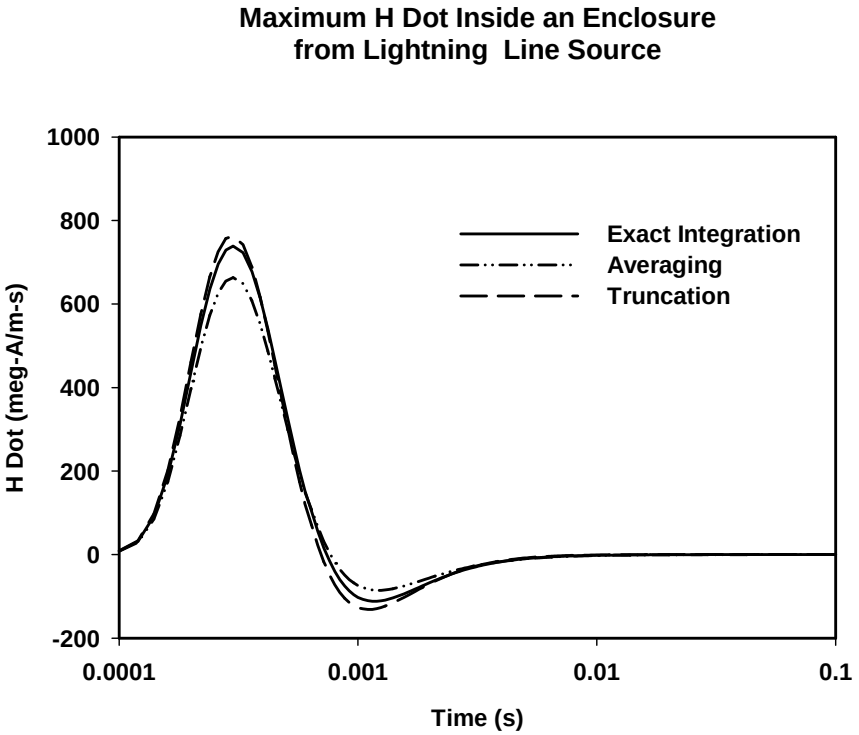

Figure 35. Comparison of the maximum magnetic field derivative inside an enclosure by various methods: exact integration, averaging, and truncation method.

Magnetic Field Away from the Wall

The magnetic field from the line source falls off spatially away from the wall. Figure 36 shows the comparison of the exact integration and the averaging results at a distance $\rho = \Delta$ and $\rho = 2\Delta$ The peak time derivative of the magnetic field decreases approximately a factor of four when the distance away from the wall double. Figure 37 shows the peak time derivative magnetic field decreases approximately 25 times and 100 times when the distance increases to $\rho = 5\Delta$ and $\rho = 10\Delta$ respectfully.

Figure 38 and Figure 39 illustrate the peak magnetic field and the peak time derivative of magnetic field are approximately proportion to the factor $\left(\frac{\Delta}{\rho}\right)^2$.

For Δ = 0.5 inches, $b \approx 72$ inches and $\rho = \Delta$, the worst case induced voltage in a single-turn loop in air occupying the full cross section of the enclosure from an impulse is

$$V < \int_{\Delta}^{\infty} \mu_0 HDOT_{in}|_{\rho=\Delta} \frac{\Delta^2 b d\rho}{\rho^2} \approx \mu_0 HDOT_{in}|_{\rho=\Delta} b\Delta = \frac{\mu_0 2\times 10^5}{0.00527} \frac{4.1608}{\alpha\tau_d} \times 1.83 \approx 19.8\ volts.$$

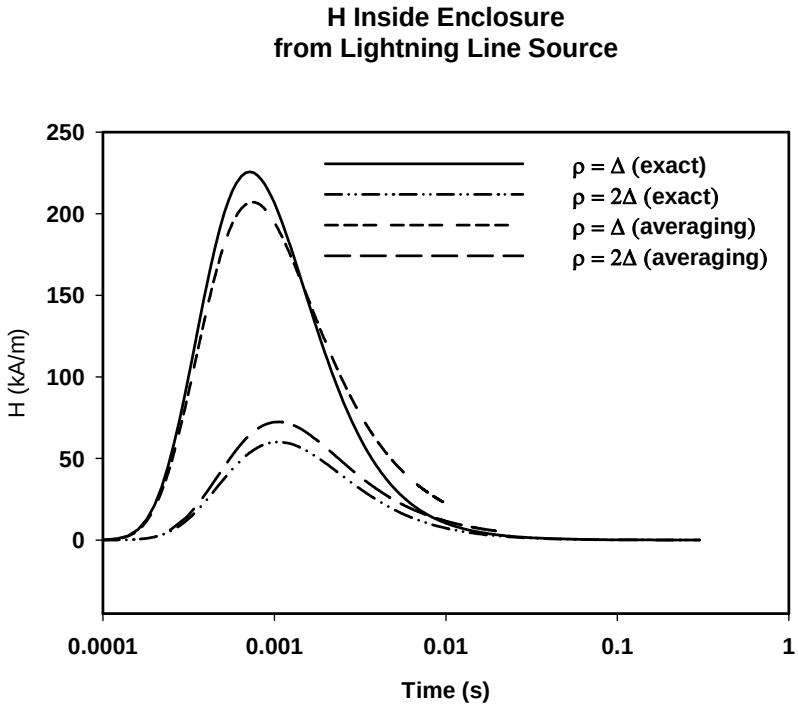

Figure 36. Comparison of the maximum magnetic field derivative inside an enclosure by exact integration and averaging method for $\rho = \Delta$ and $\rho = 2\Delta$.

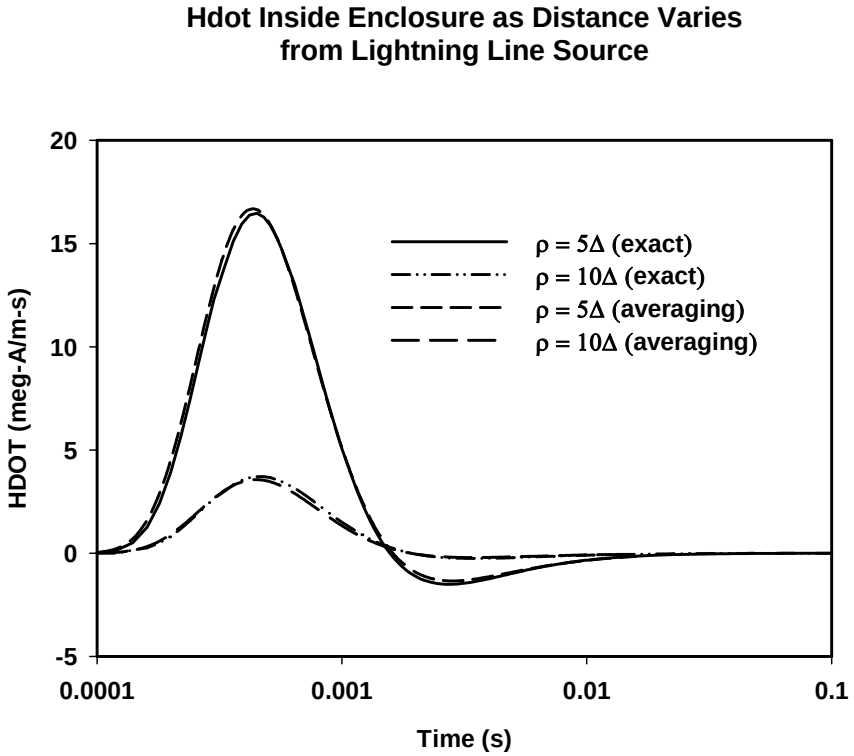

Figure 37. Comparison of the maximum magnetic field derivative inside an enclosure by exact integration and averaging method for $\rho = 5\Delta$ and $\rho = 10\Delta$.

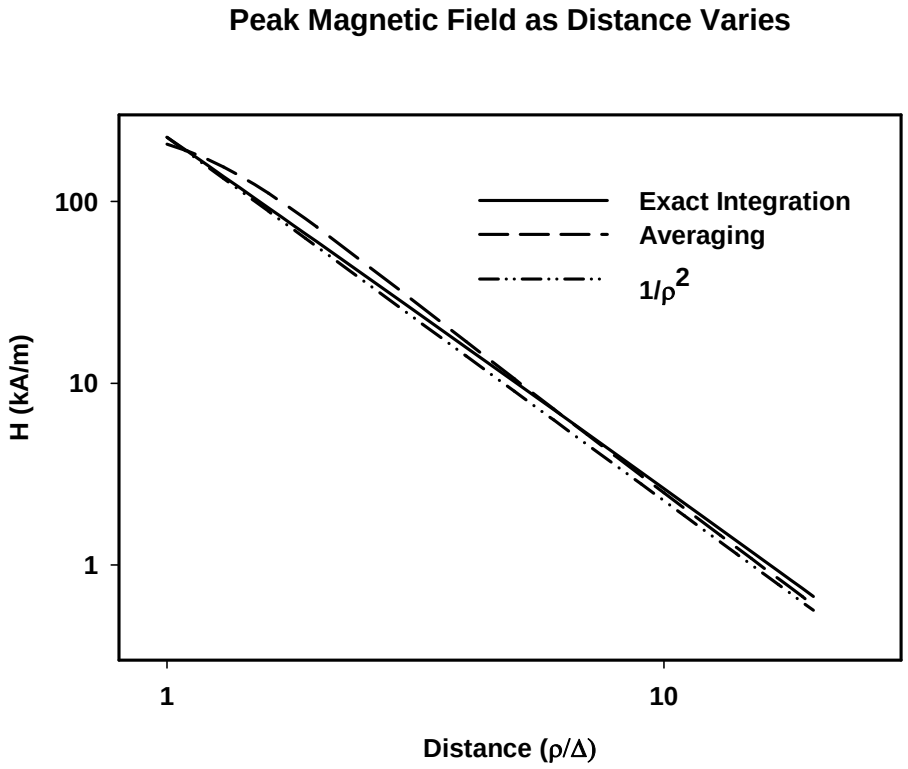

Figure 38. Peak magnetic field as distance varies away from the wall.

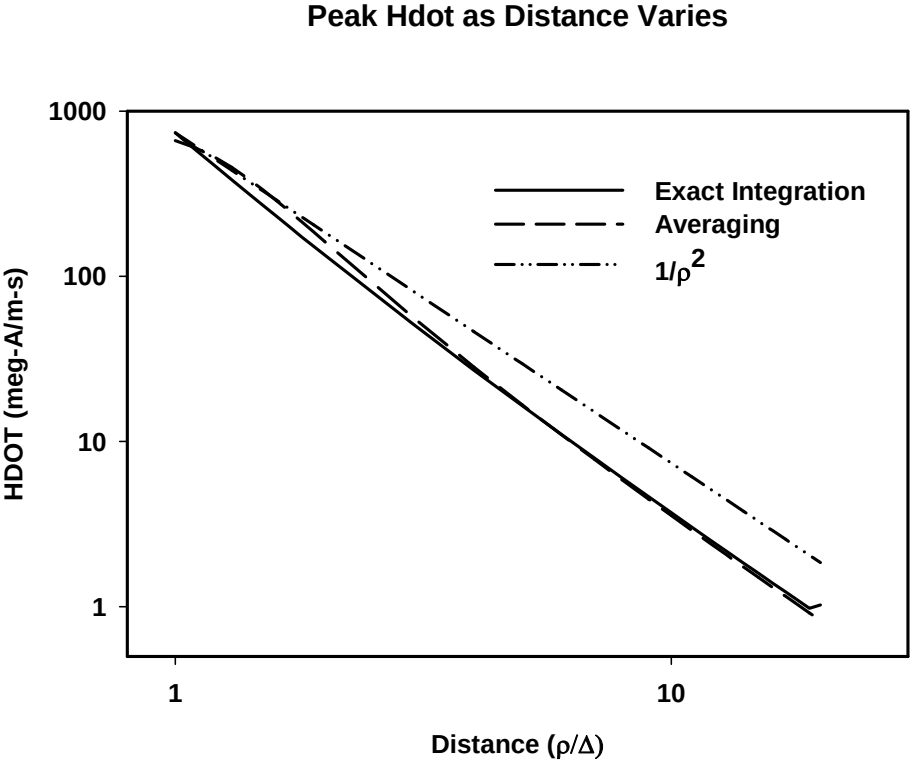

Figure 39. Peak time derivative of magnetic field as distance varies away from the wall.

Direct-Strike Response for Decaying Exponential Waveforms

The inverse Laplace transformation arising from propagating an exponential decaying function is

$$\frac{1}{2\pi i}\int_{c-i\infty}^{c+i\infty}\frac{e^{-k\sqrt{s}}}{s+\alpha}e^{ts}ds; \qquad k=F(\beta)\sqrt{\tau_d} \tag{66}$$

where $F(\beta)$ is given by (53).

The inverse transform is not given in Standard Transform Table [11]; however, if a partial fraction is applied to the denominator, the resulting function is:

$$\frac{i}{2\sqrt{\alpha}}\left[\frac{1}{\sqrt{s}+i\sqrt{\alpha}}-\frac{1}{\sqrt{s}-i\sqrt{\alpha}}\right]e^{-k\sqrt{s}} \tag{67}$$

The time-domain function is then given by

$$\frac{1}{2}\left[e^{ik\sqrt{\alpha}}e^{-\alpha t}erfc\left(i\sqrt{\alpha t}+\frac{k}{2\sqrt{t}}\right)+e^{-ik\sqrt{\alpha}}e^{-\alpha t}erfc\left(-i\sqrt{\alpha t}+\frac{k}{2\sqrt{t}}\right)\right], \tag{68}$$

which is reduced to

$$e^{\frac{-k^2}{4t}}Re\left[w\left(\sqrt{\alpha t}+\frac{ik}{2\sqrt{t}}\right)\right]. \tag{69}$$

Note that $w(iz)=e^{z^2}erfc(z)$ and $w(-x+iy)=\overline{w(x+\imath y)}$ or $w(z_1)=e^{-z_1^2}erfc(-iz_1)$.

Equation (52) can be expressed as

$$A_z^{tot}\sim\frac{2\mu_0 I}{\pi}\int_1^{\infty}\frac{\beta^2/\nu}{\left(\sqrt{\beta^2-1}+\beta/\nu\right)^2\sqrt{\beta^2-1}}e^{\frac{-k^2}{4t}}Re\left[w\left(\sqrt{\alpha t}+\frac{ik}{2\sqrt{t}}\right)\right]d\beta \tag{70}$$

To take the derivative of (70) with respect to ρ we use the function in (68) as

$$\begin{aligned}
&\frac{\partial}{\partial k}\frac{1}{2}\left[e^{ik\sqrt{\alpha}}e^{-\alpha t}erfc\left(i\sqrt{\alpha t}+\frac{k}{2\sqrt{t}}\right)+e^{-ik\sqrt{\alpha}}e^{-\alpha t}erfc\left(-i\sqrt{\alpha t}+\frac{k}{2\sqrt{t}}\right)\right]\\
&=\frac{i\sqrt{\alpha}}{2}\left[e^{ik\sqrt{\alpha}}e^{-\alpha t}erfc\left(i\sqrt{\alpha t}+\frac{k}{2\sqrt{t}}\right)-e^{-ik\sqrt{\alpha}}e^{-\alpha t}erfc\left(-i\sqrt{\alpha t}+\frac{k}{2\sqrt{t}}\right)\right]\\
&\quad-\frac{1}{\sqrt{\pi t}}\left[e^{ik\sqrt{\alpha}}e^{-\alpha t}e^{-\left(i\sqrt{\alpha t}+\frac{k}{2\sqrt{t}}\right)^2}+e^{-ik\sqrt{\alpha}}e^{-\alpha t}e^{-\left(-i\sqrt{\alpha t}+\frac{k}{2\sqrt{t}}\right)^2}\right]\\
&=\frac{i\sqrt{\alpha}}{2}e^{-\frac{k^2}{4t}}\left[w\left(-\sqrt{\alpha t}+i\frac{k}{2\sqrt{t}}\right)-w\left(\sqrt{\alpha t}+i\frac{k}{2\sqrt{t}}\right)\right]-\frac{1}{\sqrt{\pi t}}e^{-\frac{k^2}{4t}}
\end{aligned}$$

$$= \sqrt{\alpha} e^{-\frac{-k^2}{4t}} Im\left[w\left(\sqrt{\alpha t} + i\frac{k}{2\sqrt{t}}\right)\right] - \frac{1}{\sqrt{\pi t}} e^{\frac{-k^2}{4t}}$$

and $\frac{\partial}{\partial \rho} = \frac{\partial k}{\partial \rho}\frac{\partial}{\partial k} = \frac{\partial}{\partial k}\frac{\sqrt{\beta^2-1}}{\Delta}\sqrt{\tau_d}$.

The magnetic field is given by

$$H_x = -\frac{1}{\mu_0}\frac{\partial A_z^{tot}}{\partial \rho} \sim \frac{-2\sqrt{\tau_d} I}{\pi\Delta}\int_1^\infty \frac{\beta^2/\nu}{\left(\sqrt{\beta^2-1}+\beta/\nu\right)^2}\left\{\sqrt{\alpha} e^{\frac{-k^2}{4t}} Im\left[w\left(\sqrt{\alpha t} + i\frac{k}{2\sqrt{t}}\right)\right] - \frac{1}{\sqrt{\pi t}} e^{\frac{-k^2}{4t}}\right\} d\beta$$

or

$$H_x\left(\alpha\tau_d, \frac{t}{\tau_d}\right) \sim \frac{-\sqrt{\alpha\tau_d} I}{\pi\Delta}\int_0^\infty \frac{\sqrt{1+u}/\nu}{\left(\sqrt{u}+\sqrt{1+u}/\nu\right)^2}\left\{Im\left[w\left(\sqrt{\frac{\alpha\tau_d}{4T}} + i\left[\sqrt{1+u}+\lambda\sqrt{u}\right]\sqrt{T}\right)\right] - \frac{2\sqrt{T}}{\sqrt{\pi\alpha\tau_d}}\right\} e^{-\left[\sqrt{1+u}+\lambda\sqrt{u}\right]^2 T} du \tag{71}$$

where $u = \beta^2 - 1$

For $\nu = 1$, this is simplified to

$$H_x \sim \frac{-\sqrt{\alpha\tau_d} I}{\pi\Delta}\int_0^\infty \sqrt{1+u}\left(\sqrt{1+u}-\sqrt{u}\right)^2\left\{Im\left[w\left(\sqrt{\frac{\alpha\tau_d}{4T}} + i\left[\sqrt{1+u}+\lambda\sqrt{u}\right]\sqrt{T}\right)\right] - \frac{2\sqrt{T}}{\sqrt{\pi\alpha\tau_d}}\right\} e^{-\left[\sqrt{1+u}+\lambda\sqrt{u}\right]^2 T} du \tag{72}$$

For $\frac{\rho}{\Delta} = 1$,

$$H_x \sim \frac{-\sqrt{\alpha\tau_d} I}{\pi\Delta} e^{-T}\int_0^\infty \sqrt{1+u}\left(\sqrt{1+u}-\sqrt{u}\right)^2\left\{Im\left[w\left(\sqrt{\frac{\alpha\tau_d}{4T}} + i\sqrt{1+u}\sqrt{T}\right)\right] - \frac{2\sqrt{T}}{\sqrt{\pi\alpha\tau_d}}\right\} e^{-uT} du \tag{73}$$

Equations (70), (71), (72) can be numerically evaluated to be compared to (56), (57) and (55), respectively, for different fall-times (or values of $\alpha\tau_d$).

The double exponential response can be written as

$$H_x^{de} = H_x\left(\alpha\tau_d, \frac{t}{\tau_d}\right) - H_x\left(\beta\tau_d, \frac{t}{\tau_d}\right) \tag{74}$$

where each term in (74) is given by (71).

Note that when $\alpha \to 0$ (unit step limit), (66), (67) and (68) reduce to corresponding equations for the unit step discussed next.

Unit Step Responses

The unit step magnetic field response can be obtained from (52)

$$H_x = -\frac{1}{\mu_0}\frac{\partial}{\partial\rho}\left[\frac{2\mu I}{\pi}\int_0^\infty \frac{\beta^2 erfc\left[F(\beta)\sqrt{T}\right]}{\left(\nu\sqrt{\beta^2-1}+\beta\right)^2\sqrt{\beta^2-1}}d\beta\right],$$

The differentiation in ρ can be carried out to yield

$$H_x = \frac{2I\sqrt{T}}{\pi^{3/2}\Delta}\int_0^\infty \frac{\sqrt{1+u/\nu}}{\left(\sqrt{1+u/\nu}+\sqrt{u}\right)^2} e^{-\left[\sqrt{1+u}+\lambda\sqrt{u}\right]^2 T} du \tag{75}$$

For $\nu = 1$,

$$H_x = \frac{2I\sqrt{T}}{\pi^{3/2}\Delta}\int_0^\infty \left[2(1+u)^{3/2} - (1+u)^{1/2} - 2\sqrt{u}(1+u)\right] e^{-\left[\sqrt{1+u}+\lambda\sqrt{u}\right]^2 T} du \tag{76}$$

As $t \to \infty$ the unit step response approaches the static limit.

Voltage and Current Bounds for Direct Strikes

The distant time-derivative magnetic field deviates from $\frac{1}{\rho^2}$ and therefore the maximum voltage cannot be calculated from HDOT (extrapolated in ρ). A separate derivation for the maximum induced voltage is needed.

Referring to [2], the magnetic flux passing through the loop in the φ-direction (that is normal to the loop) shown in Figure 2 is calculated below using $\vec{B} = \nabla \times \vec{A}$ in a cylindrical coordinate:

$$B_\varphi = -\frac{\partial A_z^{tot}}{\partial \rho}$$

$$\emptyset > -b\int_\Delta^\infty \frac{\partial A_z^{tot}}{\partial \rho}d\rho = bA_z^{tot}|_{\rho=\Delta}$$

We can define V as the voltage bound (Figure 2) for decaying exponential as

$$V = \frac{\partial \emptyset}{\partial t} = \mu_0 bI\int_1^\infty \frac{\beta^2/\nu}{\left(\sqrt{\beta^2-1}+\beta/\nu\right)^2\sqrt{\beta^2-1}}\frac{1}{2\pi i}\int_{r-i\infty}^{r+i\infty}\frac{se^{st-\beta\sqrt{s\tau_d}}}{s+\alpha}dsd\beta \tag{77}$$

The s-integration can be carried out to yield

$$\frac{\mathrm{V}\tau_d}{\mu_0 Ib} = \frac{2}{\pi}\left\{\int_1^\infty \frac{(\beta^3/\nu)}{\left(\sqrt{\beta^2-1}+\beta/\nu\right)^2\sqrt{\beta^2-1}}\frac{e^{-\beta^2\tau_d/(4t)}}{2\sqrt{\pi(t/\tau_d)^3}}d\beta - \int_1^\infty \frac{\alpha\tau_d\beta^2/\nu}{\left(\sqrt{\beta^2-1}+\beta/\nu\right)^2\sqrt{\beta^2-1}}e^{-\frac{\beta^2\tau_d}{4t}}Re\left[w\left(\sqrt{\alpha t}+\frac{i\beta}{2\sqrt{t/\tau_d}}\right)\right]d\beta\right\} \tag{78}$$

or

$$V = \frac{\partial \emptyset}{\partial t} = \frac{2\mu_0 bI}{\pi}\frac{d}{dt}\int_1^\infty \frac{\beta^2/\nu}{\left(\sqrt{\beta^2-1}+\beta/\nu\right)^2\sqrt{\beta^2-1}}e^{-\frac{\beta^2\tau_d}{4t}}Re\left[w\left(\sqrt{\alpha t}+\frac{i\beta}{2\sqrt{t/\tau_d}}\right)\right]d\beta \tag{79}$$

For $\alpha\tau_d \to 0$ (the unit step limit),

$$\frac{\mathrm{V}\tau_d}{\mu_0 Ib} = \frac{2}{\pi}\int_1^\infty \frac{(\beta^3/\nu)}{\left(\sqrt{\beta^2-1}+\beta/\nu\right)^2\sqrt{\beta^2-1}}\frac{e^{-\beta^2\tau_d/(4t)}}{2\sqrt{\pi(t/\tau_d)^3}}d\beta \tag{80}$$

For $\alpha\tau_d \to \infty$ (the impulse limit)

$$\frac{\mathrm{V}\alpha}{\mu_0 Ib} = \frac{2}{\pi}\int_1^\infty \frac{\beta^2/\nu}{\left(\sqrt{\beta^2-1}+\beta/\nu\right)^2\sqrt{\beta^2-1}}\frac{1}{2\pi i}\int_{r-i\infty}^{r+i\infty} se^{st-\beta\sqrt{s\tau_d}}dsd\beta,$$

which can be reduced to

$$\frac{\mathrm{V}\tau_d(\alpha\tau_d)}{\mu_0 Ib} = \frac{2}{\pi}\int_1^\infty \frac{\frac{\beta^3}{\nu}\tau_d}{\left(\sqrt{\beta^2-1}+\beta/\nu\right)^2\sqrt{\beta^2-1}}\frac{d}{dt}\left\{\frac{e^{-\beta^2\tau_d/(4t)}}{2\sqrt{\pi(t/\tau_d)^3}}\right\}d\beta \tag{81}$$

where

$$\tau_d\frac{d}{dt}\left\{\frac{e^{-\beta^2\tau_d/(4t)}}{2\sqrt{\pi(t/\tau_d)^3}}\right\} = e^{-\beta^2\tau_d/(4t)}\left\{\frac{\beta^2}{8\sqrt{\pi(t/\tau_d)^7}} - \frac{3}{4\sqrt{\pi(t/\tau_d)^5}}\right\} \tag{82}$$

In order to take $\alpha\tau_d \to \infty$ of (79) we use

$$\alpha\tau_d e^{-\frac{\beta^2\tau_d}{4t}}Re\left[w\left(\sqrt{\alpha t}+\frac{i\beta}{2\sqrt{\frac{t}{\tau_d}}}\right)\right]$$

$$= \alpha\tau_d\frac{1}{2}\left[e^{ik\sqrt{\alpha}}e^{-\alpha t}erfc\left(i\sqrt{\alpha t}+\frac{\beta\sqrt{\tau_d}}{2\sqrt{t}}\right)+e^{-ik\sqrt{\alpha}}e^{-\alpha t}erfc\left(-i\sqrt{\alpha t}+\frac{\beta\sqrt{\tau_d}}{2\sqrt{t}}\right)\right]$$

$$\sim\frac{1}{2\sqrt{\pi}}e^{-\frac{\beta^2\tau_d}{4t}}\left[\frac{1}{-i\sqrt{\alpha t}+\frac{\beta\sqrt{\tau_d}}{2\sqrt{t}}}+\frac{1}{i\sqrt{\alpha t}+\frac{\beta\sqrt{\tau_d}}{2\sqrt{t}}}\right]\to\frac{\beta}{2\sqrt{\pi(t/\tau_d)^3}}e^{-\frac{\beta^2\tau_d}{4t}}$$

Therefore, as $\alpha\tau_d \to \infty$, (79) becomes (81).

As $\alpha\tau_d \to 0$, (79) becomes (80) because
$e^{-\frac{\beta^2\tau_d}{4t}}Re\left[w\left(\sqrt{\alpha t}+\frac{i\beta}{2\sqrt{\frac{t}{\tau_d}}}\right)\right]\to erfc\left(\frac{\beta\sqrt{\tau_d}}{2\sqrt{t}}\right)$ and $\tau_d\frac{d}{dt}erfc\left(\frac{\beta\sqrt{\tau_d}}{2\sqrt{t}}\right) = \frac{\beta}{2\sqrt{\pi(t/\tau_d)^3}}$.

Current bounds for an inductance dominating closed loop can be obtained by integrating (77) in time to obtain (We neglect the sign for the flux knowing that the flux change is compensated by induced voltage)

$$Li = \emptyset = \mu_0 bI\int_1^\infty \frac{\beta^2/\nu}{\left(\sqrt{\beta^2-1}+\beta/\nu\right)^2\sqrt{\beta^2-1}}\frac{1}{2\pi i}\int_{r-i\infty}^{r+i\infty}\frac{e^{st-\beta\sqrt{s\tau_d}}}{s+\alpha}dsd\beta,$$

which is

$$\frac{Li}{\mu_0 bI} = \frac{2}{\pi}\int_1^\infty \frac{\beta^2/\nu}{\left(\sqrt{\beta^2-1}+\beta/\nu\right)^2\sqrt{\beta^2-1}} e^{-\frac{\beta^2\tau_d}{4t}} Re\left[w\left(\sqrt{\alpha t}+\frac{i\beta}{2\sqrt{t/\tau_d}}\right)\right] d\beta \tag{83}$$

The corresponding bounds for the unit step and impulse are

$$\frac{Li}{\mu_0 Ib} = \frac{2}{\pi}\int_1^\infty \frac{(\beta^3/\nu)}{\left(\sqrt{\beta^2-1}+\beta/\nu\right)^2\sqrt{\beta^2-1}} erfc\left(\frac{\beta\sqrt{\tau_d}}{2\sqrt{t}}\right) d\beta \tag{84}$$

and

$$\frac{Li}{\mu_0 Ib} = \frac{2}{\pi}\int_1^\infty \frac{(\beta^3/\nu)}{\left(\sqrt{\beta^2-1}+\beta/\nu\right)^2\sqrt{\beta^2-1}} \frac{e^{-\beta^2\tau_d/(4t)}}{2\sqrt{\pi(t/\tau_d)^3}} d\beta \tag{85}$$

Some comments are in order: Our investigation is based on the early-time integral as discussed in (52). The parameters such as HDOT and voltage bounds that occur early in time are accurately determined by (52). However, in calculating H, the current bound, or the total flux for unit step excitations, the result may not be correct. The enclosure interior magnetic field due to the unit step falls off as $\frac{1}{\rho}$ from the line source (Figure 10 and Figure 13). If the upper integration of the loop area extends to infinity as done in this section, the total flux diverges and a realistic bound cannot be obtained. As discussed before, if a unit step current or flux bound is sought, it is more reasonable to limit the integration to the physical dimension of the enclosure so that a realistic bound can be obtained.

Collection of Figures

Decaying exponential waveforms with all physical parameters discussed for representative $\alpha\tau_d$ for nearby as well as direct strikes are given in this section. These parameters for nearby lightning are H and HDOT and for direct strike lightning are H and HDOT for two field points $\rho = \Delta$ and $\rho = 10\Delta$, voltage and current bounds for both $\mu = \mu_0$ and $\mu = 10\mu_0$.

H for Transition Range (Figure 40 through Figure 46)

An alternative explanation to the Laplace transform discussion in the section on general diffusion solutions for the transition is (45). $\xi = 6.088$ is used for Figure 40 through Figure 46**.** As $\alpha\tau_d \to \infty$, (45) becomes $H_{in}^e \approx \frac{H_{in}^i}{\alpha\tau_d}$ and, as $\alpha\tau_d \to 0$, (45) becomes $HDOT_{in}^e \approx H_{in}^i$ or $H_{in}^e \approx H_{in}^s$. Note also the pulse width widens as $\alpha\tau_d$ decreases. Figure 40 compares the numerical result for $\alpha\tau_d = 30$ with the approximate formula (28) with (30). The approximation is quite adequate for $\alpha\tau_d > 30$. Figure 41 indicates that a slight error in peaks if the approximation is used for $\alpha\tau_d = 6.6$. Large errors in peaks can occur for $\alpha\tau_d < 5$. Figure 40 through Figure 42 are shown with H normalized to be compared to the impulse response. Figure 43 shows the transition from large to small $\alpha\tau_d$ when the peak varies approximately $1/\sqrt{\alpha\tau_d}$. The transition implies the decaying exponential response makes the transition from an approximate unit step response to an impulse response as $\alpha\tau_d$ increases (Figure 26)

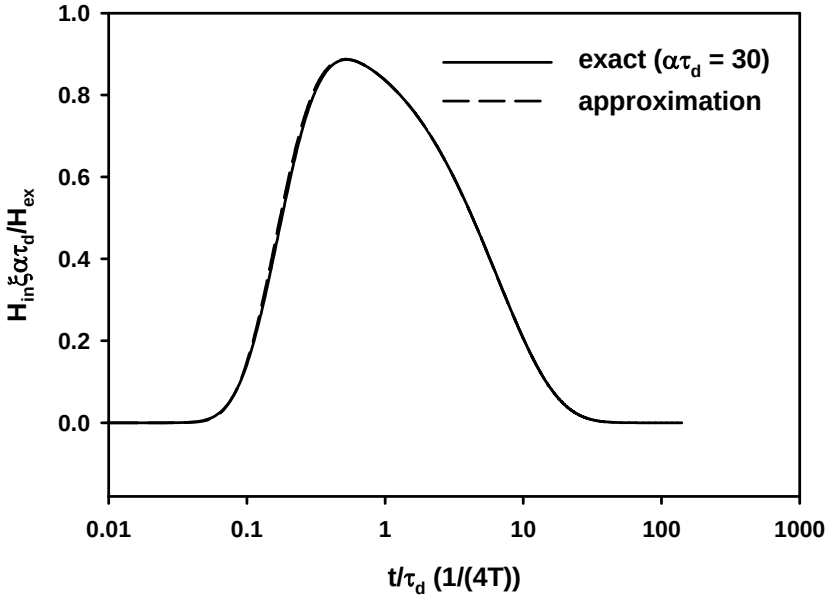

Figure 40. Comparison of exact numerical result with approximate formula (28) with (30).

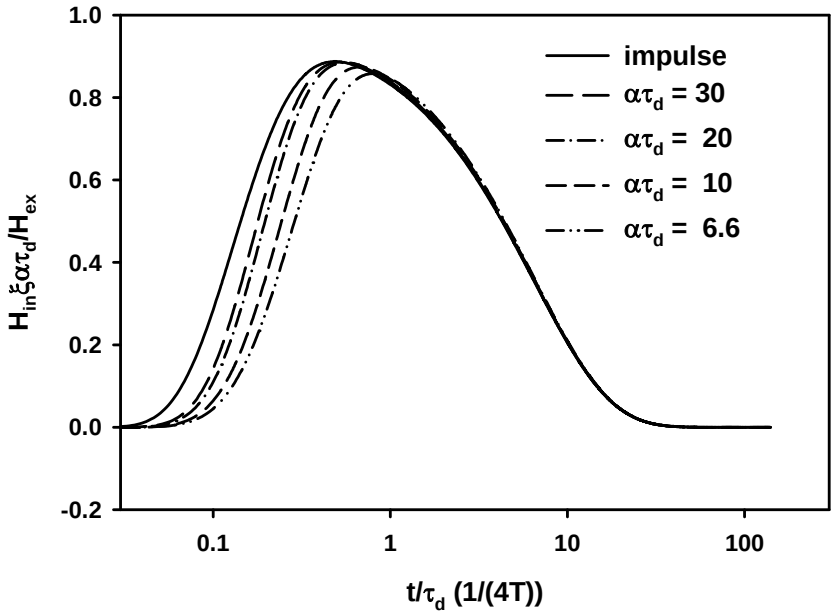

Figure 41. Numerical results for several values of $\alpha\tau_d$ are shown. If approximate formula (28) is used, slight errors in peak H result, because (28) preserves the peak from the impulse result.

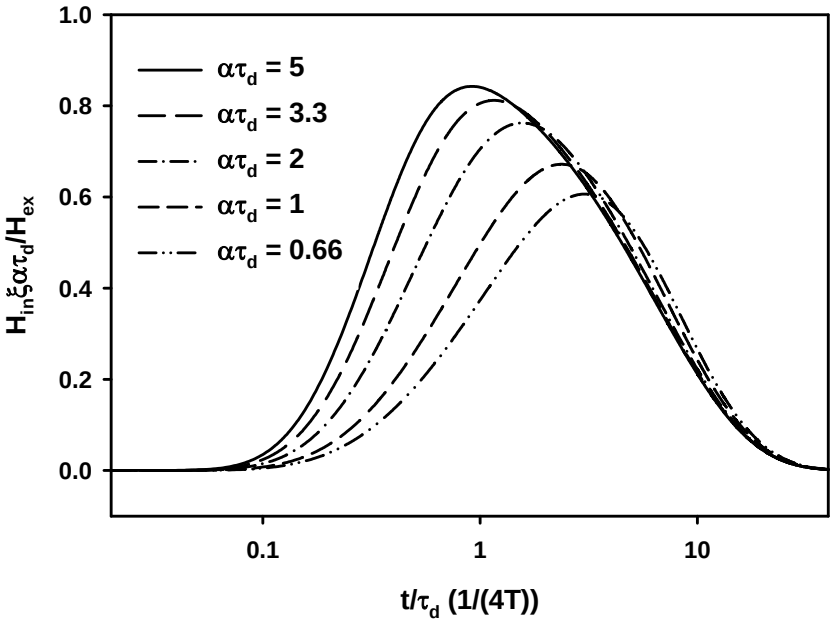

Figure 42. At these $\alpha\tau_d$ values, peak value decreases as $\alpha\tau_d$ decreases.

Figure 43 through Figure 46 are shown with H normalized to the unit step limit. Figure 44 shows that at $\alpha\tau_d = 0.01$, the peak of H almost approaches the unit step steady state limit.

Figure 45 and Figure 46 show how the approximate formula (31) compares to the numerical results for $\alpha\tau_d = 0.01$ and 0.001.

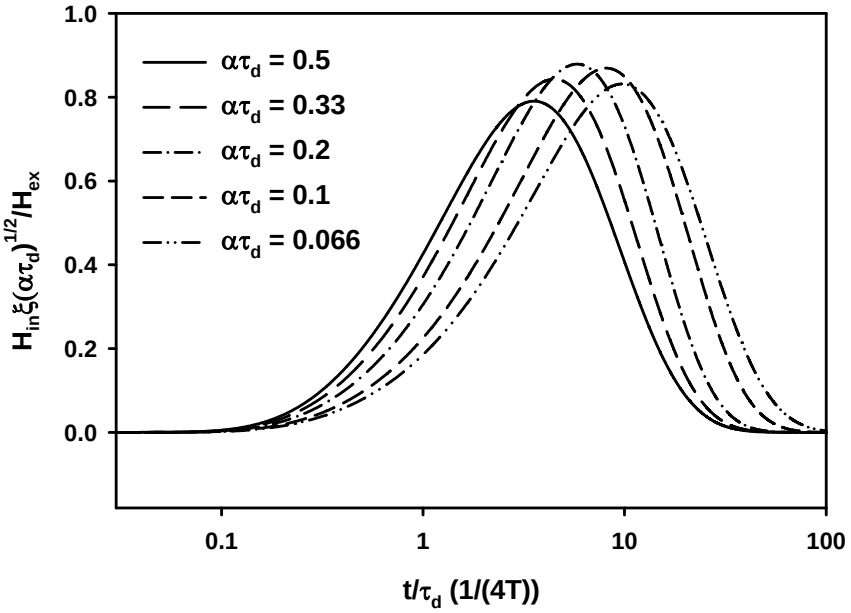

Figure 43. At these values of $\alpha\tau_d$, peak values vary approximately as $1/\sqrt{\alpha\tau_d}$ which has been scaled out. The intersection unit step peak and impulse peak in Figure 26 ($\alpha\tau_d = 0.1458$) corresponds to the occurrence of the peak response, which would have occurred between $\alpha\tau_d = 0.1$ and $\alpha\tau_d = 0.2$.

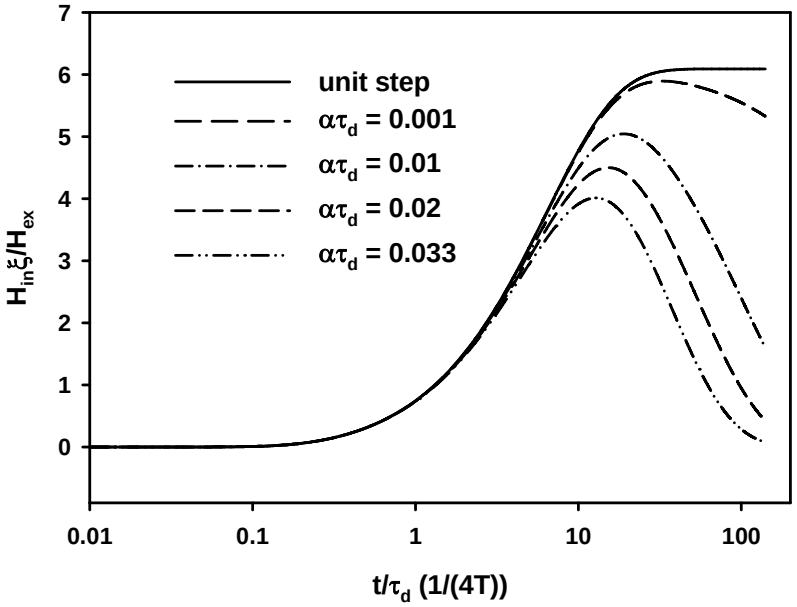

Figure 44. Peak value approaches the unit step late-time value as $\alpha\tau_d$ decreases. The unit step response approach ξ, which is 6.088.

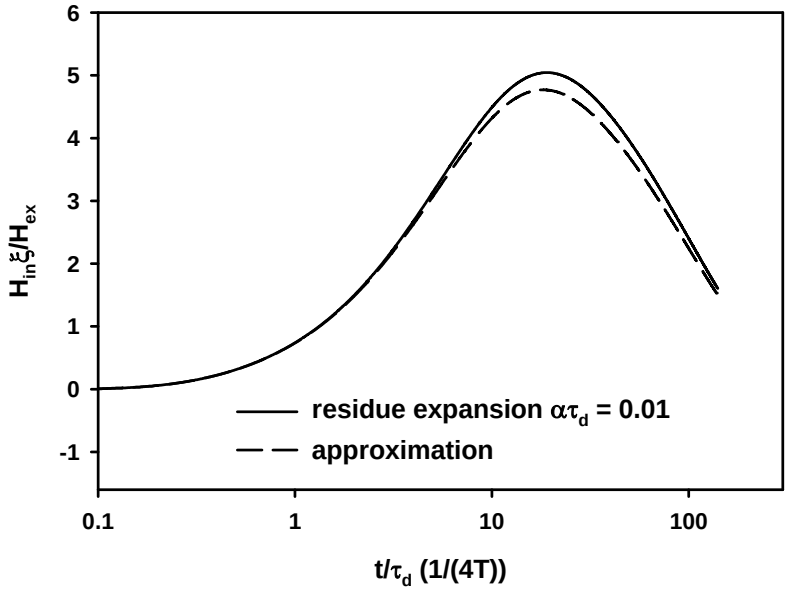

Figure 45. At $\alpha\tau_d = 0.01$, approximate formula (31) has a small error in the peak.

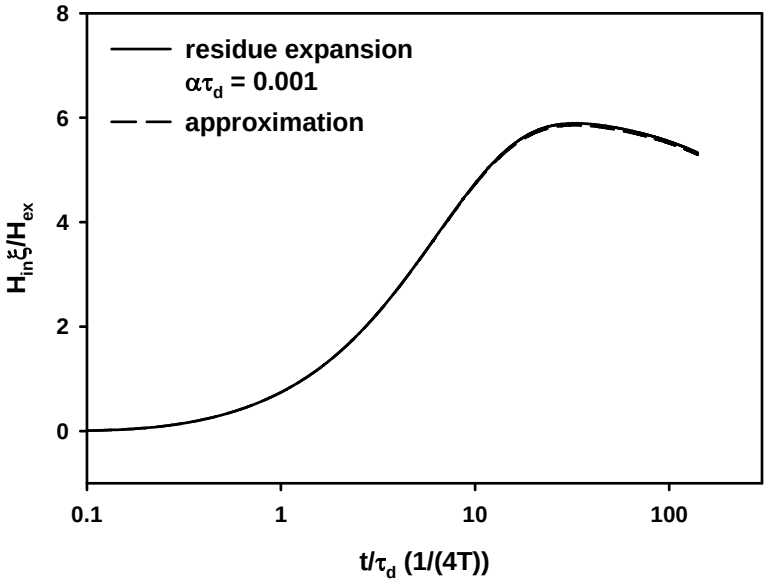

Figure 46. At $\alpha\tau_d = 0.001$, the error in approximate formula (31) is negligible.

HDOT for Transition Range (Figure 47 through Figure 51)

Figure 47 shows the transition to HDOT for the unit impulse. $\xi = 6.088$ is used for Figure 47 through Figure 51**.** It is obvious that time delay formula (29) is a good approximation to all $\alpha\tau_d$ responses shown. Again, (45) describes the transition. As $\alpha\tau_d \to \infty$, (45) becomes $HDOT_{in}^{e} \approx \frac{HDOT_{in}^{i}}{\alpha\tau_d}$ and, as $\alpha\tau_d \to 0$, (45) becomes $HDOT_{in}^{e} \approx H_{in}^{i}$. Note also the pulse width widens as $\alpha\tau_d$ decreases.

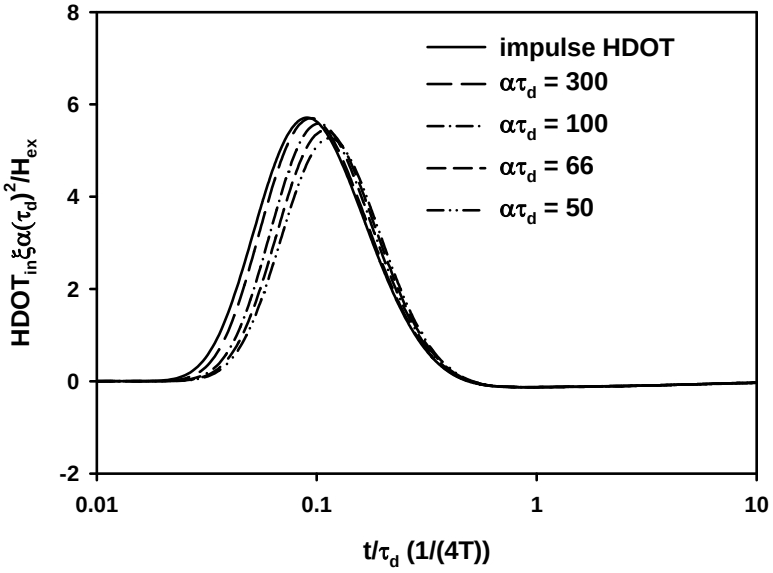

Figure 47. For large $\alpha\tau_d$, the approximate time delay formula given by (29) has small numerical discrepancy.

From $\alpha\tau_d = 30$ to $\alpha\tau_d = 0.33$, peak HDOT is reduced by approximately a factor of 4.5 (Figure 48 and Figure 49). A large transition range is described as the coefficient of (34), i.e., the peak varies approximately by $1/\sqrt{\alpha\tau_d}$. Figure 50 and Figure 51 illustrate, for $\alpha\tau_d \leq 0.2$, the peak HDOT and its waveform is approximately given by the peak impulse H response and its waveform (Figure 5).

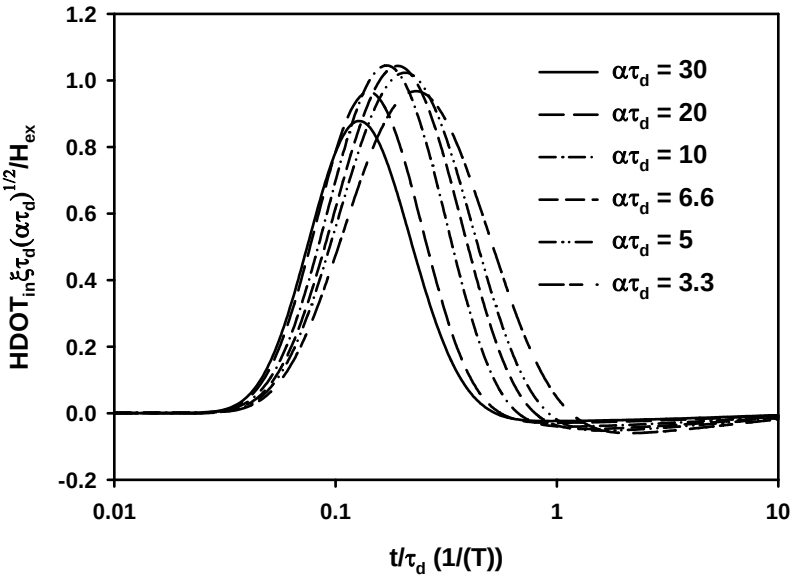

Figure 48. Peak HDOT is approximately inversely proportional to $\sqrt{\alpha\tau_d}$, which has been scaled out. Peak occurs near the curve $\alpha\tau_d = 6.6$, because of the intersection of the unit step and impulse peaks at 6.4351 shown in Figure 1.

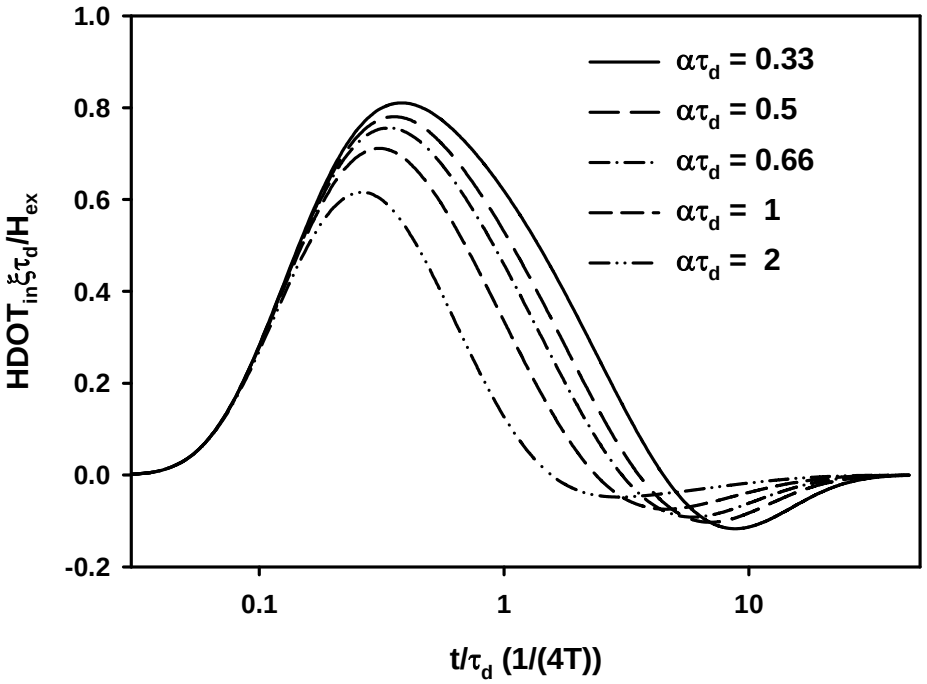

Figure 49. In this $\alpha\tau_d$ range, peak HDOT has a large decrease as $\alpha\tau_d$ decreases.

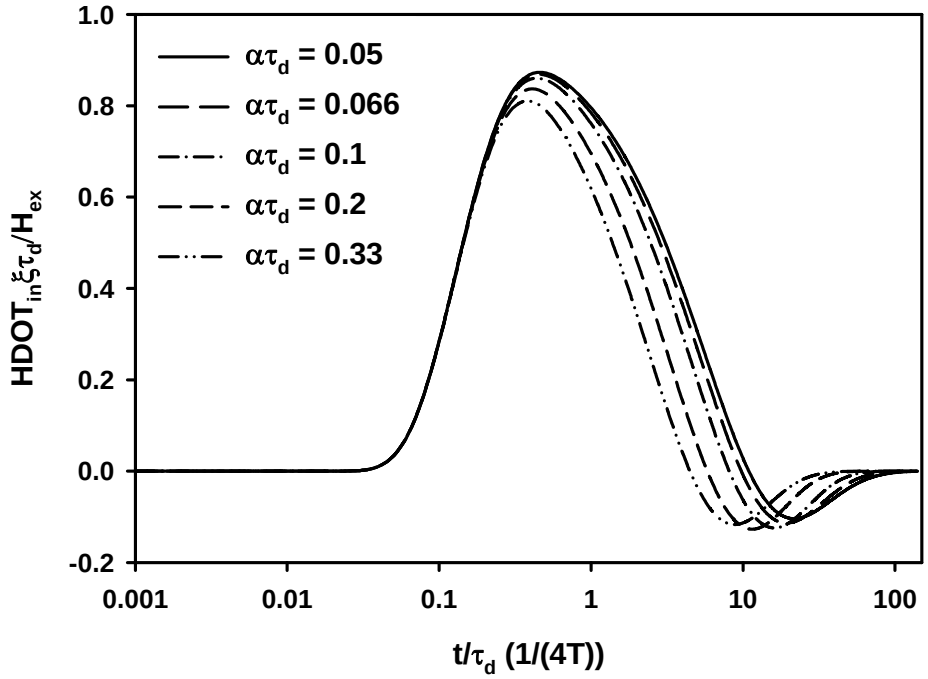

Figure 50. In this $\alpha\tau_d$ range, peak *HDOT* approaches the impulse *H* response (32).

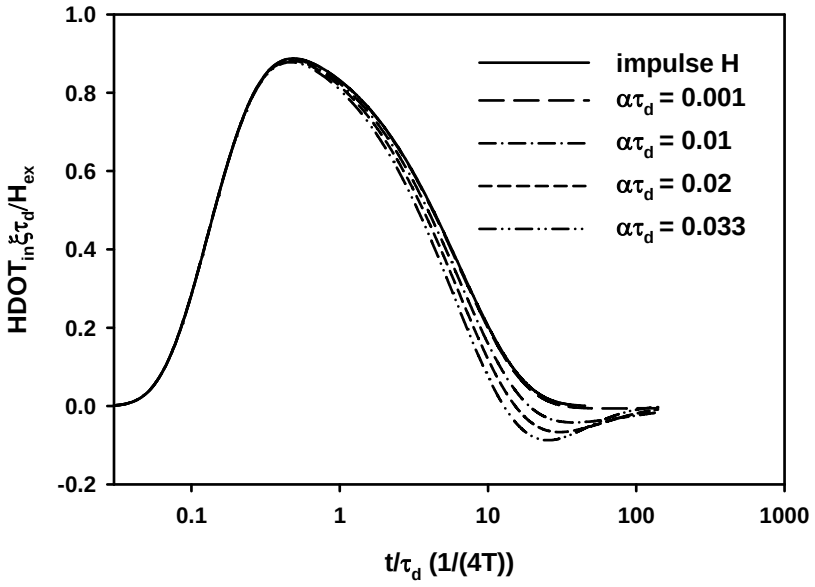

Figure 51. The waveform approaches the impulse response (32) at these $\alpha\tau_d$ values.

H Transition for $\rho = \Delta$, $\mu = \mu_0$, (Figure 52 through Figure 55)

All figures for direct strikes to be presented are labeled as H_{in} rather than H_x. They are derived from a planar wall. However, the solution is valid for most enclosures because other walls can be assumed to be distant from the source. The difference between the nearby planar excitation and the direct strike attachment to the insulated cable in proximity (that results in a line source) is the geometric parameter ξ (19).

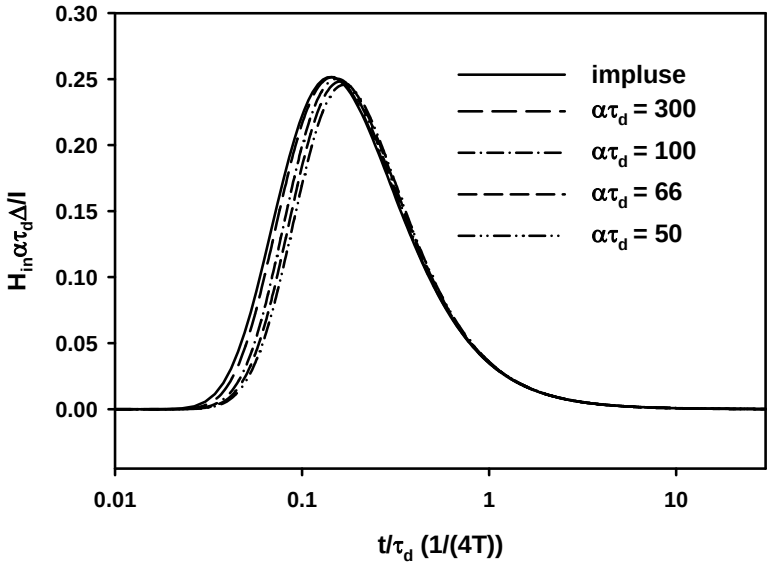

Figure 52. For all values of $\alpha\tau_d$, approximation 28 with (30) works well. Exponential decaying responses are time-delay of impulse H.

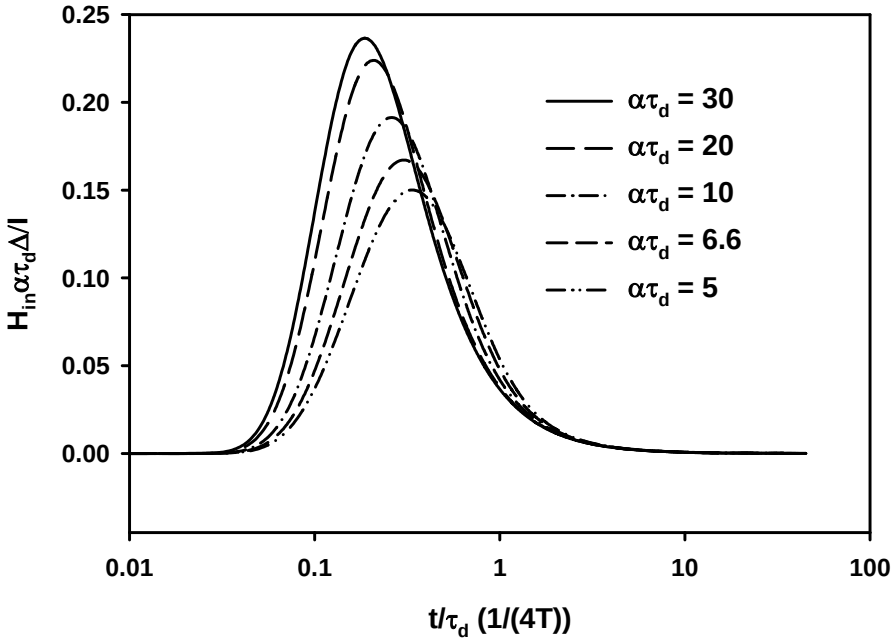

Figure 53. The peak and waveform deviate noticeably from those of Impulse H at $\alpha\tau_d = 30$. For corresponding nearby responses, see Figure 41.

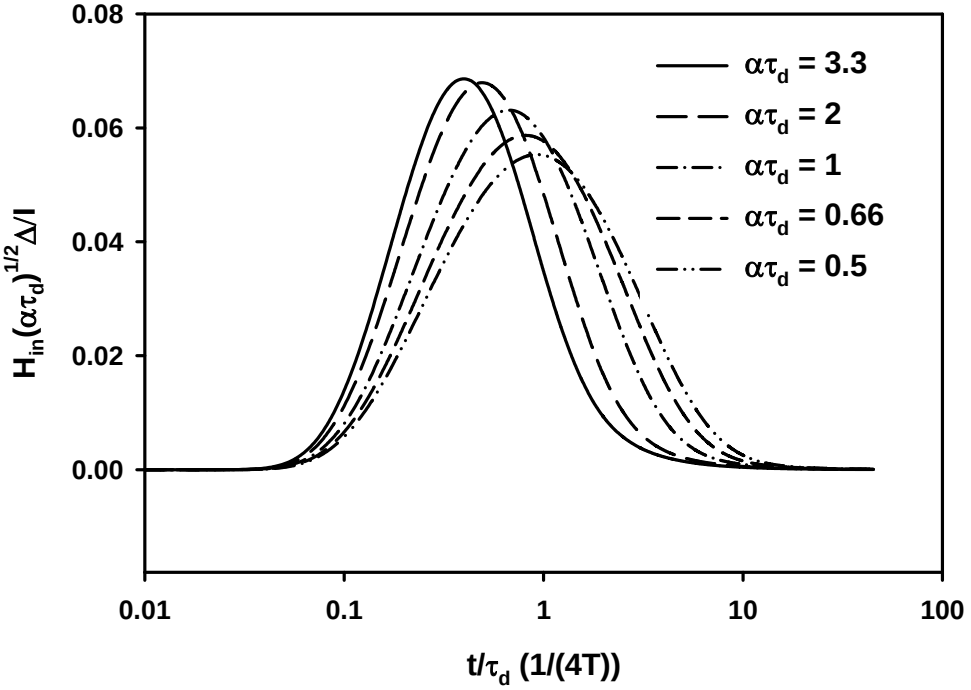

Figure 54. Vertical quantity has been scaled to $\sqrt{\alpha\tau_d}$ resulting in comparable peaks. The intersection of unit step and impulse peaks shown in Figure 27 occurs at $\alpha\tau_d = 1.5804$, which would corresponding to peak in the scaled quantity shown.

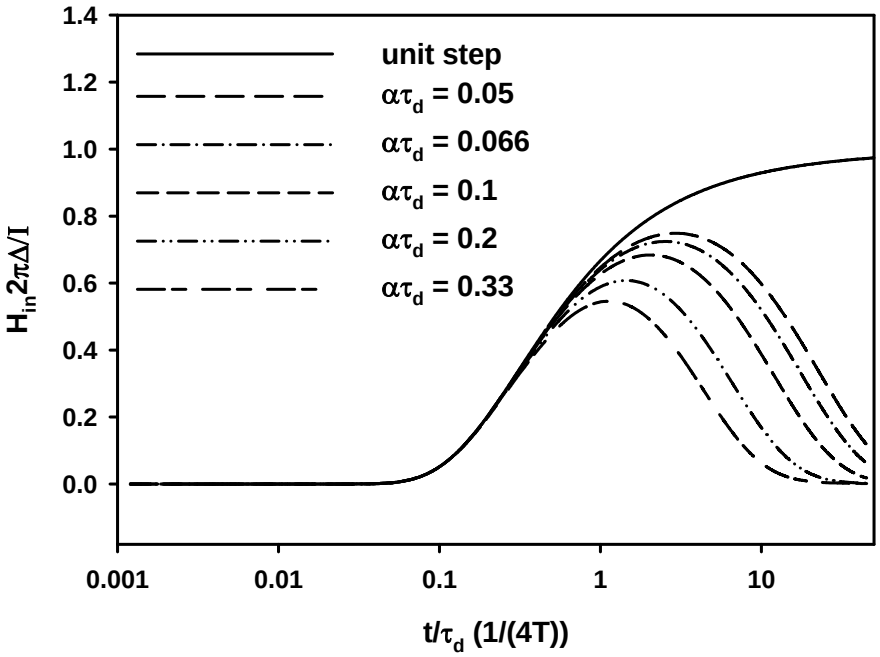

Figure 55. The unit step response is the same as shown in Figure 9. For small values of $\alpha\tau_d$, (31) is a good approximation.

HDOT Transition for $\rho = \Delta, \mu = \mu_0$ (Figure 56 through Figure 59)

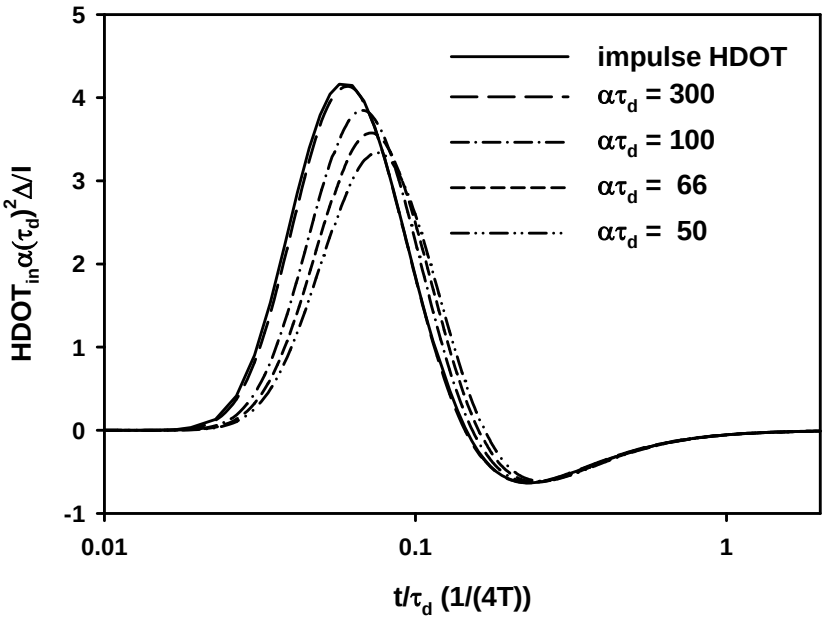

Figure 56. For $\alpha\tau_d = 300$, the response the same as impulse HDOT.

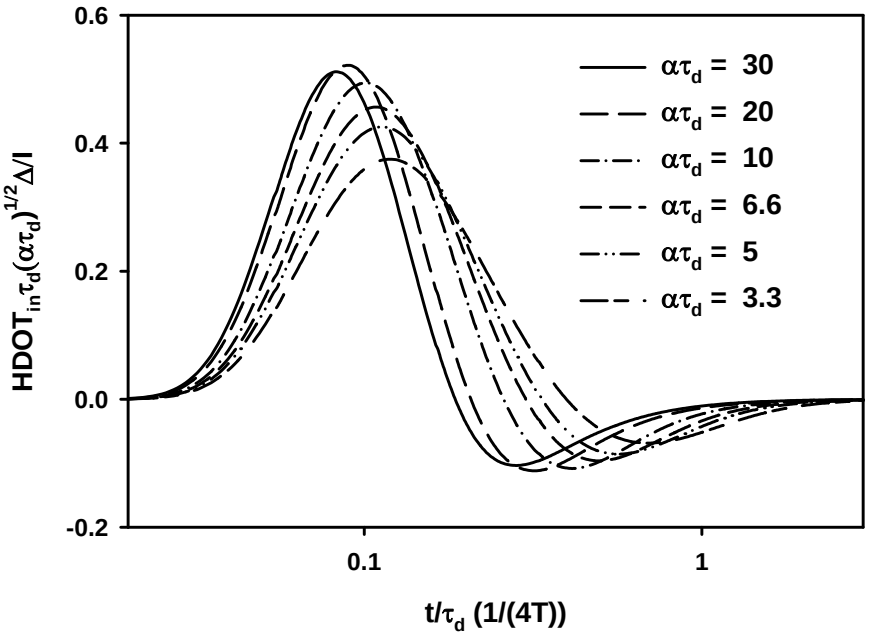

Figure 57. Vertical quantity has been scaled to $\sqrt{\alpha\tau_d}$ resulting in comparable peaks. The intersection of unit step and impulse peak occurs at $\alpha\tau_d = 16.5374$.

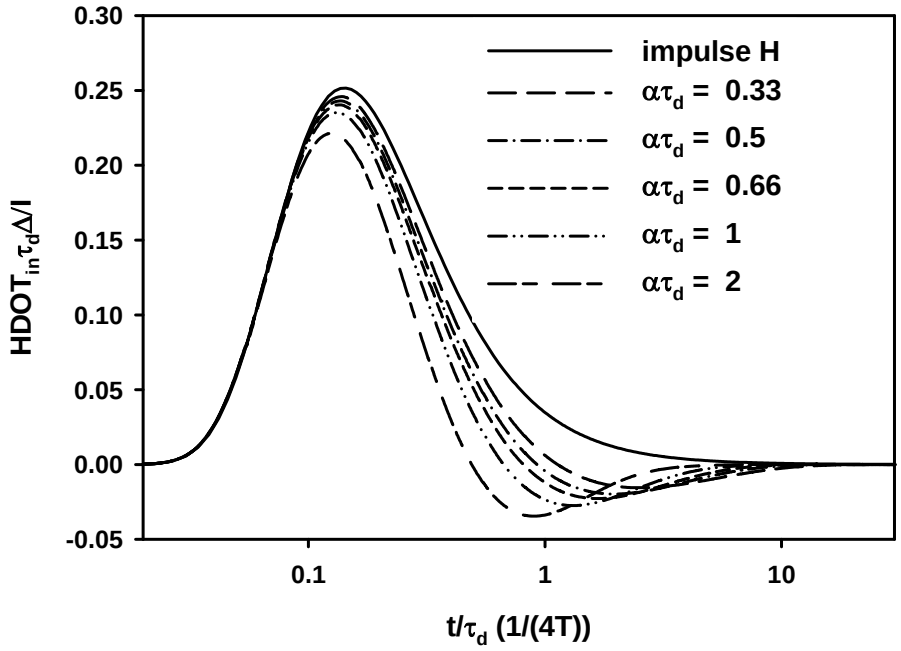

Figure 58. These *HDOT* responses for these values of $\alpha\tau_d$ are well approximated by the impulse *H*.

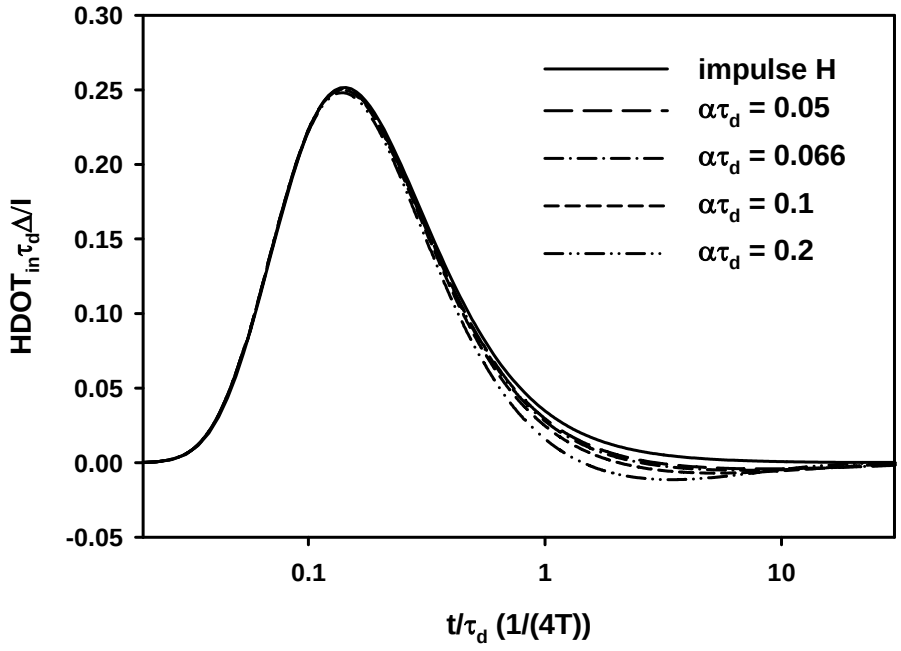

Figure 59. Impulse *H* (32) is a very good approximation to these *HDOT*.

H Transition for $\rho = 10\,\Delta$, $\mu = \mu_0$ *(Figure 60 through Figure 64)*

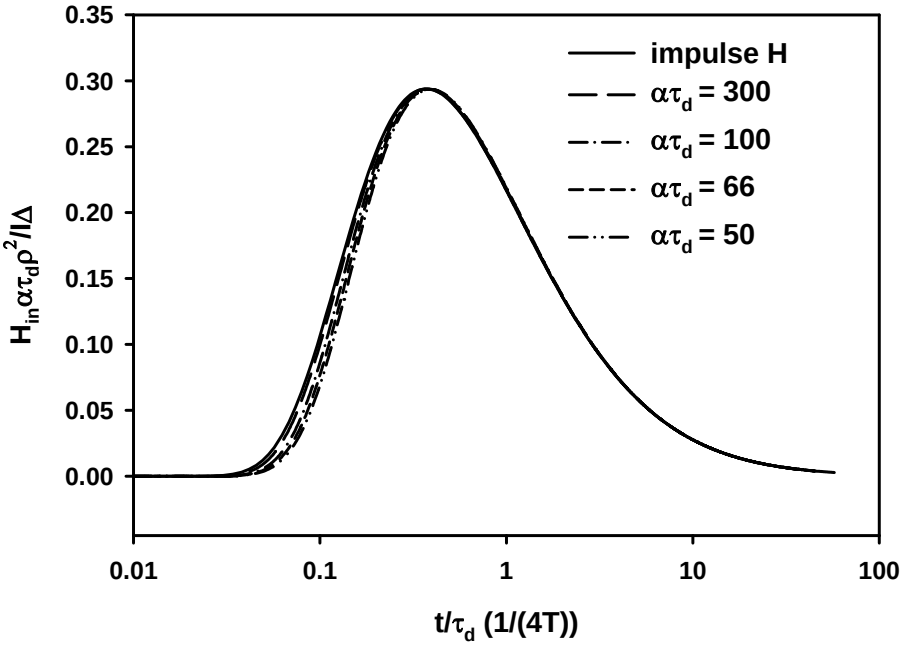

Figure 60. Impulse *H* (28) with (30) is an excellent approximation to these values of $\alpha\tau_d$.

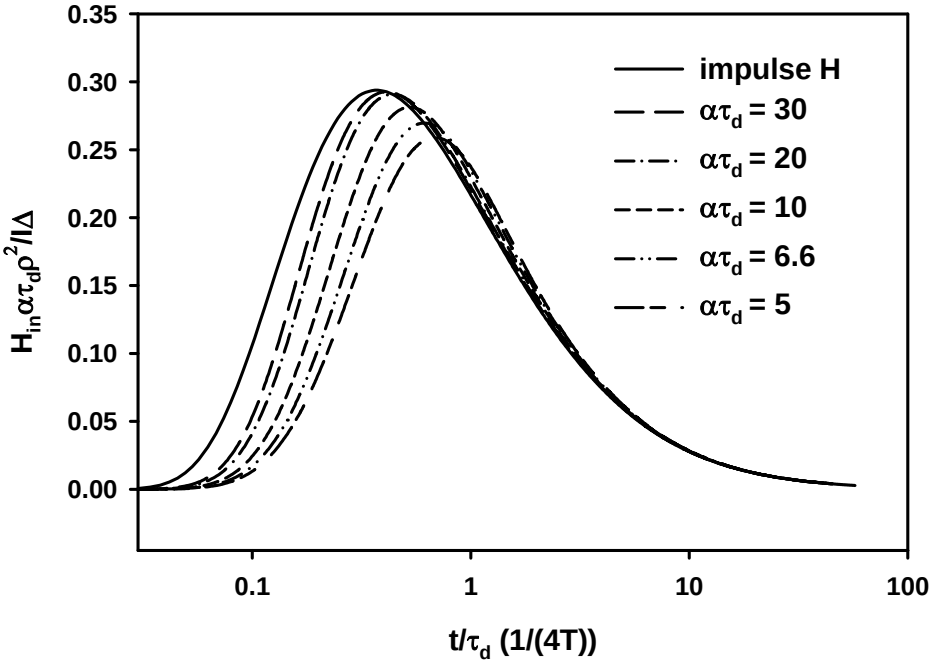

Figure 61. Transition values for $\rho = 10\Delta$ is close to that for the nearby response (Figure 41).

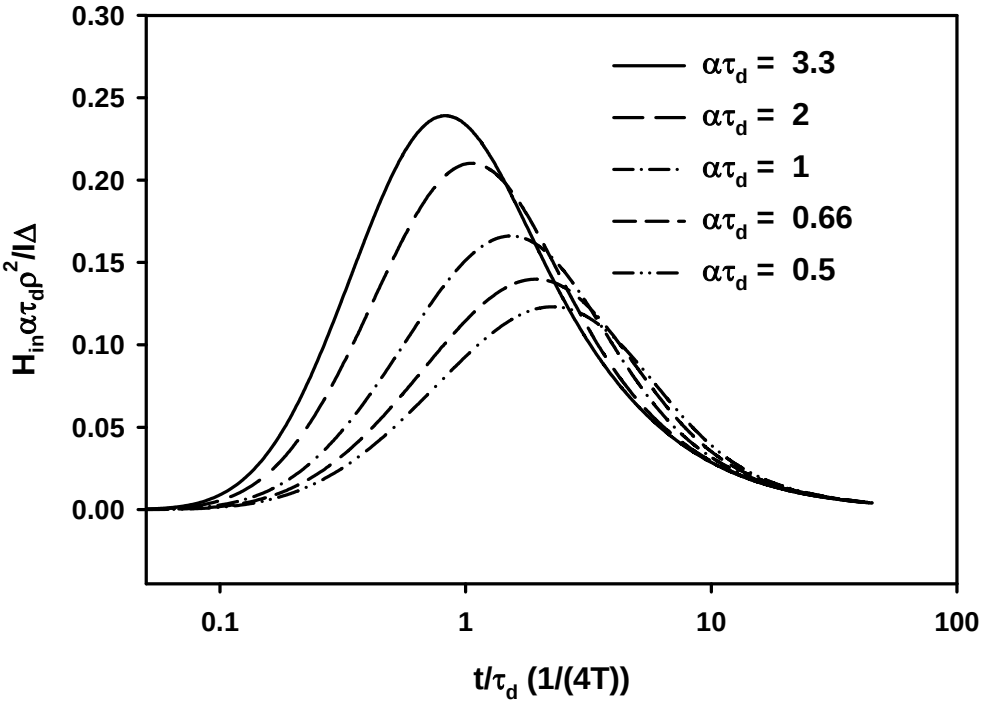

Figure 62. Peak H decreases quite a bit from the impulse *H* given in Figure 61.

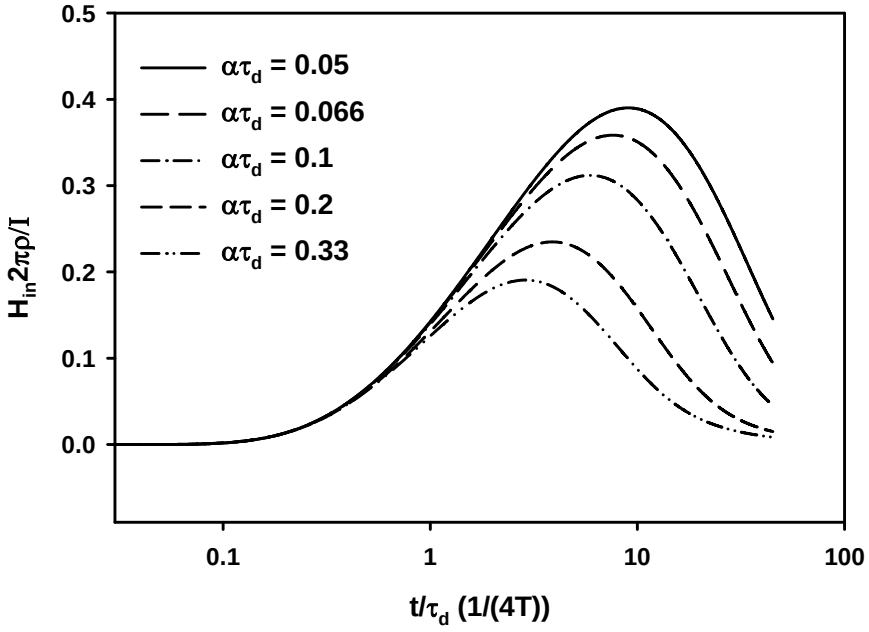

Figure 63. These curves should be compared to unit step response shown in Figure 64. The intersection of peak unit step and impulse responses occurs at $\alpha\tau_d = 0.1845$; however, the transition peak in the scaled vertical axis ($\sqrt{\alpha\tau_d}$) is not shown.

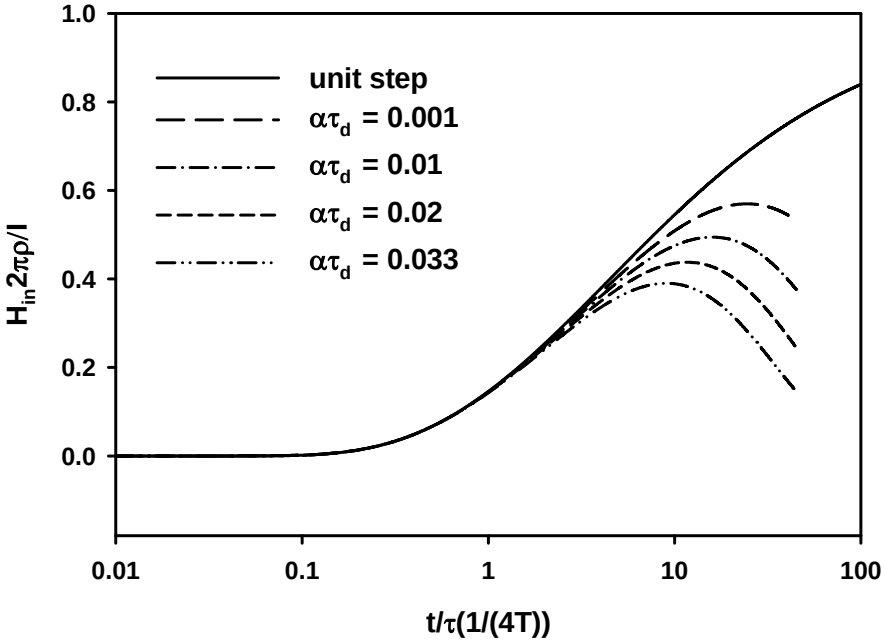

Figure 64. Transition to unit step response is shown. (31) is a good approximation to these curves.

HDOT Transition for $\rho = 10\Delta$, $\mu = \mu_0$ (Figure 65 and Figure 68)

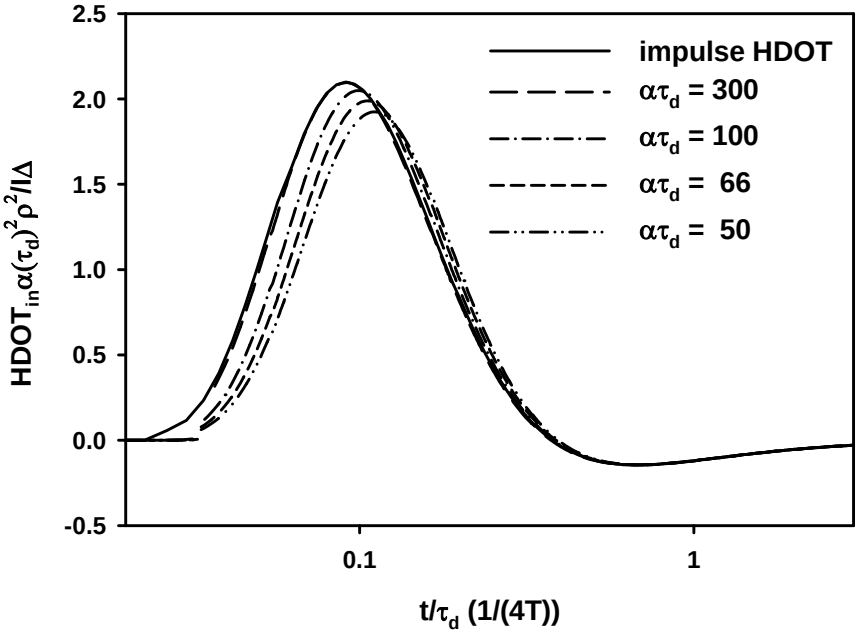

Figure 65. For $\alpha\tau_d = 300$, the response is well approximated by impulse HDOT.

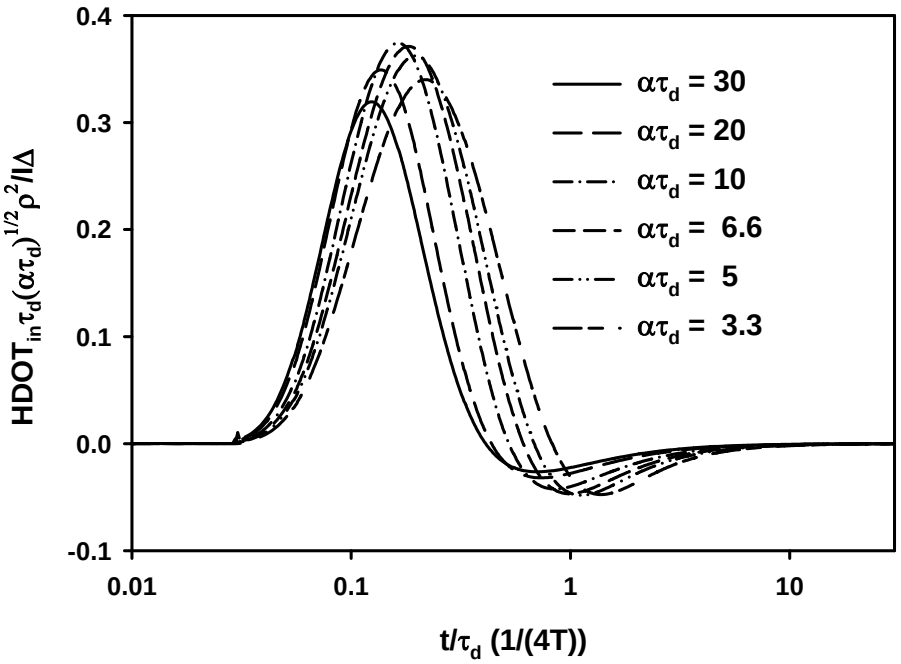

Figure 66. Vertical quantity has been scaled to $\sqrt{\alpha\tau_d}$ resulting in closer peak values. The intersection of peak unit step and impulse responses occurs at $\alpha\tau_d = 7.1467$.

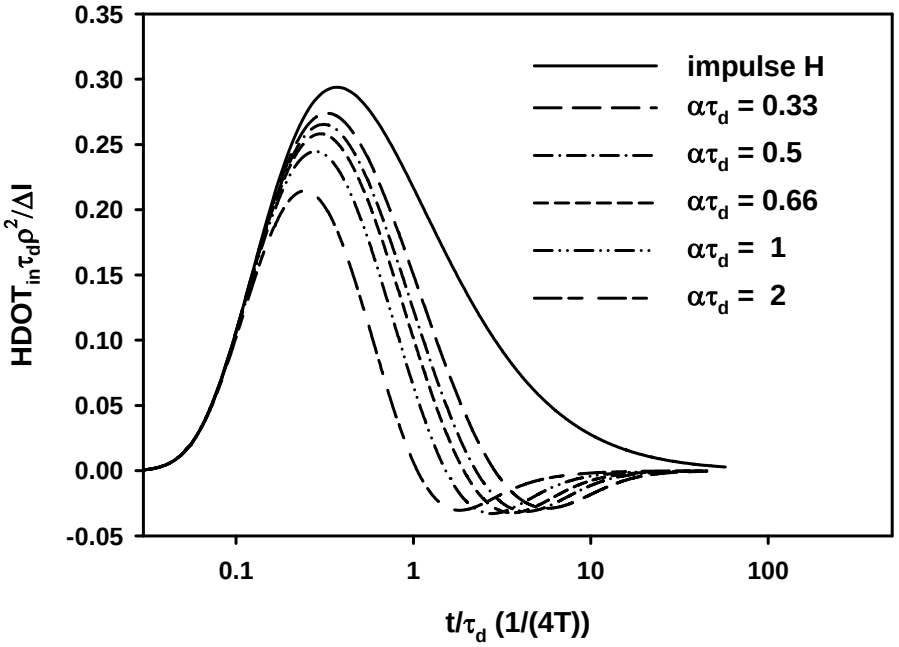

Figure 67. At these values of $\alpha\tau_d$ the impulse *H* is a fair approximation for peaks.

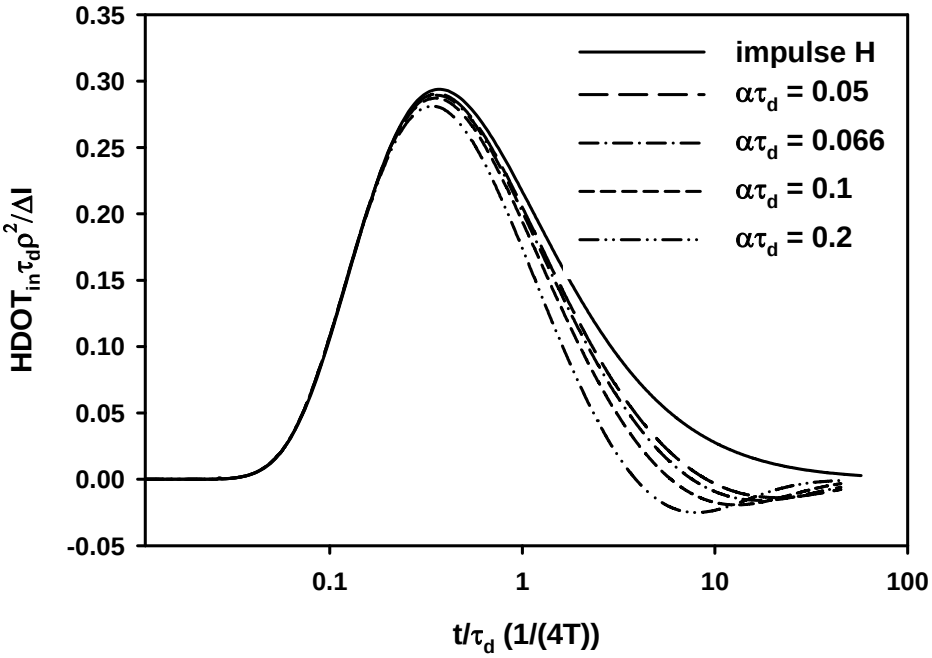

Figure 68. Impulse *H* or (32) is a good approximation to these value of $\alpha\tau_d$.

H Transition for $\rho = \Delta$, $\mu = 10\mu_0$ (Figure 69 through Figure 72)

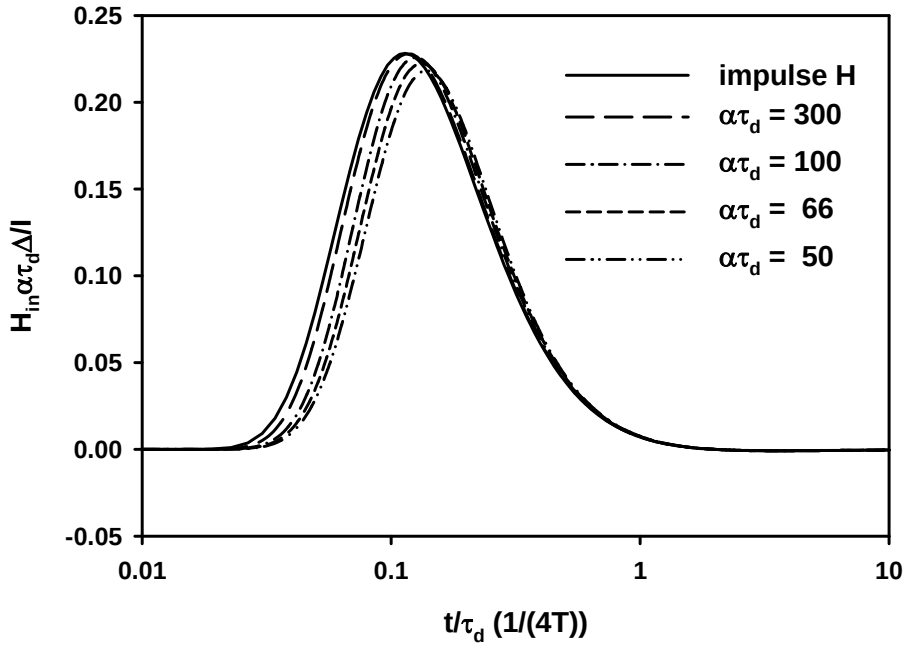

Figure 69. These responses are well approximated by (28) with (30). Some errors in peak for $\alpha\tau_d \leq 66$.

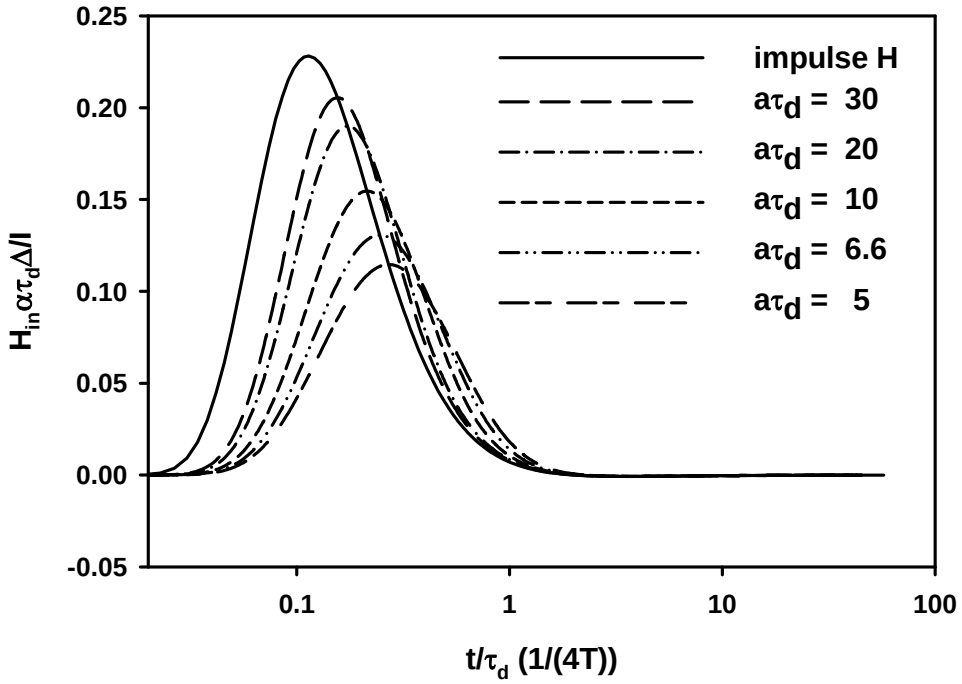

Figure 70. The peak decreases by almost a factor of *2* as $\alpha\tau_d$ reduces from *30* to *5*.

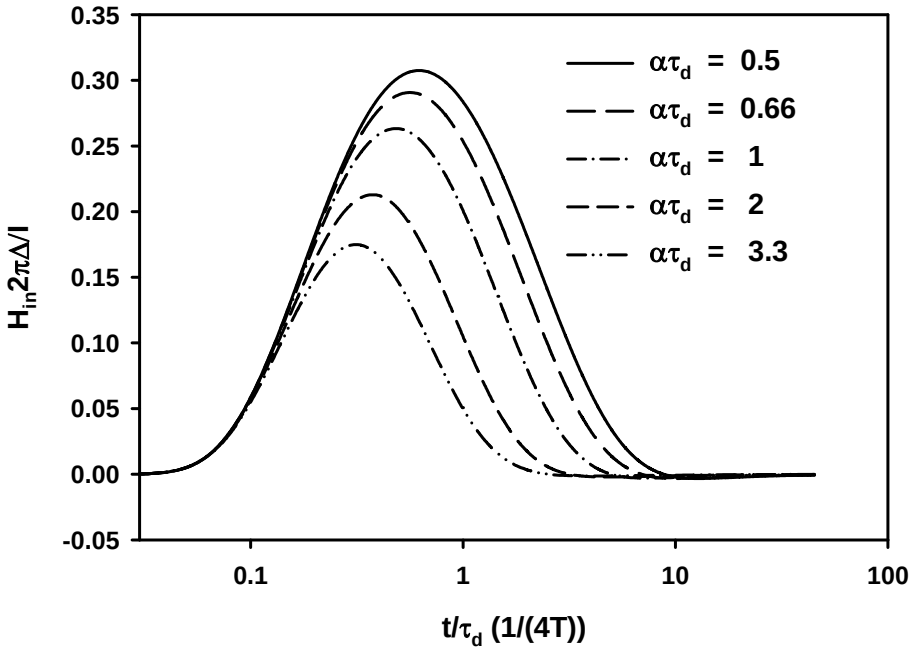

Figure 71. This should be compared to the unit step response shown in Figure 72. (31) is a good approximation for these curves. The intersection of the unit step and impulse peaks occurs at $\alpha\tau_d = 3.4249$, which is between the value shown in Figure 70 and the current figure.

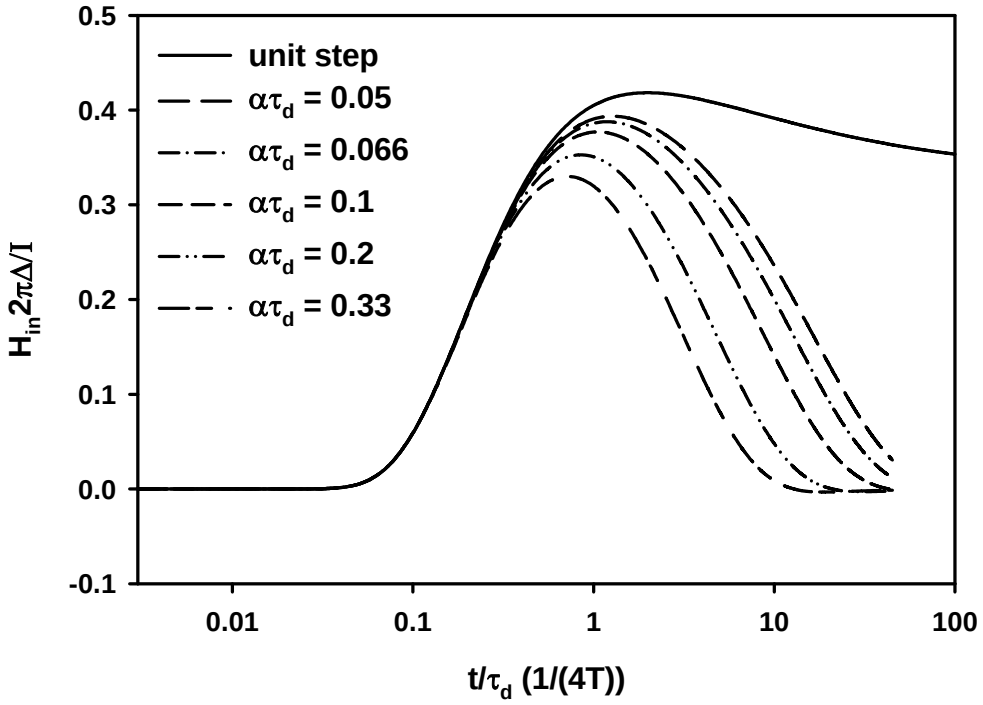

Figure 72. For these values of $\alpha\tau_d$, responses can be approximated by (31).

HDOT Transition for $\rho = \Delta$, $\mu = 10\mu_0$ (Figure 73 through Figure 76)

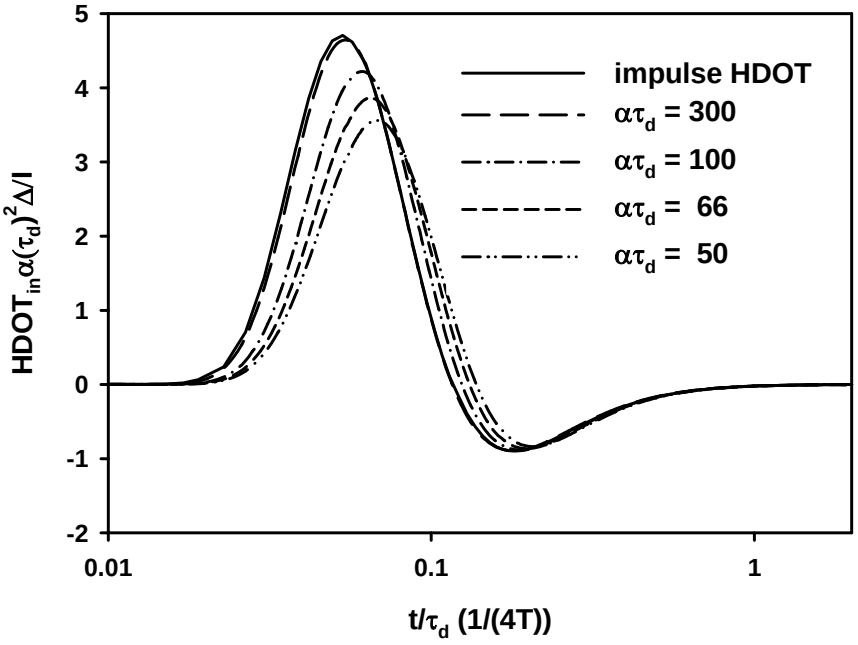

Figure 73. For $\alpha\tau_d = 300$, the response is well approximated by impulse HDOT.

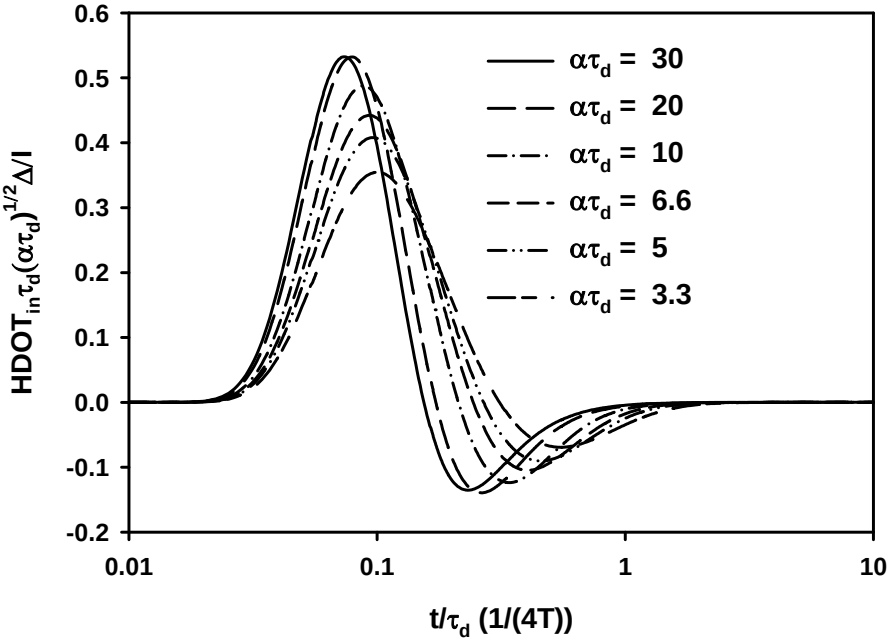

Figure 74. Vertical quantity has been scaled to $\sqrt{\alpha\tau_d}$ resulting in closer peak values. Figure 23 indicates the intersection of the unit step and impulse peaks occurs at $\alpha\tau_d = 20.63$. Notice the near peak for curve shown for $\alpha\tau_d = 20$.

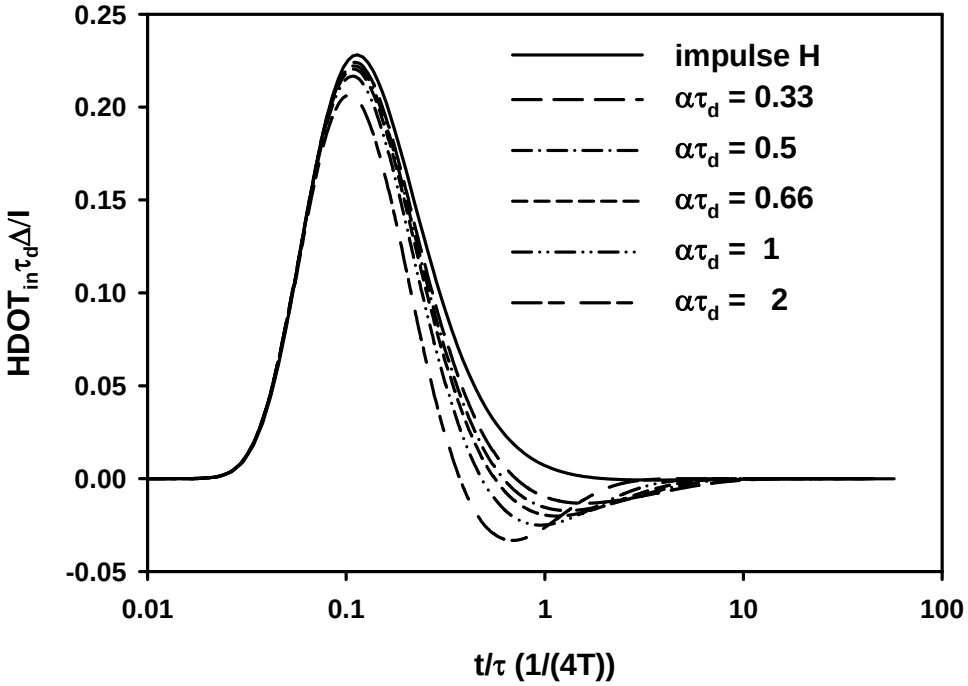

Figure 75. Impulse *H* or (32) is a good approximation to responses for these values of $\alpha\tau_d$. $\alpha\tau_d = 1$ is when the transition starts.

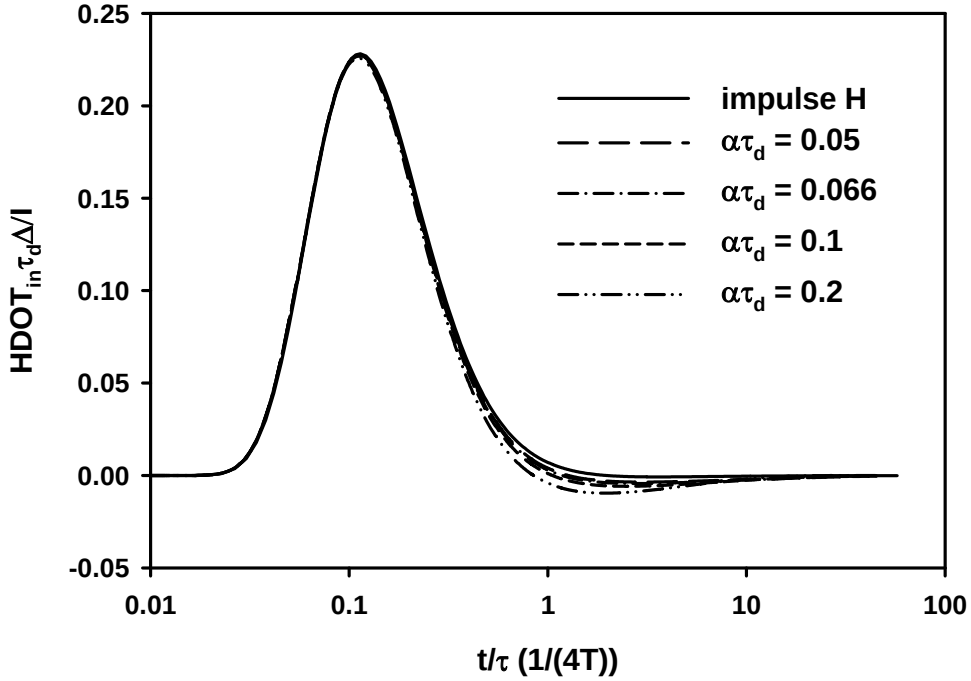

Figure 76. Impulse *H* or (32) is an excellent approximation to the responses for these values of $\alpha\tau_d$.

H Transition for $\rho = 10\Delta$, $\mu = 10\mu_0$ (Figure 77 and Figure 80)

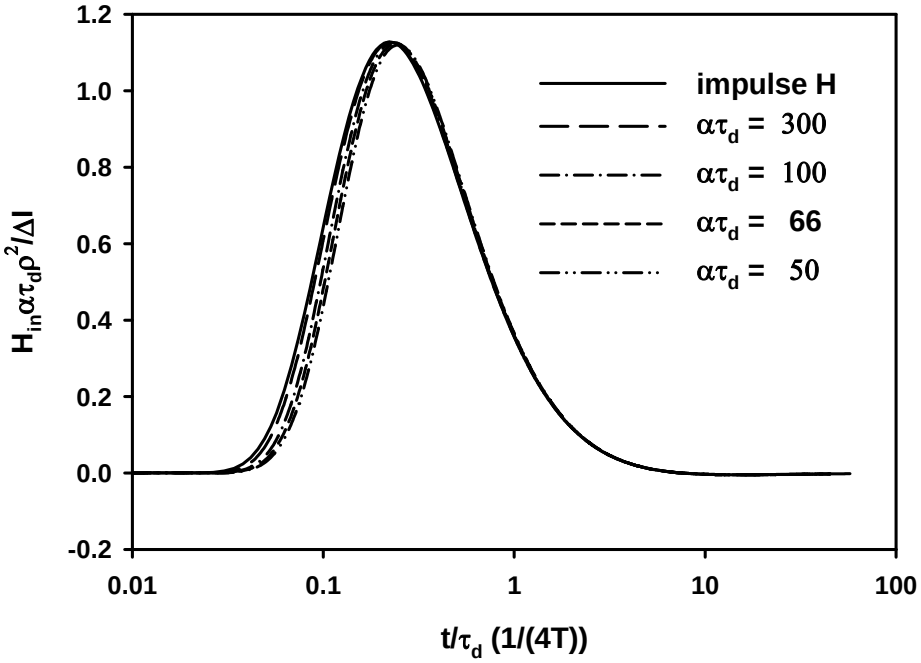

Figure 77. (28) with (30) is an excellent approximation to responses for these values of $\alpha\tau_d$.

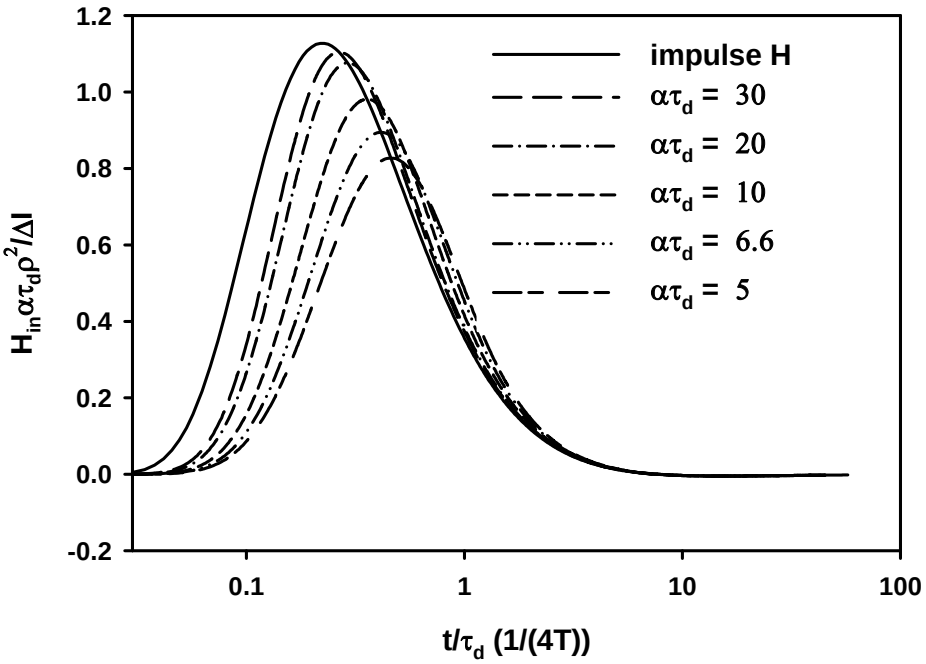

Figure 78. The peak H decreases considerably in the range $5 < \alpha\tau_d < 30$.

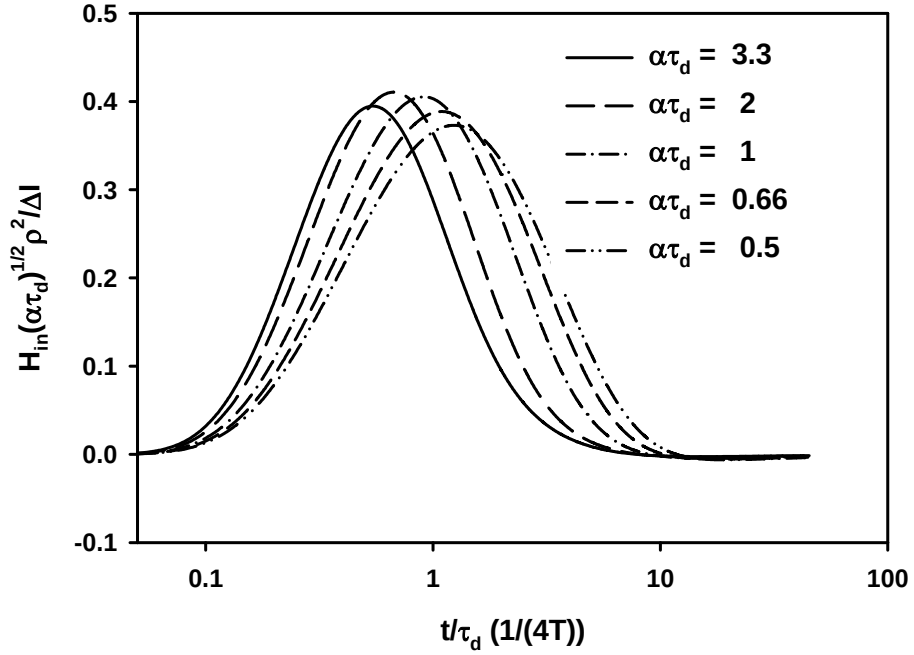

Figure 79. Vertical quantity has been scaled to $\sqrt{\alpha\tau_d}$ resulting in closer peak values. Note the intersection of unit step peak and impulse occurs at $\alpha\tau_d = 1.0956$, which corresponds to the peak value shown.

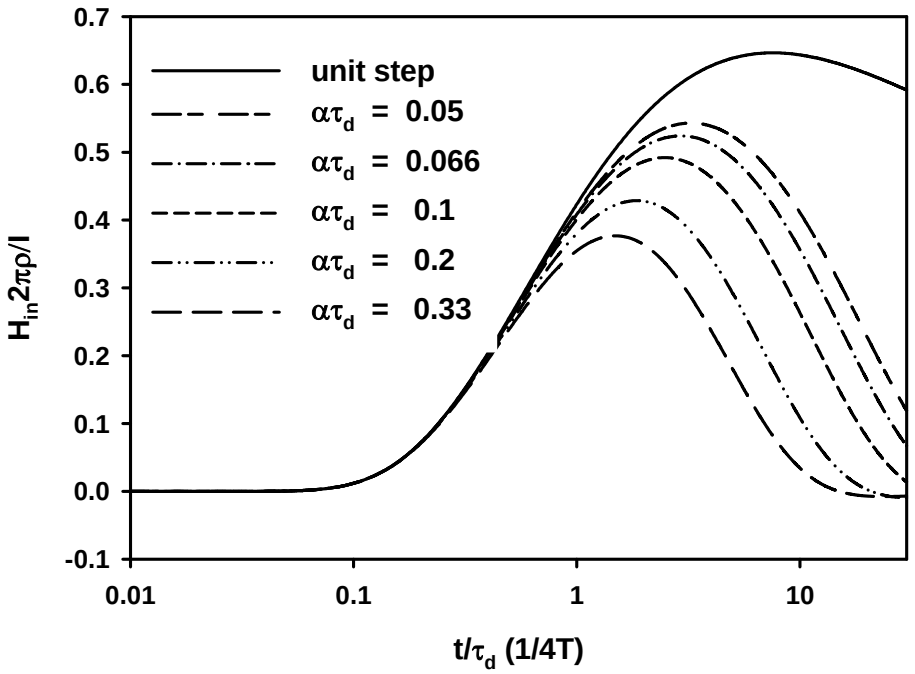

Figure 80. For these values of $\alpha\tau_d$, responses can be approximated by (31).

HDOT Transition for $\rho = 10\ \Delta$, $\mu = 10\mu_0$ (Figure 81 and Figure 84)

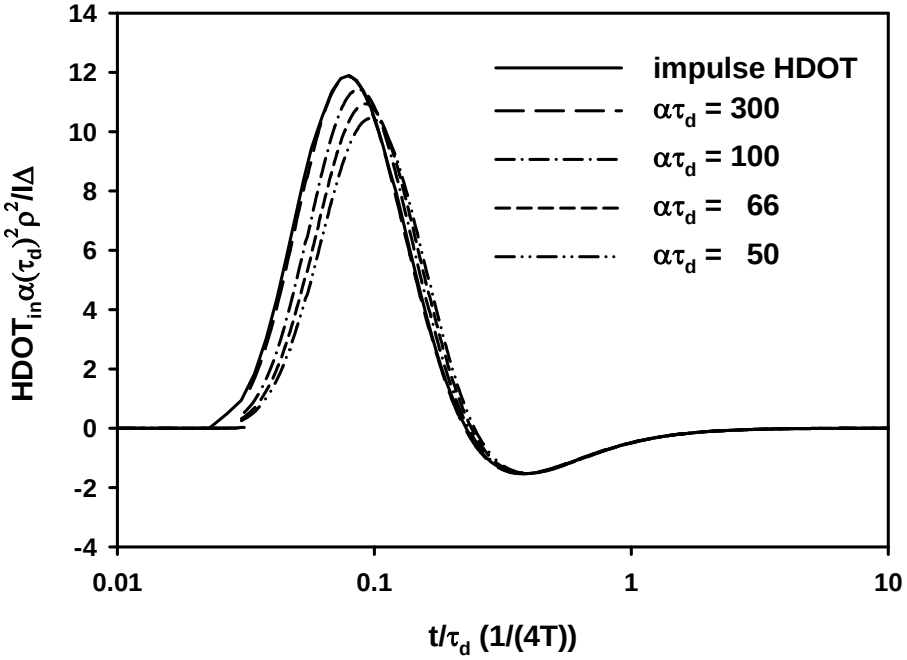

Figure 81. HDOT for $\alpha\tau_d = 100$ can be approximated by (29) with (30).

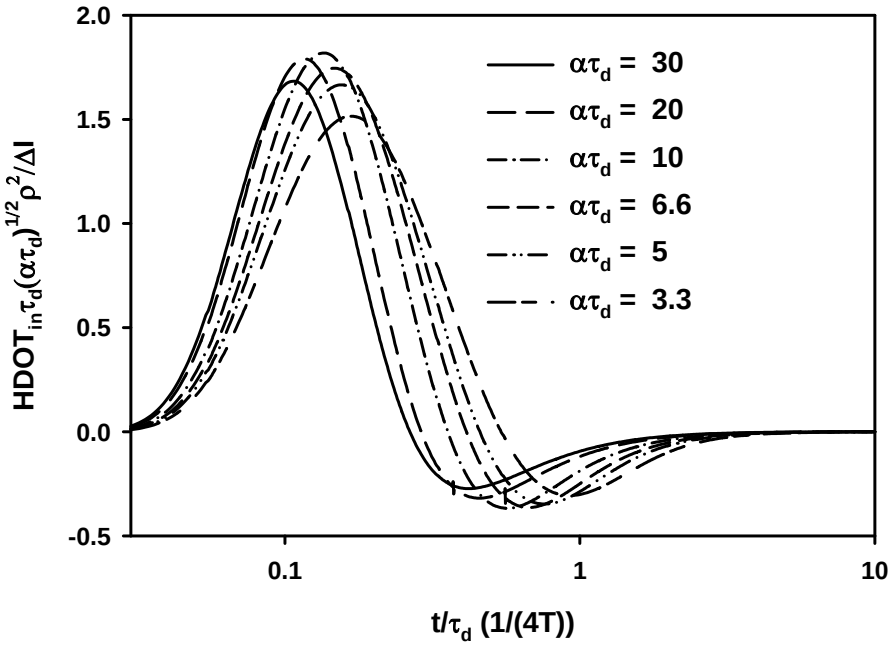

Figure 82. Vertical quantity has been scaled to $\sqrt{\alpha\tau_d}$ resulting in closer peak values. Intersection of the unit step and impulse responses occurs at $\alpha\tau_d = 10.5552$, as shown in Figure 24 the near peak for the curve $\alpha\tau_d = 10$.

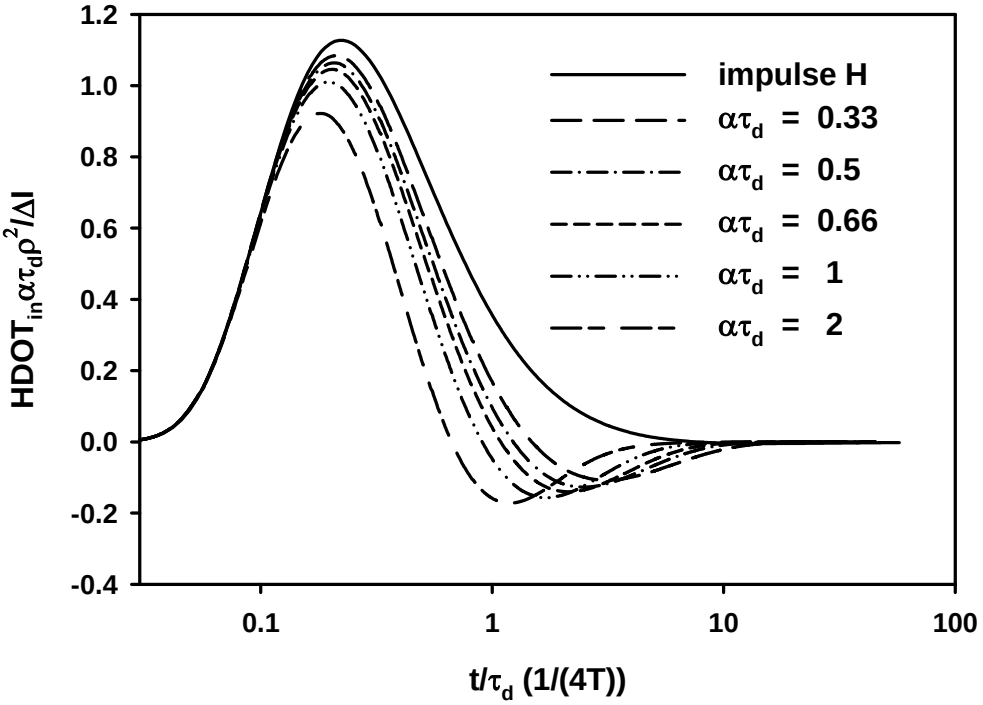

Figure 83. Impulse H or (32) is a good approximation to responses for these values of $\alpha\tau_d$.

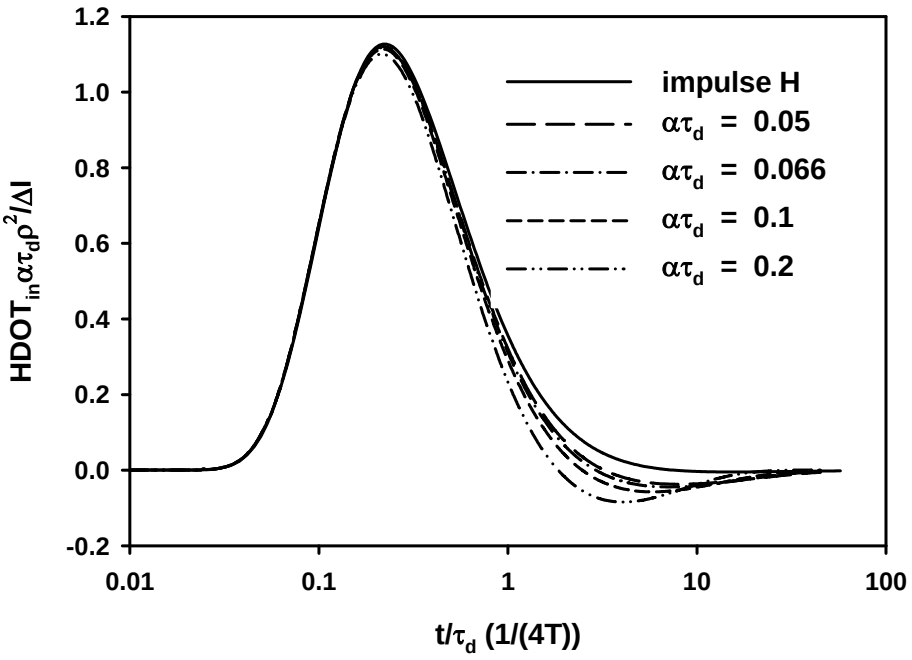

Figure 84. Impulse H or (32) is an excellent approximation to responses for these values of $\alpha\tau_d$.

Voltage Bounds μ = μ₀ (Figure 85 through Figure 88)

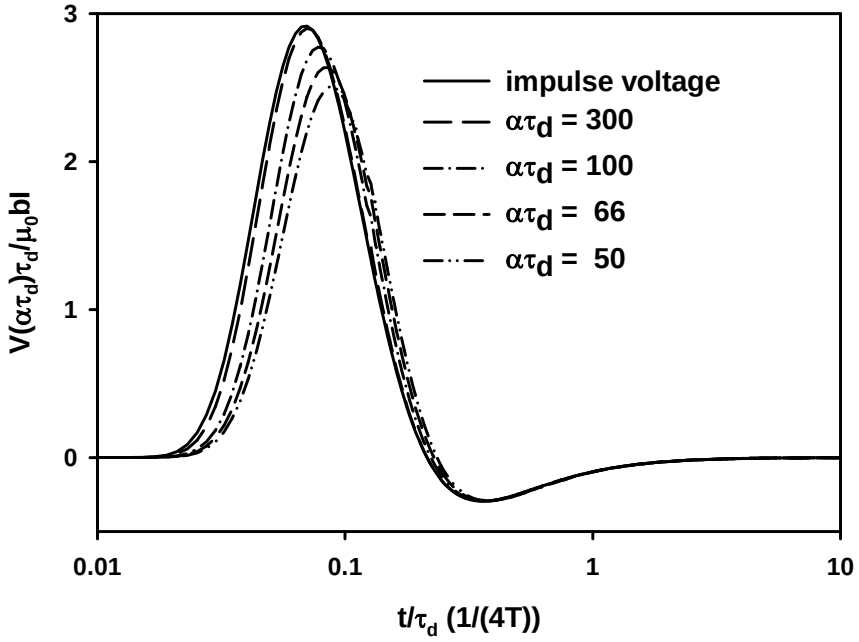

Figure 85. Voltage bounds for direct strikes (μ = μ₀).

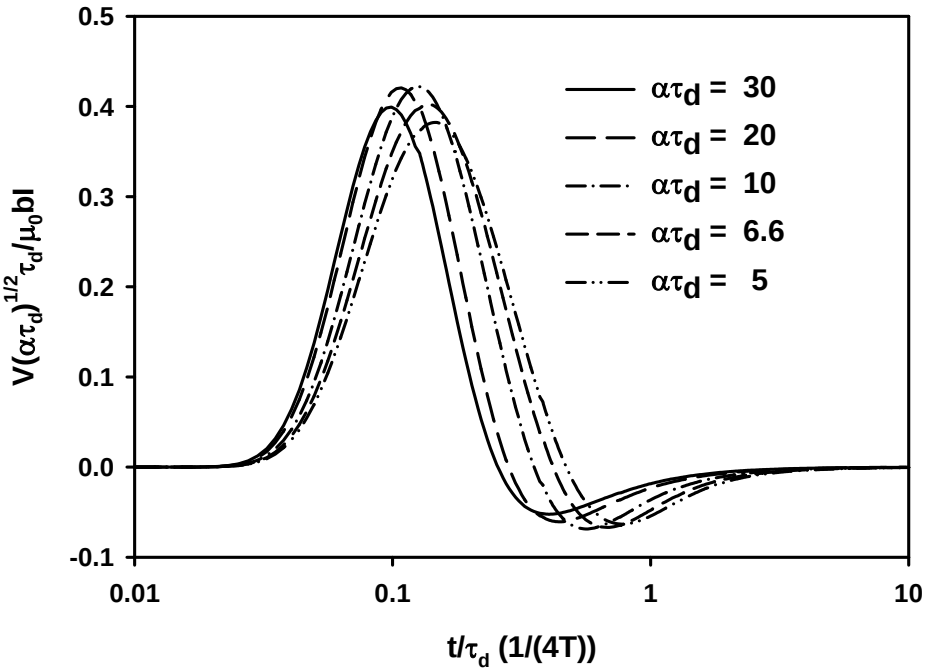

Figure 86. Voltage bounds for direct strikes. The intersection of unit step and impulse peak occurs at $\alpha\tau_d = 11.4263$ ($\mu = \mu_0$).

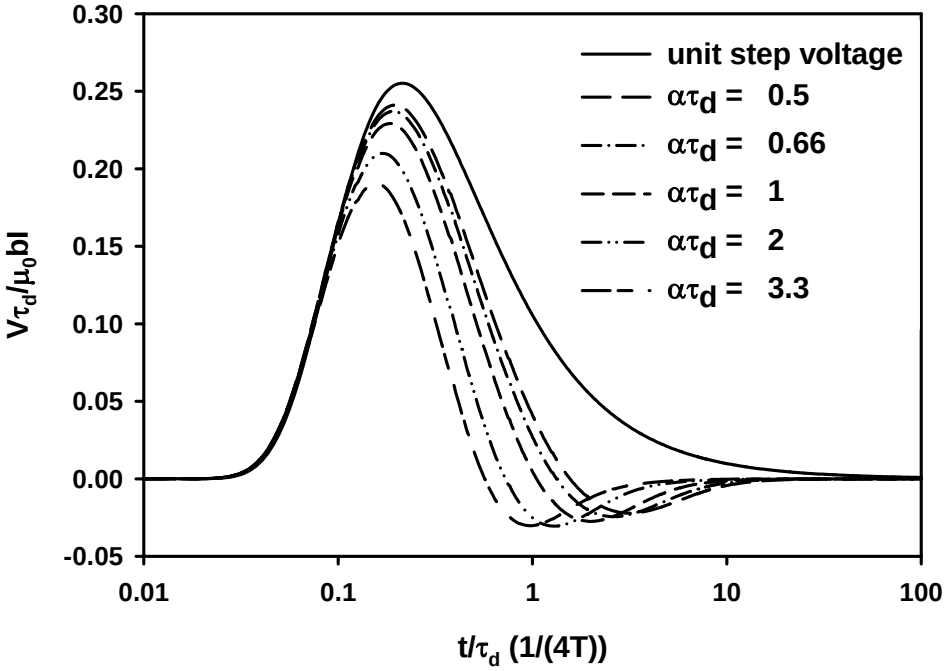

Figure 87. Voltage bounds for direct strikes ($\mu = \mu_0$).

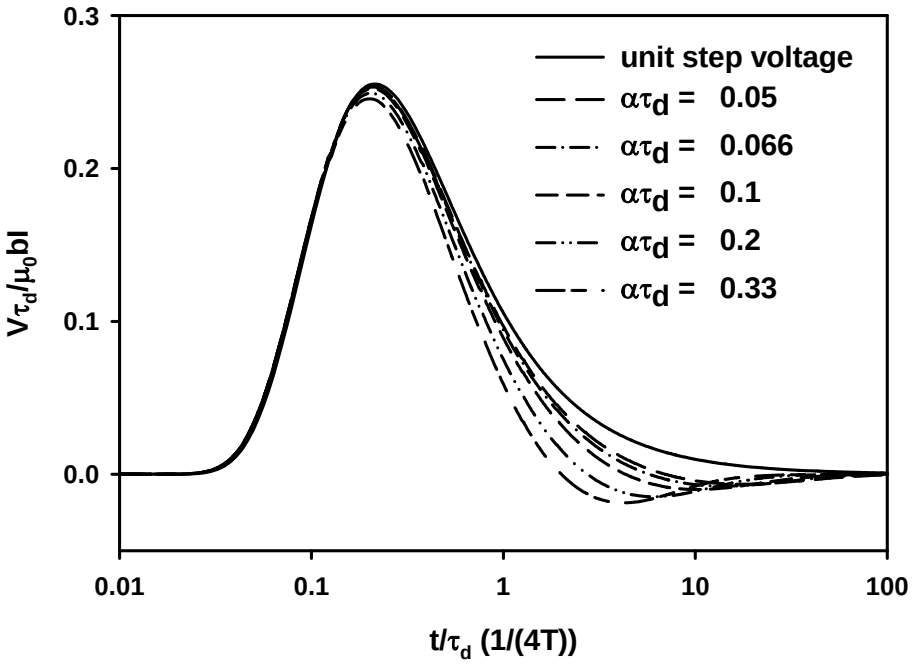

Figure 88. Voltage bounds for direct strikes ($\mu = \mu_0$).

Voltage Bounds $\mu = 10\mu_0$ (Figure 89 and Figure 92)

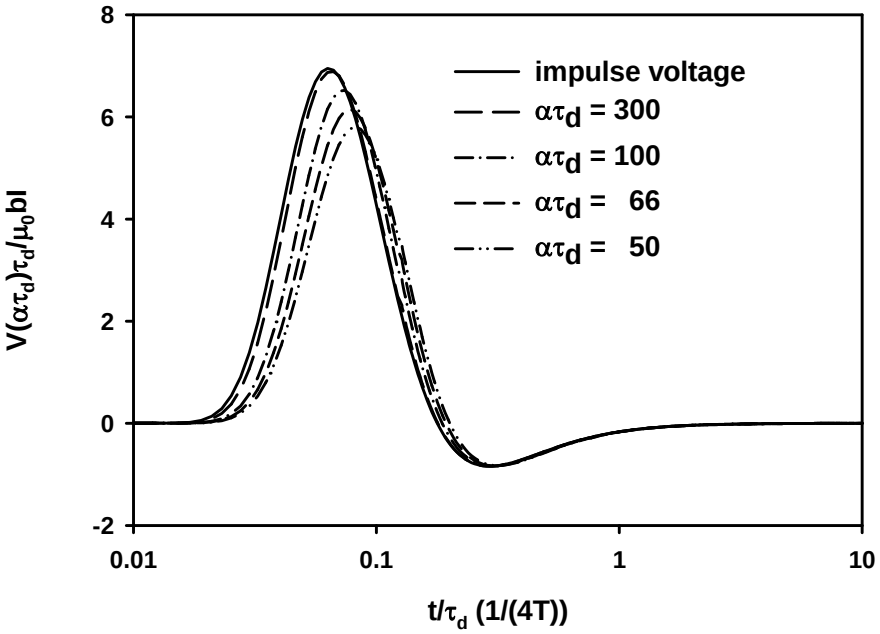

Figure 89. Voltage bounds for direct strikes ($\mu = 10\ \mu_0$).

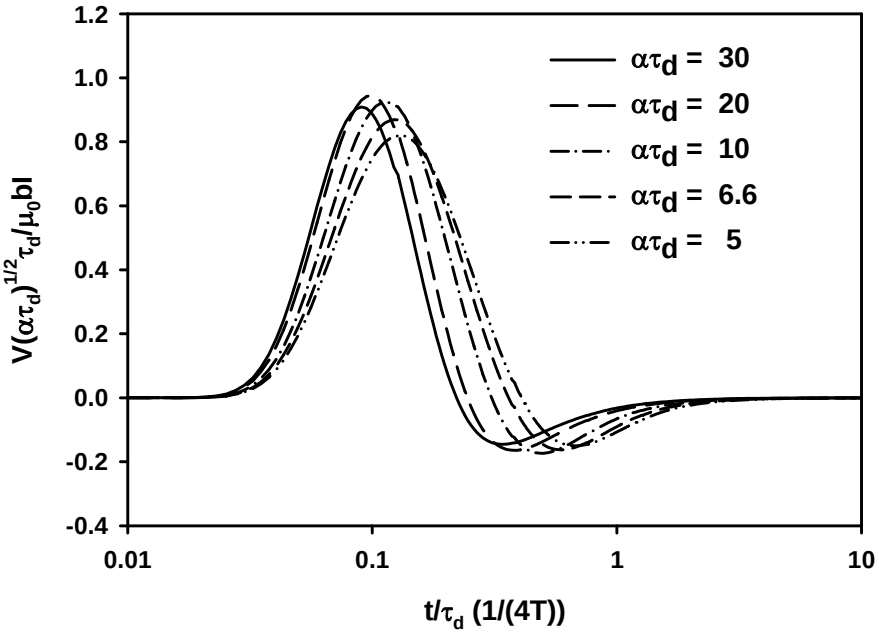

Figure 90. Voltage bounds for direct strikes. The intersection of unit step and impulse peak occurs at $\alpha\tau_d = 13.4488$ ($\mu = 10\ \mu_0$).

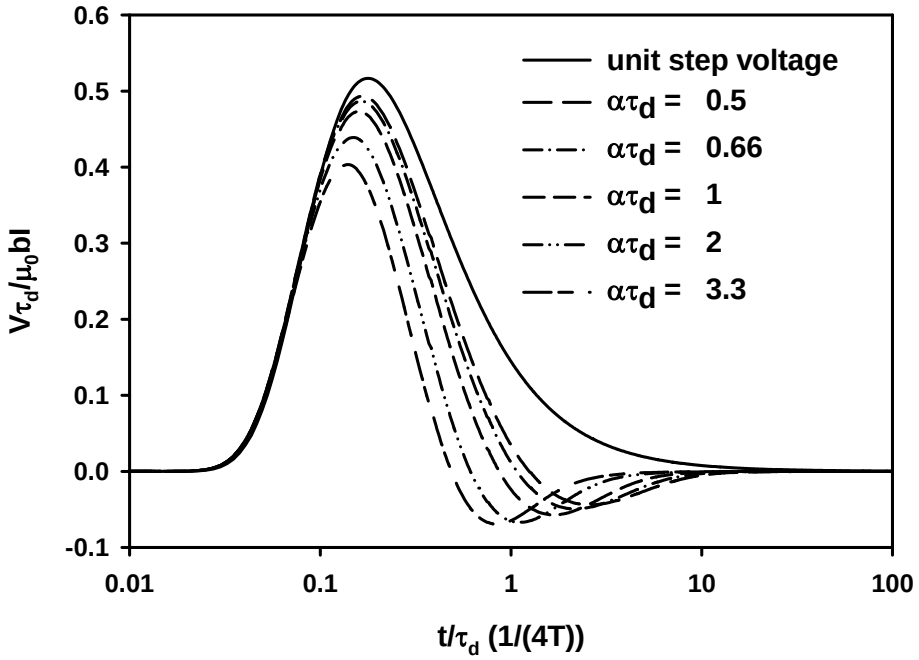

Figure 91. Voltage bounds for direct strikes ($\mu = 10\ \mu_0$).

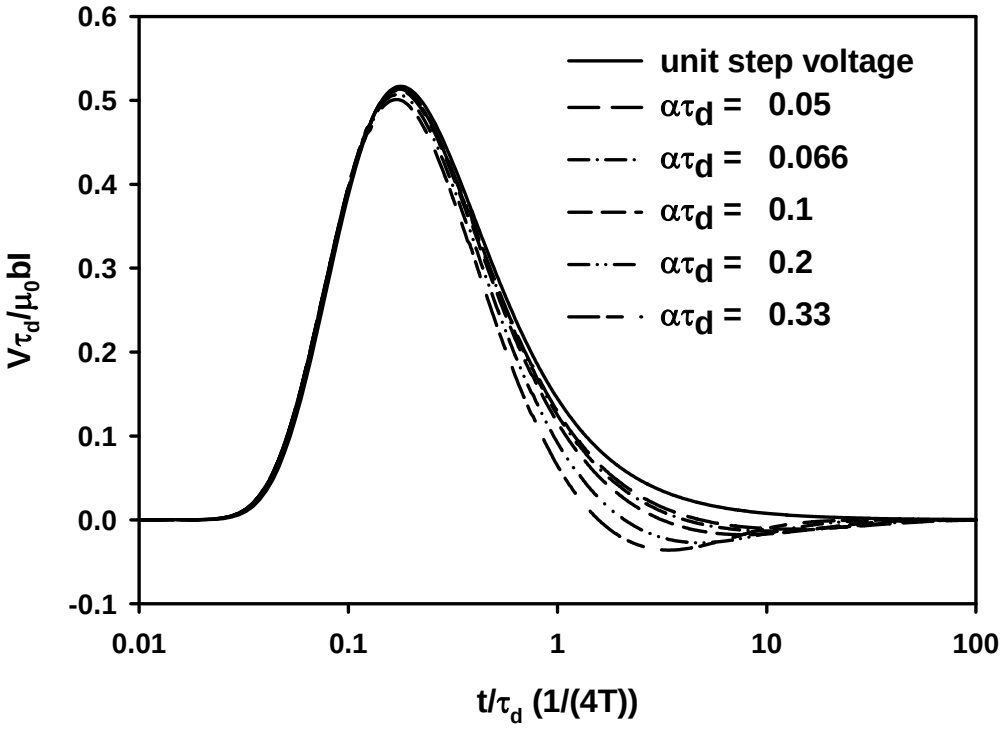

Figure 92. Voltage bounds for direct strikes ($\mu = 10\ \mu_0$).

Current Bounds $\mu = \mu_0$ (Figure 93 and Figure 96)

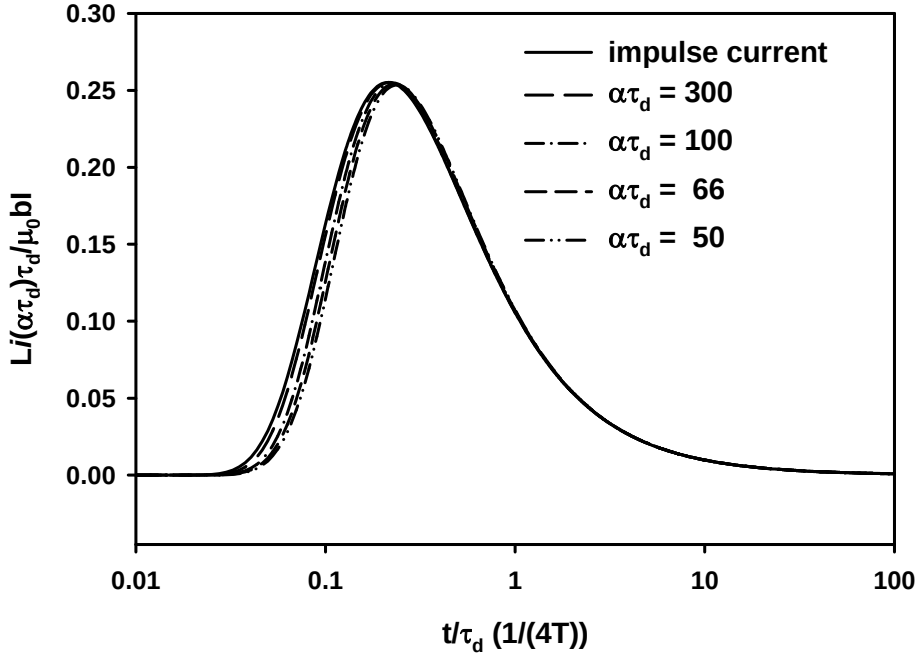

Figure 93. Current bounds for direct strikes ($\mu = \mu_0$).

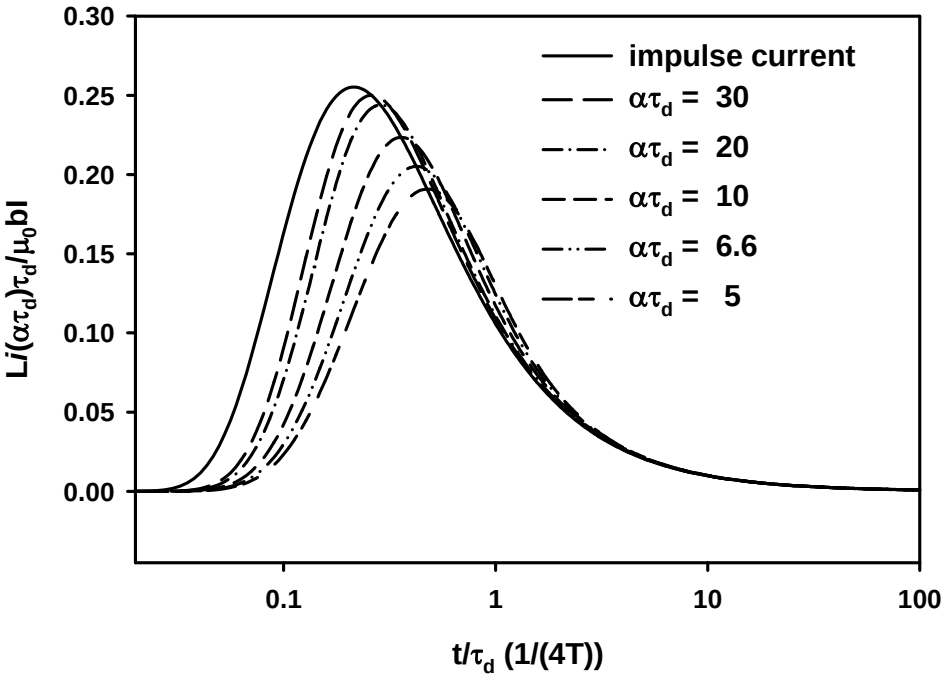

Figure 94. Current bounds for direct strikes ($\mu = \mu_0$).

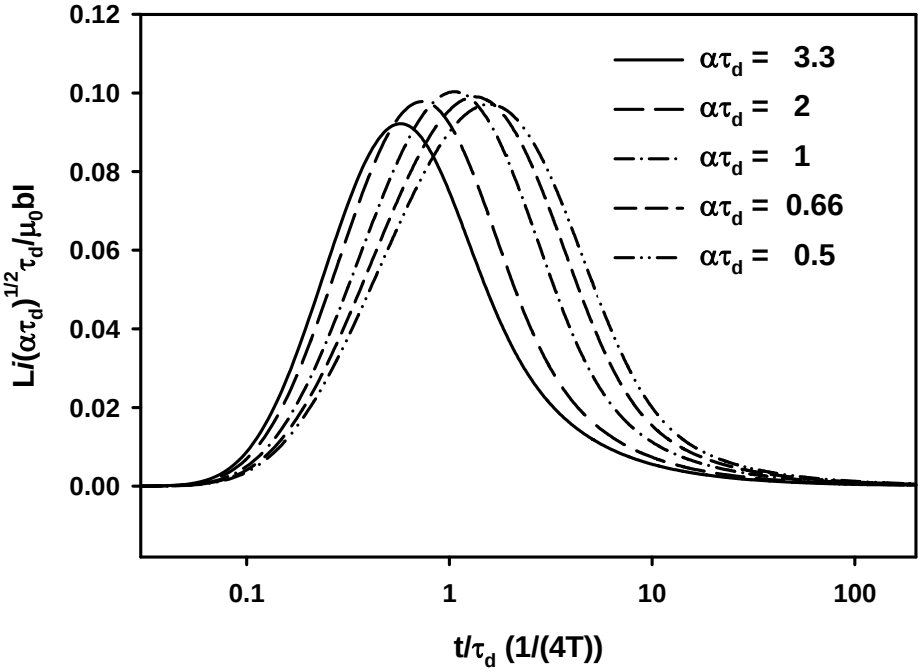

Figure 95. Current bounds for direct strikes ($\mu = \mu_0$). The peak on the scaled "*i*" appears to occur near $\alpha\tau_d \approx 1$.

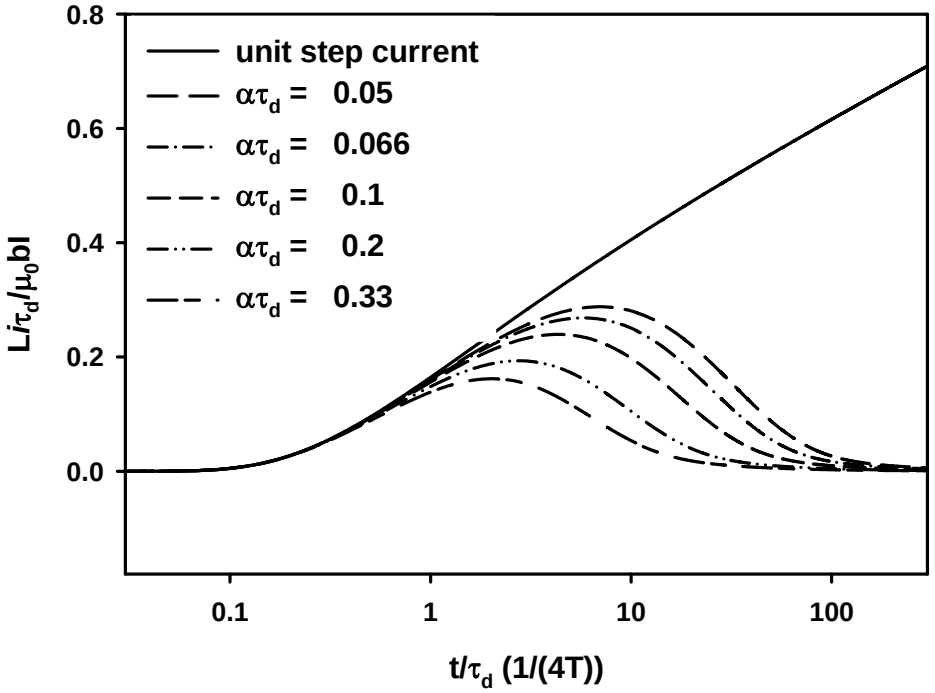

Figure 96. Current bounds for direct strikes ($\mu = \mu_0$).

Current Bounds $\mu = 10\mu_0$ (Figure 97 and Figure 100)

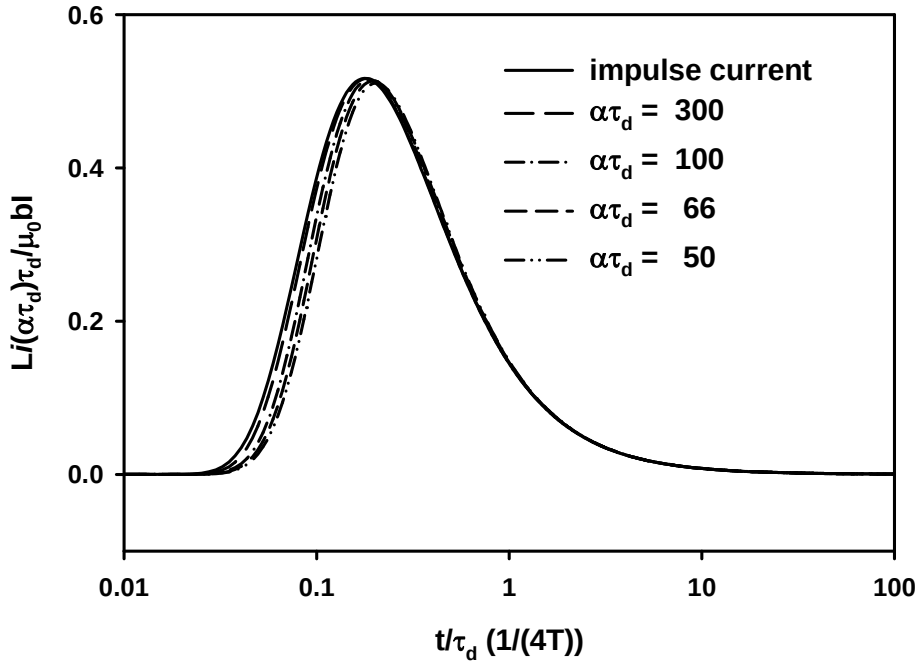

Figure 97. Current bounds for direct strikes ($\mu = 10\ \mu_0$).

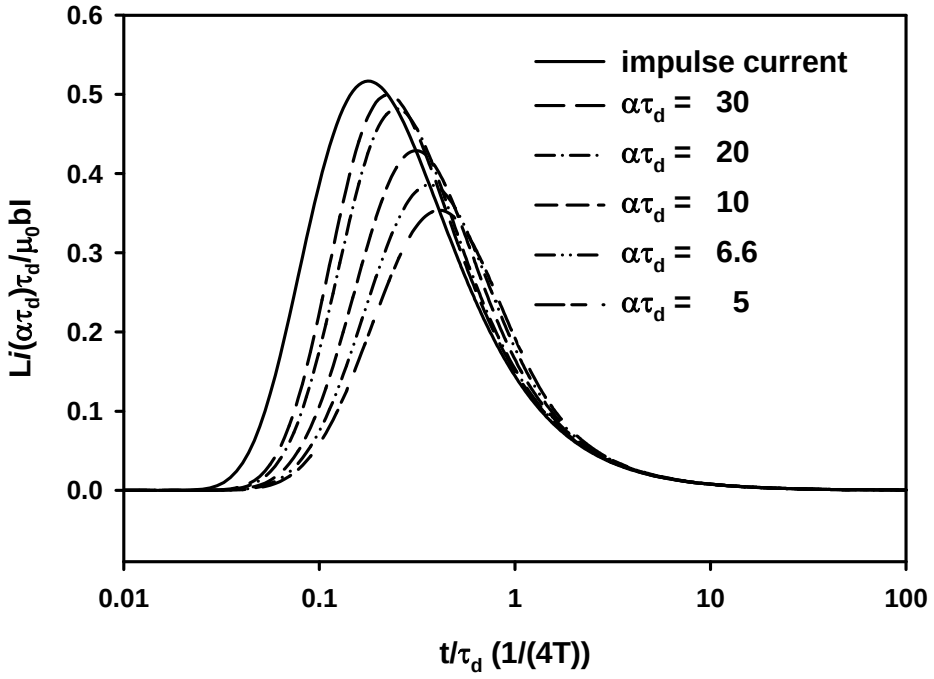

Figure 98. Current bounds for direct strikes ($\mu = 10\ \mu_0$).

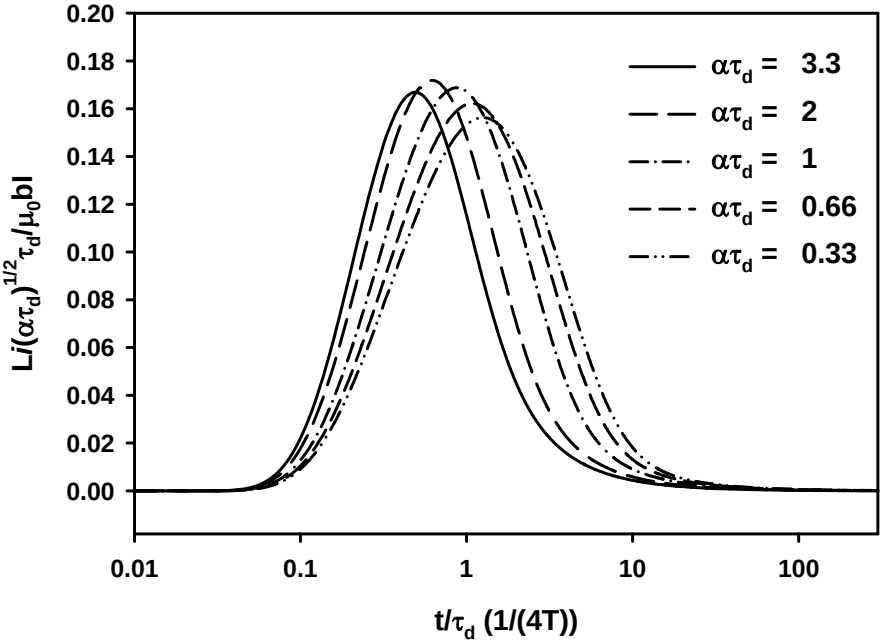

Figure 99. Current bounds for direct strikes ($\mu = 10\ \mu_0$). The peak on the scaled "*i*" appears to occur near $\alpha\tau_d \approx 2$.

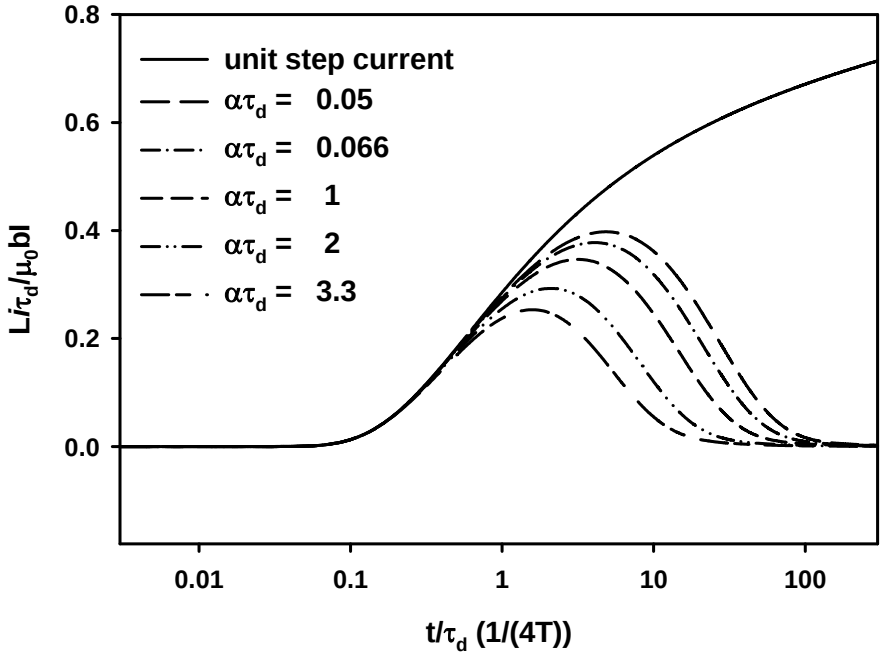

Figure 100. Current bounds for direct strikes (μ = 10 μ_0).

Conclusions

Linear magnetic diffusion into a metallic enclosure has been studied with a more realistic decaying exponential incident waveform. Lightning parameters are used to illustrate a field excitation by nearby lightning and a line source excitation by a direct strike to a metallic cable insulated from the enclosure.

For a transient magnetic field incident on a metallic enclosure, the existing simple formulas for the impulse response on the enclosure interior are compared to the exact residue expansion. This expansion is also used to numerically calculate enclosure interior responses for decaying exponentials. For a line source excitation of a metallic enclosure, the existing enclosure interior response for a unit step excitation is extended to the impulse excitation as well as to the case of a decaying exponential. The physical parameters studied include H and HDOT at the wall $\rho = \Delta$ as well as $\rho = 10\Delta$, voltage and current bounds for any single–turn coupling loops.

The governing parameter $\alpha\tau_d$ is identified and numerically investigated to determine the peak response and waveform transition of a decaying exponential response from the unit step response to the impulse response.

The enclosure interior responses as a function of the product of metallic enclosure parameter constant and lightning decaying constant $\alpha\tau_d$ have been extensively tabulated. The enclosure interior responses for any enclosure wall with linear material properties can be determined

from the curves presented. The only exception to the use of data is the transparency limit $\Delta \rightarrow 0$ due to the use of the double exponential lightning waveform.

Those who read and understand the executive summary will develop a feel for how to estimate the induced voltage on any loop inside the enclosure from a transient magnetic field such as the nearby lightning magnetic field. They can also determine the maximum voltage on a single loop inside an enclosure from a worst-case direct strike lightning coupling to the enclosure. But before embarking on such tasks, they should study the whole report together with the relevant references to fully appreciate the limitations of such a treatment. We believe that this report is a useful addition to the current literature on the linear magnetic diffusion through a metallic wall.

Appendix A. Impulse Charge Statistics

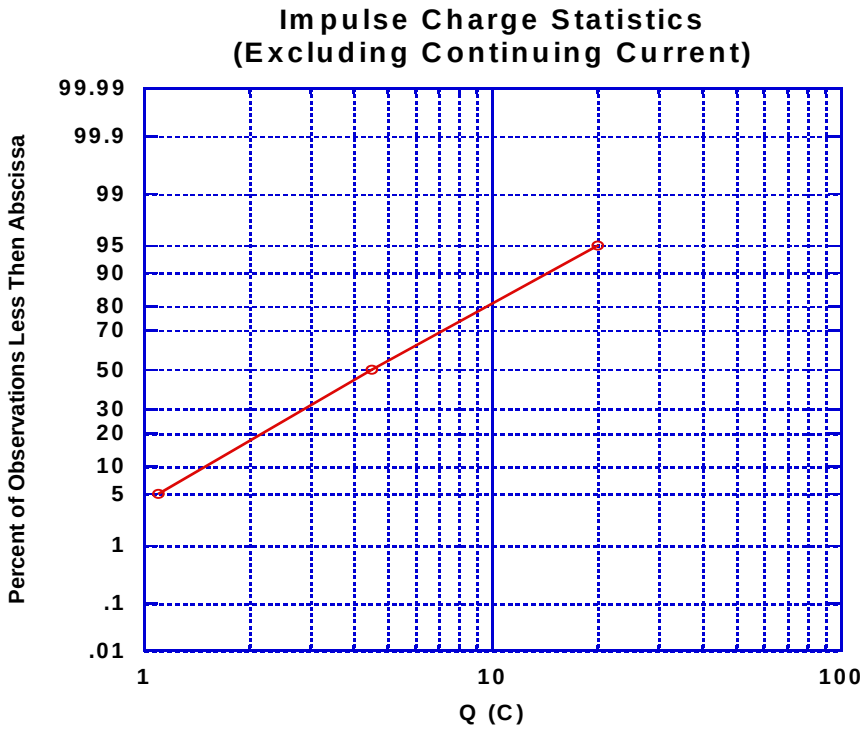

Figure 101. Impulse charge statistics (excluding continuing current). Adapted from Berger et al. (1975).

References

[1]. Lee, K. S. H. Editor, **EMP Interaction: Principle, Techniques, and Reference Data**, Revised Printing, Hemisphere Publishing Corporation and Taylor & Francis, 1986 and 1995, pp.559-573.
[2]. Warne, L. K., W. A. Johnson and K. C. Chen, "Maximum Interior Voltage and Magnetic Field Penetration through a Linear Conducting Layer," Journal of Electromagnetic Waves and Applications, Vol. 9, No.4, 1995, pp. 569-598.
[3]. "EMP Engineering and Design Principles," Bell Laboratories Report, Whippany, NJ, Chapter 2, 1975.
[4]. Dorf, R. C., **The Electrical Engineering Handbook**, Second Edition, IEEE Press, 1997.
[5]. Cianos, T. and E. T. Pierce, A Ground-lightning Environment for Engineering Usage, TS-3141/7723, Stanford Research Institute, Menlo Park, August 1972.
[6]. Uman, M. A., **The Lightning Discharge**, Academic Press, Inc., New York, 1987, pp. 124-125.
[7]. Kaden, H., **Wirbelstrome und Schirmung in der Nachrichtentechnik** , Springer-Verlag, Berlin, 1959.
[8]. Bedrosian, G. and K. H. S. Lee,"EMP Penetration through Metal Skin Panels and Into Aircraft Cavities," AFWL Interaction Note 314, August 1976.
[9]. Merewether, K. O. "Linear magnetic field diffusion through cylindrical shields for nearby and direct-strike lightning," in preparation.
[10]. Chen, K. C. and L. K. Warne, "Improved Asymptotic Expansions of Time Domain Antenna Current," Radio Science, Volume 26, Number 5, Page 1205-1208, September-October 1991.
[11]. M. Abramowitz and I. A. Stegun (editor), **Handbook of Mathematical functions**, Washington DC: National bureau of Standards, 1027.
[12]. Warne, L. K., W. A. Johnson and K. C. Chen , "Nonlinear Diffusion and Internal Voltages in Conducting Ferromagnetic Enclosures subjected to Lightning Current," IEEE Transactions on Electromagnetic Compatibility, Vol. 37, No. 2, May 1995, pp.145-154.
[13]. Johnson, W. A., L. K. Warne, K. C. Chen and E. M. Gurrola, "Linear Diffusion Internal Voltages in Conducting Enclosure Subject to a Direct Lightning Strike," Electromagnetics, 15:189-207, 1995.
[14]. Chen, K. C., L. K. Warne and T. T. Wu, "Accurate Formulas and Asmptotic Expansions of Transient Antenna Current," Journal of Electromagnetic Waves and Applications, Vol. 6, No. 3, 297-308, 1992.

Distribution

1	MS0492	J. D. Brewer, 411
1	MS0492	T. D. Brown, 411
1	MS0492	D. A. Hoke, 411
1	MS0492	L. L. Luna, 411
1	MS0492	R. L. Meyers, 411
1	MS0492	M. R. Taylor, 411
1	MS0492	K. J. Maloney, 411
3	MS0492	K. C. Chen, 411

1	MS0405	K. O. Merewether, 433
1	MS0405	J. McLaughlin, 433
1	MS0405	T. N. Hennerichs, 433
1	MS0405	J. L. Means, 433
3	MS1152	L. K. Warne, 1652
1	MS1152	R. E. Jorgenson, 1652
1	MS1152	M. A. Dinallo, 1653
1	MS0447	P. D. Hoover, 2111
1	MS0447	M. E. Morris, 2111
1	MS0899	RIM-Report Management, 9532 (electronic copy)